UNIVERSITY OF GENOVA

DISTAV

Department of Earth, Environmental and Life Sciences - PhD course on Sciences and Technologies for the Environment and the Territory (Curriculum: Earth Sciences)

31st PhD Cycle

Rip currents in Mediterranean environment: a case study along eastern Ligurian coast

PhD Supervisors:

Prof. Marco Ferrari
Prof. Marco Firpo

PhD Candidate:

Luca Carpi

Year

2019

ii

Preface

The rip currents (or cross-shore currents) are an interesting phenomenon occurring along the coasts of the whole world, playing a key role in near-shore circulation and coastal processes. These currents, as well as for the environmental implications, are also well known as risk source for beachgoers. For these reasons, rip currents are widely investigated by coastal scientists, but most of studies concern rip currents development along the oceanic coasts. The "Mediterranean rips" are (wrongly) commonly perceived as less important, and this probably due to the absence of recognised accident statistics along the Mediterranean coasts. The "rip hazard" is in fact the main rip implication known to public opinion. In this thesis we applied several research methodologies, integrated between them, to investigate rip currents behaviour within a micro-tidal embayed beach on the eastern Ligurian coast (north-eastern Italy). The main target is to provide an accurate description of rip dynamics, and propose a reliable investigation method for rip currents research in Mediterranean environment.

iv

Acknowledgements

I would like to express my special thanks and appreciation to Prof. Marco Ferrari and Prof. Marco Firpo, for their efforts on following and supporting my PhD research project.

I would like to thank my "coastal research colleague" Luigi Mucerino, for all the discussions and input he provided during my PhD course.

I would like to thank Dott. Alessio Rovere, for all the precious input and counsels during my period of study at MARUM (University of Bremen) and ZMT (Leibniz Centre for Tropical Marine Research). I also would like to thank the entire Sea Level and Coastal Changes research group at MARUM and ZMT, for all the support during my period in Germany.

I would like to thank Prof. Giovanni Besio and the entire MeteOcean research group (DICCA - University of Genova) for providing offshore wave dataset, essential for my PhD project.

During my PhD course I had an opportunity to work with many good colleagues. I thank them for the good time and discussions, which contributed to this thesis as well.

Finally, I would thank my parents and my girlfriend for all the unconditional support during my long student career.

Abstract

This thesis proposes a study on the rip currents development within a Mediterranean embayed beach. The rip (or cross-shore) currents are among the most investigated phenomena in the field of coastal research, and their fame is due to their environmental and socio-economic implications. The coastal areas are considered as transition environments, where hydrosphere, lithosphere, biosphere, atmosphere and (often) anthroposphere meet. The rip currents are a crucial component of the coastal hydro-morphodynamic processes (hydrosphere and lithosphere) (Short, 1999; Castelle et al., 2016), play a role in larval recruitment processes (biosphere) (Shanks et al., 2010), and they are also well known as risks source for beachgoers (anthroposphere) (Short and Hogan, 1994; Austin et al., 2012). However, the rip currents role along the Mediterranean coasts is often neglected, and most of the literature concerns the rip currents in oceanic environments. The aim of this research is a detailed description of the rip currents behaviour along a Mediterranean embayed beach, also considering the possible sea-level rise implications. The study area was identified within Levanto bay, along the eastern Ligurian coast (NW Italy). The research activity has been conducted through an integrated application of several investigation methodologies, in order to obtain the best possible results in therm of phenomena description. The rip currents individuation is performed through a coastal video-monitoring system installed on the Levanto

beach, and the collected data were processed through a dedicated software for coastal video-monitoring (Brignone et al., 2012). Several field surveys were performed to obtain a full description of the geomorphological boundary conditions (topo-bathymetric surveys and sedimentological sampling). The rip currents description and evaluation were executed through the application of the XBeach model (Roelvink et al., 2009), which is a well-known tool for coastal modelling. Moreover, the modelling approach allowed the evaluation of the possible rip currents response under different sea-level rise scenarios (local sea-level projections to 2100) (Kopp et al., 2014). The obtained results show a detailed description of the rip currents phenomena, showing their essential role in the local coastal dynamics. The proposed research approach has proved to be reliable for the rip currents investigation in the Mediterranean environment, and it can be applied along any stretch of coast of the Mediterranean Sea. Moreover, the modelling results showed a significant relation between sea-level rise and rip currents behaviour. The results of this study highlight the role of the rip currents in the Mediterranean environment and represent a firm basis for the rip currents investigation along the Mediterranean coasts.

Contents

Chapter 1

Introduction

1.1 The aim of research

The integrated coastal zone management (ICZM) is a necessary practice for the sustainable development of the coastal areas (Thia-Eng, 1993; Pickaver et al., 2004; Moksness et al., 2009). In this regard, the development of integrated study approaches is a well-known challenge for coastal scientists, and the broad knowledge of coastal processes is a crucial factor for the correct management of coastal environments. Moreover, forecasting the effects of climate change is one of the main challenges for the international scientific community (Marcos et al., 2012). This challenge can be won only through an in-depth knowledge of current environmental dynamics, which allows developing reliable projections for the future. Coastal areas are fundamental resources for European countries that border the Mediterranean, and the Liguria region (north-western Italy) is a clear example of interdependence between coastal areas and local communities. The presence of reasonably extensive beaches, often nestled in rocky coasts with cliffs and promontories (embayed or pocket beaches) characterises the Ligurian coast, and the effects of human activity

1

are also evident with the massive presence of coastal structures (e.g. groynes, piers, seawalls, breakwaters) to prevent coastal erosion processes (Fierro et al., 2010, 2015). The local hydrodynamic regime is conditioned by the local geo-morphological features which, in their turn, are conditioned by the hydrodynamic regime itself. The interdependence between hydrodynamics and coastal morphology is an essential feature for the coastal environments (Short, 1999), and the term "morphodynamics" define the mutual adjustment of morphology and fluid dynamics (Wright and Thom, 1977). The aim of this research is the study, through the integrated use of several methodologies of the investigation, of the behaviour of rip currents (or cross-shore currents) on a typical Ligurian beach. The rip currents are narrow and concentrated seaward-directed currents, that extend from close to the shoreline, through the surf zone, and varying distances beyond (Castelle et al., 2016). These currents are a crucial component of the near-shore circulation (Inman and Brush, 1973; MacMahan et al., 2005; Aagaard and Masselink, 1999), involving a water interchange between near-shore and offshore area. The Levanto bay, on the eastern Ligurian coast, was chosen as the study area. This stretch of coast shows the characteristic features of the Ligurian beaches (embayed beach, the presence of coastal structures, high anthropic pressure). The research activity was focused on individuation, observation and evaluation of the rip currents along the Levanto beach. Furthermore, an investigation of possible sea-level change effects on the rips' behaviour was also performed. The developed approach has been based on the integration of several methodologies of investigation; in details, we used direct methods (field sampling, coastal video-monitoring) and indirect methods (coastal modelling, GIS analysis). The use of several techniques allowed compensation among the weaknesses of single methodologies. The XBeach model (Roelvink et al., 2009) application represents a research key component

and its application, calibration and validation on a Mediterranean study case is a further purpose of this research. The obtained results represent a firm basis for the future rip currents researches in the Mediterranean environment and reliable support for authorities and administrators involved in the coastal areas management.

Chapter 2

Coastal Dynamics

2.1 Beach morphodynamics

Coastal areas are among the most dynamic and energetic environments on earth, and coastal morphology is shaped mainly by the action of waves and currents (Dronkers, 2005). The several processes that play a role on coastal dynamics (e.g. waves, currents, tides and sediment transport) are not dependent only on external forces, but they are also conditioned by the local topography and composition of the seabed (Dronkers, 2005). The interdependence between water motion and bottom morphology is a crucial factor of coastal processes, and this aspect is commonly summarised with the term "morphodynamics". The term morphodynamics was introduced into the coastal literature by Wright and Thom (1977). They define it as a mutual adjustment of topography and fluid dynamics involving sediment transport. This definition implies that the topography of the beach will adjust to accommodate the fluid motions produced by waves, tides and currents, which in turn will influence the wave and tide processes (Short, 1999). According to Cowell and Thom (1994), the essential properties of coastal morphodynamics processes are the

feedback loops between topography and fluid dynamics, which drive sediment transport producing morphological change. Short (1999) highlights this reaffirming that: "beach morphodynamics therefore involve the mutual interaction of waves (tides, currents) with the beach topography, such that the wave processes modify the topography, which in turn will modify the waves and so on". This small literature collection focuses attention to the dynamic nature of coastal systems and (in details) beach environments. Among the recurring cited terms we find "waves" and "currents" that represent two of the most important forces on coastal processes. It is also worth highlighting that the tides have an essential role in beach morphodynamics, but their importance is not equivalent in all the environments. For example, in enclosed basins (such as the Mediterranean Sea) the role of tides is limited than in the oceanic environments.

2.2   Embayed beaches

It is generally accepted that about half of the world's coastline features typical beach morphology in the presence of hard rock headlands (Short and Masselink, 1999). The rocky headlands are independent of the formative beach processes and which in fact can have a major influence on beach development (Short and Masselink, 1999). A typical characteristic of embayed beaches is a mountainous coastal topography, where we can find beaches (more or less extended) nestled along the rocky coasts. The length of these beaches is dependent on the topography of pre-existing bedrock. However, embayed beaches are not only shaped by natural features (e.g. headlands), but they can also be shaped by anthropic structures. Structurally embayed beaches are more common adjacent to coastal structures as groynes, walls and breakwaters (Short

and Masselink, 1999). In literature, we can find a plethora of terms, including zeta bays, crenulate shaped bays, spiral beaches, curved beaches, hooked beaches, headland bay beaches (Yasso, 1965; Schwartz, 1982; Short, 1991, 1996; Finkl, 2004), which are used as synonyms, although they are sometimes described as specific morphologies. However, the term "pocket beach" is widely accepted in international literature to define the embayed beach morphology. Headlands and structures more condition the hydrodynamics of these beaches and, if they jut out enough, the sedimentary exchange with adjacent sectors are very limited or absent (Simeoni et al., 2012). Development of pocket (or embayed) beaches is strictly related to incident waves; in fact, Davies (1958) concluded that "the orientation and planform of embayed beaches are controlled by the refraction pattern associated with the prevailing (swell) waves". Subsequently, Rea and Komar (1975) and LeBlond (1979) confirmed, through numerical models, the importance of refraction and diffraction phenomena. As regards to the hydrodynamic pattern on these beaches, longshore currents may be present, driven by the alongshore gradient in the wave height (O'Rourke and LeBlond, 1972). However, a key role was also played by the cross-shore currents. The study of Martens et al. (1999) highlighted the role of breaking wave height (H_b) and shoreline length (S_1) on the hydrodynamic pattern. Martens et al. (1999) observed that when a wave height increases and a shoreline length decreases, a critical threshold is reached where the wave-dominated beach model is strongly modified. On beaches with widely spaced headlands or structures we find a transitional circulation, with cross-shore currents around headlands (or structures) and longshore currents in the central sector of the beach. When wave height increases and (or) the headlands (or structures) are close together, the transitional circulation turns into cellular circulation, with effect on beach topography. In extreme conditions, with wave height exceed-

ing a few metres, large scale, topographically controlled rip systems, called megarips, prevail (Short, 1985). The degree of headland impact on circulation pattern can be predicted using the non-dimensional embayment scaling parameter δ' (Short and Masselink, 1999). Based on the value we can define the circulation type:

- δ' > 19 normal beach circulation,

- δ'= 8 -19 transitional circulation,

- δ' < 8 cellular beach circulation.

The parameters which describe the morphodynamics of embayed beaches, and in particular the embayment degree (Silvester et al., 1994; Short and Masselink, 1999), are variable on time and they are controlled by feedback processes. Beaches characterised by an increasing trend will be more exposed to swell events and may be subject to erosion events. Conversely, beaches characterised by a shoreline retreating will be more protected (by storm events), and consequently more stable.

2.3   The surf zone currents

The surf zone is that area located between the zone of wave shoaling and the swash zone, where the incident waves break, and breaking-induced processes dominate the fluid motion, and thus sediment transport processes (Aagaard and Masselink, 1999). According to Aagaard and Masselink (1999), "The surf zone is characterised by a complex mixture of wave and current motions operating over a range of frequencies. These motions are related to the breaking of incident waves and consist of high-frequency turbulence, incident, infragravity and far-infragravity wave motion, and mean currents". In international

literature, we can find several studies on the surf zone dynamics and the wave-current interaction processes. (Grant and Madsen, 1979; Grant et al., 1984; Signell et al., 1990; Soulsby et al., 1993). Wave-current interaction represents an essential factor for the surf zone dynamics and coastal environments in general. Surf zone currents are defined as currents generated by wave action in (or near) the breaker zone (Shepard and Inman, 1951), and historically we know three types of currents: (1) bed return currents (undertow), (2) rip currents, (3) longshore currents (Aagaard and Masselink, 1999). Rip currents and bed return currents are directed perpendicular to the beach (on seaward direction), while longshore currents are parallel to the shore. These currents are fundamentals for the beach morphodynamics feed-back processes.

2.3.1 Rip currents

The "rip current" term was coined by Shepard (1936) to distinguish these currents from "undertow" (or bed return currents) and "rip tides". These terms were commonly used in literature and public vernacular (Davis, 1925), but they were often misleading and incorrect (Brander and MacMahan, 2011). The term "undertow" (or bed return currents) described an offshore-directed flow near the bed and has been recognised for some time (Johnson, 1919; Evans, 1938; Bagnold, 1940). Nowadays this term remains in use between the coastal scientists, but describe a laterally homogeneous current that flows offshore near seabeds at a lower velocity than rip currents (Faria et al., 2000; Aagaard and Vinther, 2008). "Rip tide" is an incorrect term because rip currents are not tides, and tidal rips are different currents associated with tidal inlet during an ebbing tide (Brander and MacMahan, 2011). The first studies that described the rip currents phenomena came from the Scripps Institution of Oceanography at La Jolla, California (Shepard et al., 1941; Shepard and In-

man, 1950; Inman and Quinn, 1951), and the foundations of our conventional understanding of rip current systems effectively originated from these studies (Brander and MacMahan, 2011). Rip currents are now identified as "narrow and concentrated seaward-directed flows that extend from close to the shoreline, through the surf zone, and varying distances beyond" (Castelle et al., 2016). This definition is widely accepted by coastal scientists and also largely used by the population. This description is connected with the traditional rip currents paradigm that describes the rip currents are a key component of an idealised near-shore circulation cell (Inman and Brush, 1973; Aagaard and Masselink, 1999; MacMahan et al., 2005) involving an interchange of water between surf zone and off-shore areas. From a "physical viewpoint" the rip currents are constituted by three essential parts (Figure 2.1): (1) rip-feeder, (2) rip-neck and (3) rip-head (Aagaard and Masselink, 1999; Fuell et al., 2005).
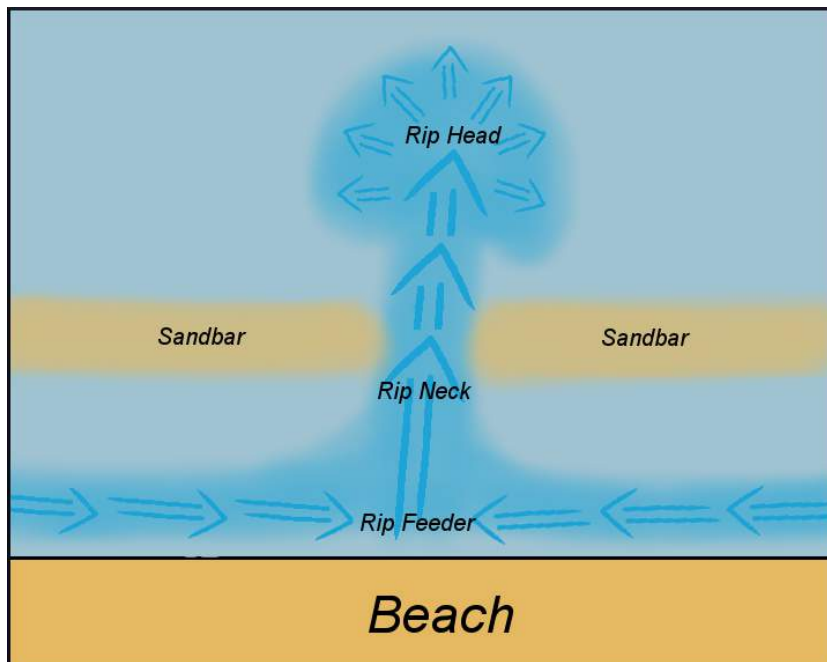

Figure 2.1: Rip current schematic structure.

The description of rip currents is often simplified by a mass balance description (Brander and MacMahan, 2011). This explanation is partially correct because the water mass balance between nearshore and off-shore areas is essential but rip currents are also driven by gradients in wave momentum, referred to as radiation stresses (Longuet-Higgins and Stewart, 1964). The relationship between the rip currents intensity and waves direction, waves height and tidal stages (Shepard et al., 1941; McKenzie, 1958; Sonu, 1972; Lushine, 1991; Drønen et al., 2002), are well-known (Nelko and Dalrymple, 2011). An increase in rip currents magnitude has been observed with more shore-normal wave incidence, increasing wave height and decreasing tide level (Nelko and Dalrymple, 2011). The off-shore development of rip currents is related to the height of incident waves (Shepard et al., 1941; Bowen, 1969). An additional force that plays a role in rip currents dynamics is the alongshore variation in wave set-up (that causes an additional driving force for alongshore currents) (Nelko and Dalrymple, 2011). In general, the alongshore currents transport water from sectors of high set-up to sectors of low set-up, where rip currents are often located (Nelko and Dalrymple, 2011). It can be said that rip currents are complex phenomena, and many possible mechanisms play a role in their genesis and development (MacMahan et al., 2006; Dalrymple et al., 2011). We can find these currents on barred beaches with rip channels (Sonu et al., 1967; Bowen, 1969; Sonu, 1972; Noda, 1974; Dalrymple and Lozano, 1978; Wright and Short, 1984; Lippmann and Holman, 1990; Chen et al., 1999), cuspidal beaches (Hino, 1974), on beaches where coastal structures, such as groynes, are present (Pattiaratchi et al., 2009; Scott et al., 2016; Castelle et al., 2016), at embayed beaches (Aagaard and Masselink, 1999; Loureiro et al., 2012), and at beaches with natural barriers such as islands and dredge holes (Mei and Liu, 1977; Pattiaratchi et al., 1987). Rip currents also occur along the coasts of en-

closed basins (seas and great lakes) (Sabet and Barani, 2011; Meadows et al., 2011; Castelle et al., 2016; Benassai et al., 2017). In general, we can affirm that local bathymetry and wave climate are critical factors for determining the type of rip currents that occur on a given beach (Nelko and Dalrymple, 2011). Castelle et al. (2016) propose a robust rip current type classification based on hydrodynamic and morphological features (Figure 2.2).
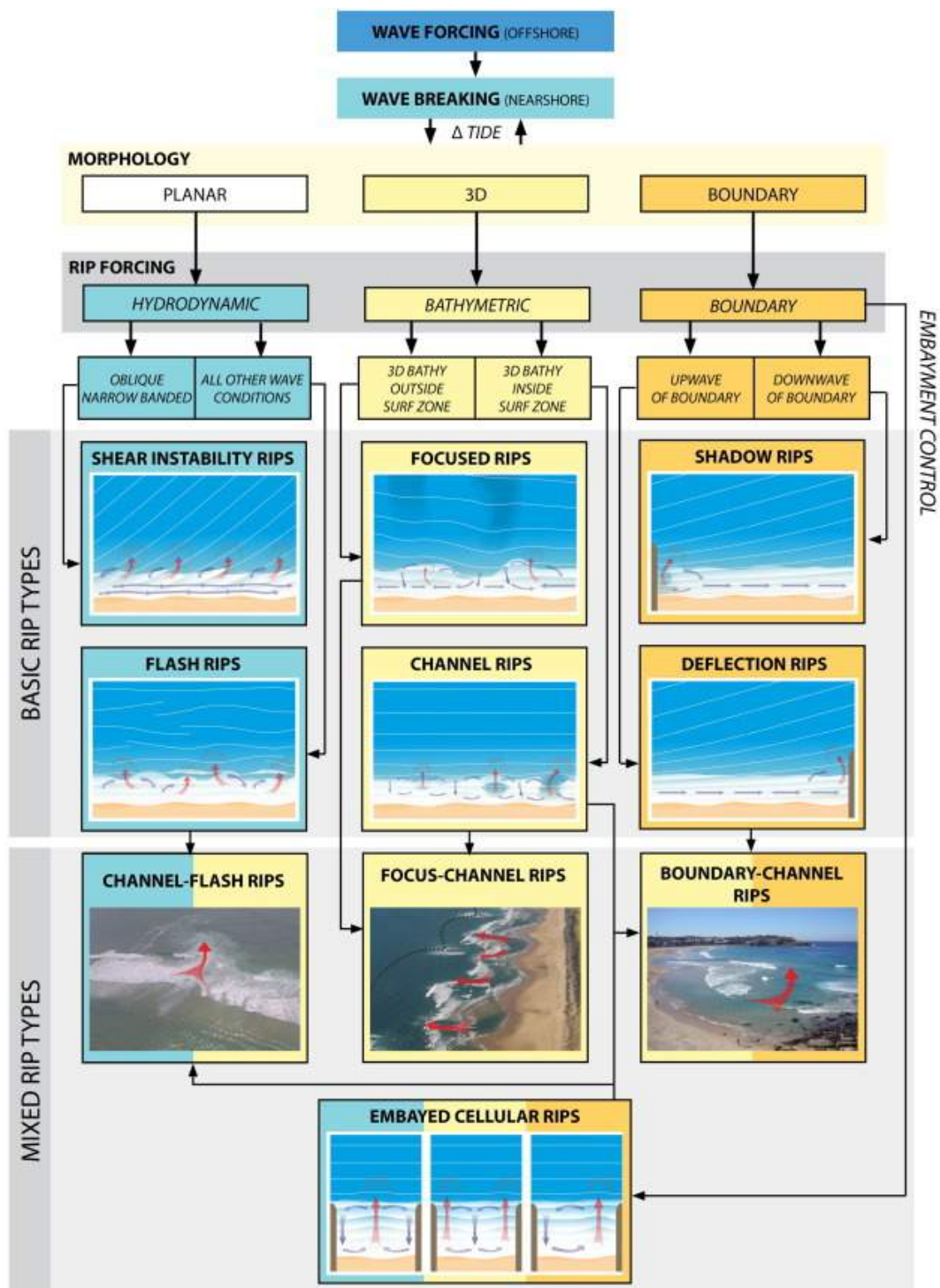
Figure 2.2: Rip current type classification (Castelle et al. 2016).

This classification provides a clear framework to understand the rip currents generation processes (and development) in the surf-zone area. According to Castelle et al. (2016) we can classify three broad categories of rip currents, based on the dominant controlling forcing. Each category is further divided into two types owing to the different physical driving mechanism. We observed six fundamentally rip current types: hydrodynamically-controlled (1) shear instability rips and (2) flash rips, which are transient in both time and space and prevalently occur on alongshore uniform beaches; bathymetrically-controlled (3) channel rips and (4) focused rips, which occur at relatively fixed locations and are related to hydrodynamic processes forced by natural alongshore variability of the morphology in both the surf zone and inner shelf zone; and boundary-controlled (5) deflection rips and (6) shadow rips, which are controlled by rigid lateral boundaries as natural headlands or anthropogenic structures (e.g. groynes and piers) (Castelle et al., 2016). Rip currents play a crucial role in coastal environments and are also important to preserve the coastal ecosystems. It is well recognised that rip currents are essential for transport, mixing and dispersion of heat, pollutants, nutrients and biological species (larval recruitment) (Talbot and Bate, 1987; Shanks et al., 2010; Sinnett and Feddersen, 2014). Furthermore, their flow (often strong and sustained) allows the transport of large volumes of sediments, particularly during storm events (Cook, 1970; Thornton et al., 2007; Loureiro et al., 2012; Castelle et al., 2015).

2.3.2   Rip current hazards

Rip current hazards are well known since recreational beach swimming became popular in early 1900 (Brander and MacMahan, 2011). Rip currents are the leading deadly hazard to recreational beach users (Brander and Scott, 2016)

and represent a severe public health issue with major personal, societal, and economic costs associated with drowning deaths, near-miss drowning, injuries, and trauma (Sherker et al., 2008). The United States Lifesaving Association (USLA) estimates that rip currents account for 80% of surf rescues and the annual number of fatalities due to rip currents exceeds 100 (Brander and MacMahan, 2011). However, other estimates vary from as low as 35 (Gensini and Ashley, 2010) up to 150 (Lushine, 1991). In Australia, 89% of more than 25000 annual surf rescues are caused by rip currents (Short and Hogan, 1994) with an estimated 40 to 50 drownings/year (Sherker et al., 2008; Surf Life Saving Australia, 2009). Other countries and regions with rip current problems include New Zealand, United Kingdom, Europe, Israel, the Middle East, South Africa, Asia, and Central and South America (da F. Klein et al., 2003; Carey and Rogers, 2005; Hartmann, 2006; Short, 2007; McCool et al., 2008; Scott et al., 2009). If we considered that an Olympic swimmer reach around 7 km/h (1.95 ms^{-1}) (Short, 1999) and rip currents can reach 2 ms^{-1} (Short, 1999), we have an idea on the rip currents hazard. Broad knowledge of the rip currents phenomena is essential to prevent rip currents accidents, and, for this reason, the role of rip current science (and scientists) is fundamental.

Chapter 3

The study case of Levanto

3.1 The eastern Ligurian coast

The Ligurian coast is characterized by fairly extensive beaches, nestled in a rocky coast with cliffs and promontories. The sea is very depth close to the coast, and it is characterized by a wide incident waves direction (more than 120 nautical degree). The eastern Ligurian coast (from Genoa to Tuscany border) shows variable geomorphological features, showing also some important effects of human activity. The Portofino promontory area can be considered as the meeting point between eastern Ligurian coast and Genoa coastline. The Portofino promontory represents the most important morphological structure along the Ligurian coast, and it is an insurmountable limit for coastal sediment transport. The stretch of coast from the Portofino promontory to rocky head of Punta Baffe is characterized by rocky cliff and pocket beaches, and subsequently is followed by a continuous depositional coast. In this sector, rocky coast preserves fairly natural features (except for the urban area of Santa Margherita Ligure and Rapallo). Between the municipalities of Chiavari and Sestri Levante, the human impact on beaches is heavy and highlighted by of
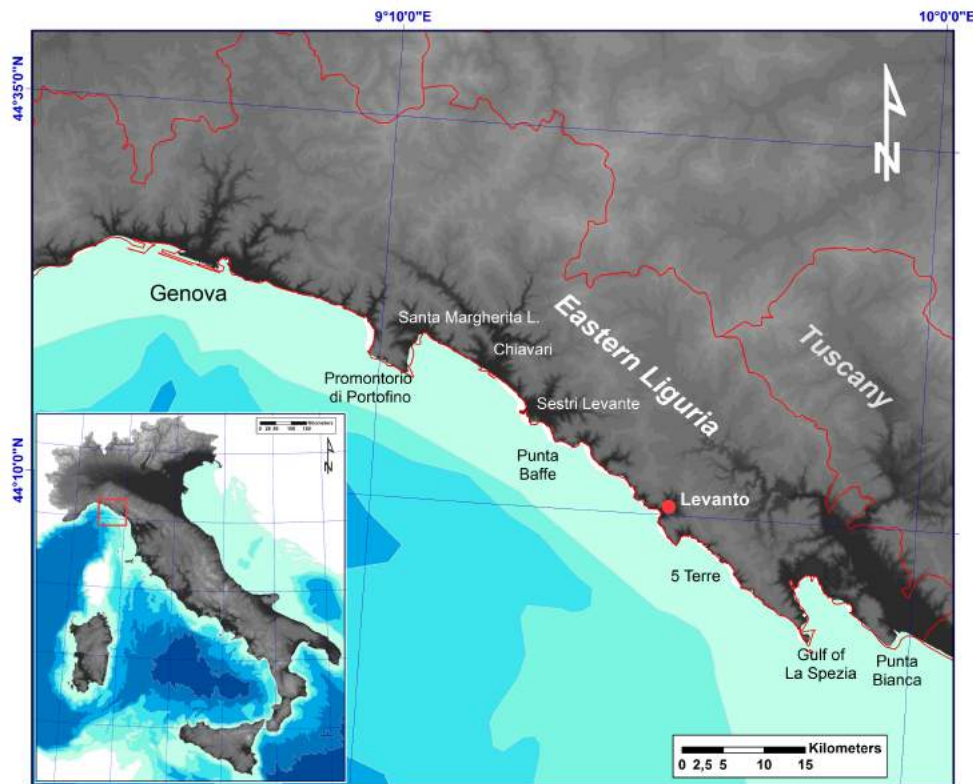
Figure 3.1: The eastern Ligurian coast: Portofino promontory (Promontorio di Portofino) is the meeting point between eastern Ligurian coast and Genoa coastline.

the presence of harbours (e.g., Chiavari, Lavagna and Sestri Levante) which play a key role in sedimentary dynamics. The eastern most coastal stretch extends from the rocky head of Punta Baffe to the Tuscany border. In this coastal section it can be observed the main morphological variability. From Punta Baffe up to Punta Bianca extensive rocky cliffs occur; subsequently, due to some important rivers as the Magra river, wide depositional coasts are present in the proximity of the Tuscany border. The area comprised between Punta Baffe and Monterosso, together with the area around the Gulf of La Spezia, is characterized by rocky coast and widespread pocket beaches. Differently, in the area of Cinque Terre, the beaches are very small, ephemerals

and unstable. This coastal sector is characterized by a quite natural coastal setting, apart from some local situations near the urban settlements and the areas of Fiumaretta and Marinella (in the extreme eastern sector), where the beaches show a severe erosive trend (Fierro et al., 2010, 2015). The our study area is located within the Levanto bay (Figure 3.2), between the eastern side of the Monte La Guardia promontory (i.e., Punta Gone) and the western side of the Punta Mesco promontory (i.e., Punta Picetto), on the stretch of coast comprised between Punta Baffe and Monterosso.
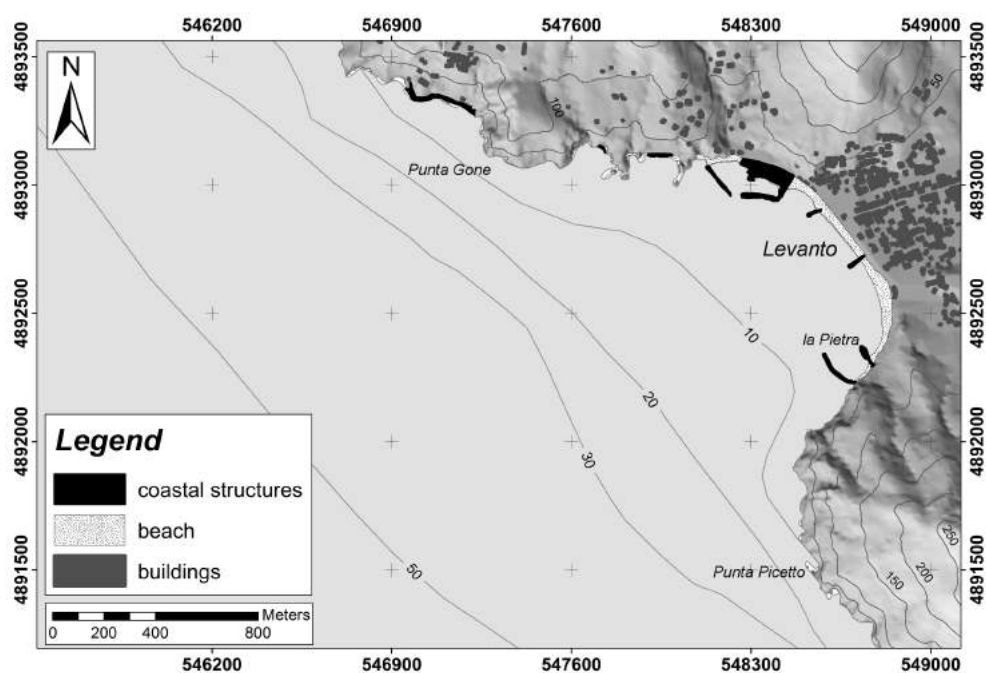

Figure 3.2: Map of the Levanto bay. Coastal structures (groynes, piers and harbours) are clear evidence of the anthropic impact along the coast.

3.2 Geological and geomorphological framework

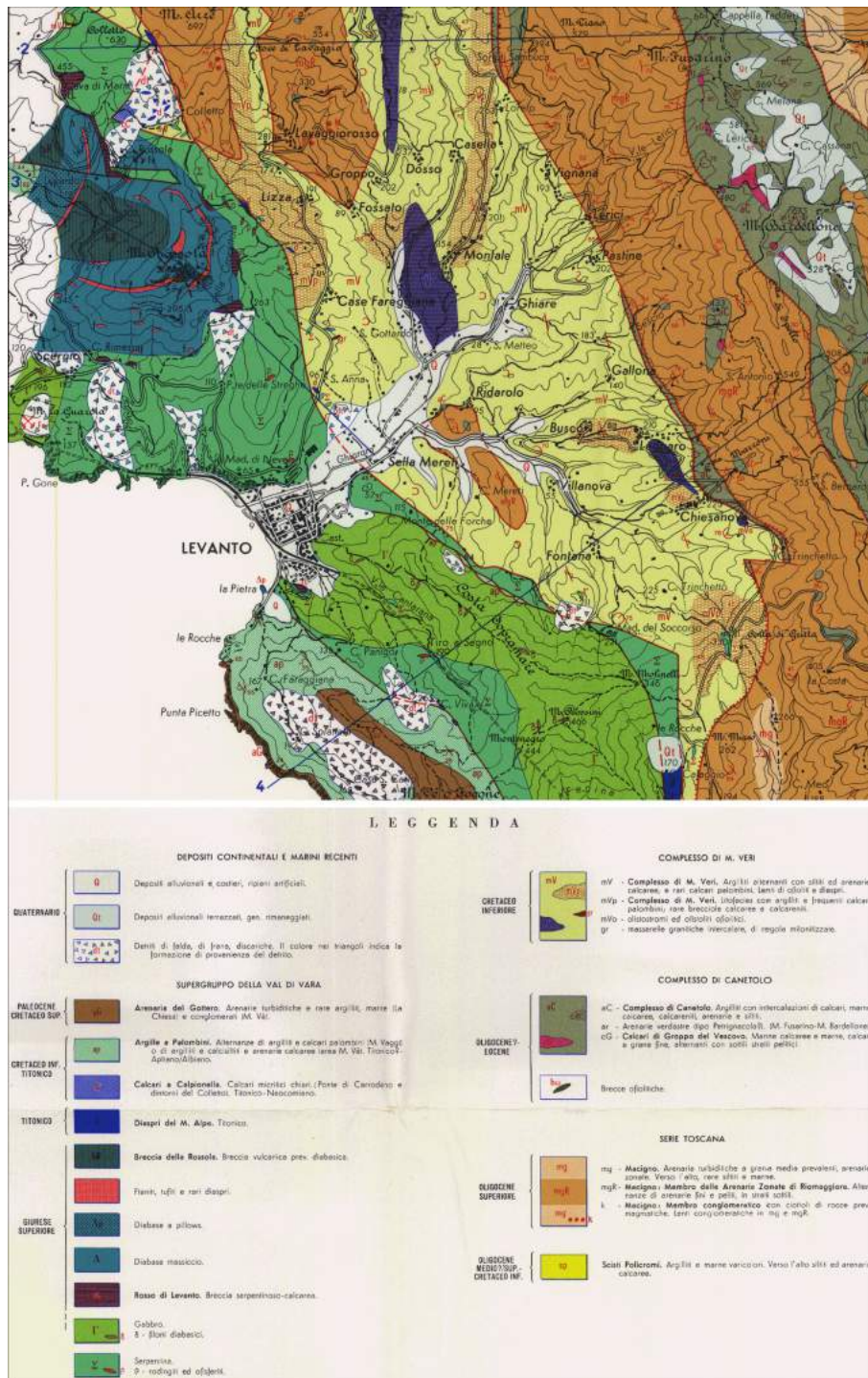### 3.2.1 Geological features

Figure 3.3: Geological map of the Levanto area (Abbate, 1969).

From a geological viewpoint the area of Levanto belongs to a segment of the northern Apennines, which is a mountain belt formed during the Tertiary by the tectonic superimposition of the Ligurid units onto the Adria plate margin. In the study area, northern Apennines show a complex geological setting characterized by rocks pertaining to the following paleogeographic domains (bottom to top)(Abbate, 1969; Abbate et al., 2005): Tuscan Domain, Sub-ligurid Domain, External Ligurid Domain, and Internal Ligurid Domain (known as the succession of the Vara Supergroup). These successions are mainly made up of sedimentary and ophiolitic sequences that were piled up during the orogenesis constituting four tectonic units, from bottom to top: the Tuscan Nappe (Tuscan Domain), Canetolo Complex (Sub-Ligurid Domain); Ottone unit (External Ligurid Domain), Bracco-Val Graveglia, Gottero and Lavagna units (Internal Ligurid Domain).

Tuscan Domain

It is a turbiditic arenaceous succession showing thickness of about 3500 m (Zaccagna, 1935; Mucchi et al., 1968). In the study area it can be only observed its upper side, represented by the Macigno Fm. (Upper Oligocene - Lower Miocene), which widely outcrops in the high sector of the Ghiararo catchment. Macigno Fm. is composed by arenaceous turbiditic layers (from thin to very thick), with medium to coarse grain size and with good gradation. Sandstones are mainly made up of quartz, feldspar, abundant lithic fragments and mica. Turbidite sandstone layers are also alternated with siltstone layers and sporadic hemipelagic claystone levels. The thickness of sandstone layers decreases moving to the top of the sedimentary sequence whereas siltstones and claystones become simultaneously more common. At the top of the sedimentary succession it can be observed the tectonic contact (thrust fault) with

rocks belonging to the Sub-Ligurid Domain.

Sub-Ligurid Domain

In the study area, the Sub-Ligurid Domain is represented by claystones with limestones and silty sandstone turbidites (Canetolo shales and limestones Fm.-Medium Eocene) and by marly limestones and calcarenitic turbidites (Groppo del Vescovo limestones Fm.- Late and medium Eocene) (Abbate et al., 2005). The former is characterized by high heterogeneity, because of it includes thin and medium layers of dark-grey/black shales, with interbedded dark-grey limestones, calcareous-marly turbidites and thin layers of siltstones. The latter is made up of calcareous and calcareous-marly turbidites, with layers about 15-30 cm thick (sometimes up to 1 m). Canetolo shales and limestones Fm. outcrops in the higher part of the Levanto basin, in proximity of the main watershed separating the Ghiararo catchment from the Vara valley. On the other hand, the Groppo del Vescovo limestones Fm. is characterized by few and small scattered outcrops .

External Ligurid Domain

The External Ligurid Domain is only represented by the Monte Veri Complex (Ottone Unit - Late Cretaceous), a highly tectonized grey-brown shales with beds and fragments of dark grey calcilutites; bodies of polygenic breccias with ophiolite, ophiolite breccia, granite, and limestones clasts are present. This complex outcrops along a wide area, mainly located in the middle sector of the Ghiararo catchment. The Monte Veri Complex is in tectonic contact (thrust fault) with the Canetolo Unit (at the bottom) and with the Gottero-Val Graveglia Unit (at the top).

Internal Ligurid Domain

The Internal Ligurid Domain includes rocks belonging to two tectonic units (from bottom to top): the Bracco-Val Graveglia Unit and the Gottero Unit. These units belong to the Vara Supergroup, which includes turbiditic formations lying on carbonatic-siliceous pelagic formations of oceanic crust environment, with basaltic flows and breccia bodies at the bottom. The succession lies on a mantle ultramafic basement and suffered intense polyphasic deformations. In the study area, the rocks belonging to the Internal Ligurid Domain mainly outcrop in the lower sectors of the Ghiararo catchment and along the coast.

Ophiolitic Basement

- Serpentinites: dark serpentinites with massive structure and with relics of tectonic structures. Fractures are generally filled by lizardite, clorite and opaque minerals (Piccardo et al., 1994). Sometimes gabbroic and basaltic dikes occur, usually affected by oceanic metamorphism.

- Gabbros: magnesian gabbros (Medium Jurassic) generally characterized by massive and isotropic structure(Cortesogno et al., 1987).

Volcano-Clastic Cover

The volcano-clastic cover is characterized by a high variability both of rock types and of thickness. The coverage is represented by massive and pillows basalts and by ophiolitic breccias of sedimentary nature (known as Breccia di Levanto).

- Basalts: they outcrop extensively in the proximity of Monte Rossola area, along the ridge between the municipalities of Levanto and Bonas-

sola. Such basalts are green-grey when fresh and light brown if weathered. Usually, such rocks lack of clear bedding structures and in some locations (e.g., eastern slope of Monte Rossola) they appear heavy fractured. Pillow-lavas are present along the southern side of Le Gronde hill. Pillows are not generally well developed, showing on average size around 50 cm, with maximum size reaching 1.5 m.

- Breccia di Levanto: the volcano-clastic succession is completed by ophiolitic-breccias, outcropping along the eastern slope of Monte Rossola. This outcrop is characterized by breccia with clasts mainly of serpentinite bonded by micro-crystalline calcite cements (Abbate, 1969). Minor components of breccia clasts are also represented by basalts, gabbros, fine sandstones, red siltstones and shalestones (radiolarites).

Sedimentary Cover

- Monte Alpe Cherts Fm.: they are red cherts with radiolarians relicts, characterized by very thin layers, alternated to finely bedded red claystones. The thickness of the succession varies from less than 10 to more than 100 m.

- Palombini Shales Fm.: the Palombini Shales Fm. outcrops along a wide area located western of Levanto urban settlement. This rock formation pertains to the Monte Gottero Unit, representing the lowest stratigraphic limit. This formation is made up of grey shales and siltstones interbedded with micritic dark grey limestones rarely with a calcarenitic base. The thickness of the formation is highly variables and can reach some hundred meters. Analysis of the paleontological content dated it to Hauterivian/Barremian (early Cretaceous) (Cobianchi et al., 1994).

- Scisti Zonati Fm.: this formation is included in so called Lavagna Group and is characterized by finely bedded siltstones, silty sandstones, shale and marls. This succession can be interpreted as the distal section of the Monte Gottero Sandstones turbiditic system. The age of the formation is Albian-Cenomanian (early Cretaceous) (Decandia and Elter, 1972) while its thickness, badly measurable due to intense tectonization, is not below 250 m.

- Monte Gottero Sandstones Fm.: it outcrops south of the Levanto urban settlement, along the rocky coast between the locality of Le Rocche and Punta Mesco promontory. They are quartz-feldspatic sandstones in medium to thick beds, alternating with shales. Near the bottom of the succession sometimes microconglomeratic or conglomeratic layers occur. The formation is attributable to late Campanian - Paleocene (Marroni and Perilli, 1990) while its thickness is from 600 to 800 m.

3.2.2   Geomorphological features

The beach of Levanto extends for about 800 meters and it is located in the central part of the Levanto Bay, which is geographically delimited by two promontories: Punta Gone to the West and Punta Picetto to the East. Therefore, it can be defined as a pocket beach (Silvester et al., 1980). The beach is divided into three sectors by two groynes: a western sector (150 m long, 35 m wide), a central sector (240 m long, 35 m wide) and an eastern sector (400 m long, 43 m wide) (Schiaffino et al., 2015). The beach is originated by the alluvial deposits of the Ghiararo Stream, which is the main stream of the area. Behind the Levanto beach there is a small alluvial coastal plain (about 2.5 km long and 700 m large). The Levanto urban settlement is mainly built on the
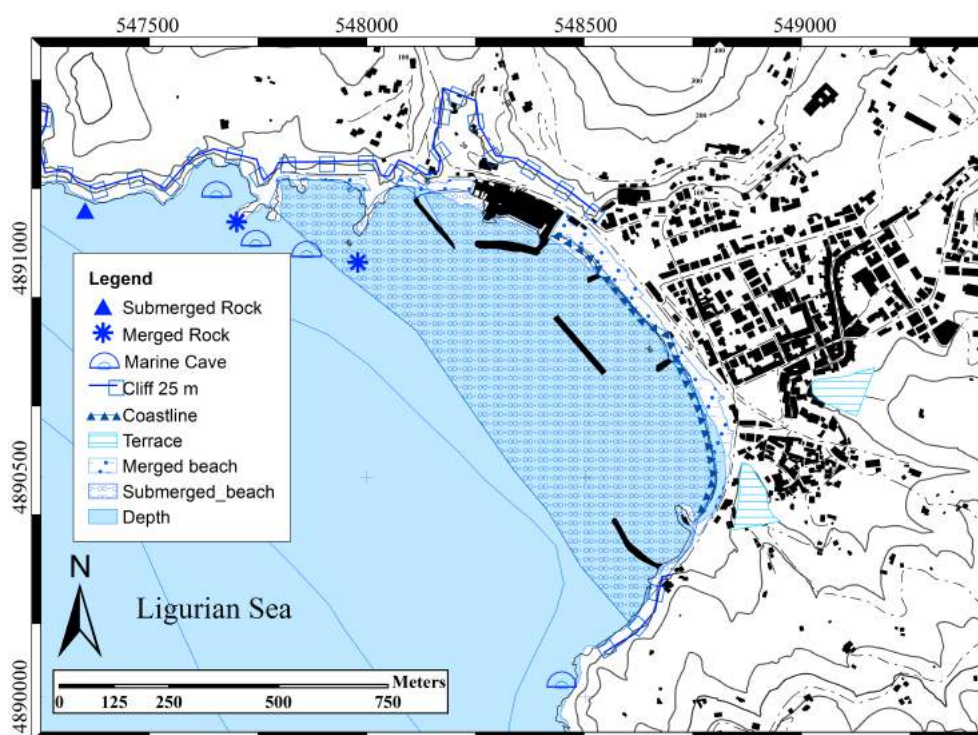
Figure 3.4: Geomorphological features of the Levanto coastal area (Mastronuzzi et al., 2017).

small Ghiararo coastal plains. The alluvial deposits of the Ghiararo Stream represents the main sedimentary input for the beach. The Ghiararo catchment has a drainage basin area of about 16.4 km^2 (Brandolini et al., 2002). In the study area, Two other minor basins are present: the Cantarana catchment(1.9 km^2) to the East and the Rio Rossola (about 1 km^2) to the West. As other Ligurian Tyrrhenian basins, the Ghiararo basin watershed is located very close to the coastline. In the north-eastern side of the basin the distance of the coastline from the watershed amount to 4 - 4.5 km, and this is the greater distance reached. The Ghiararo Stream has a maximum length of around 4.88 km, a mean slope of 9.23% while the difference between the elevation of the source and the out let is about 450 m (Brandolini et al., 2002). From West

to East, the maximum elevations of the basin are: Monte Rossola (559.5 m a.s.l.), Monte Persico (535.2 m a.s.l.), Monte Fusarino (716.2 m a.s.l.), Monte Bardellone (678 m a.s.l.), Monte Crocettola (609.2 m a.s.l.), Monte Rossini (465.8 m a.s.l.). The historical evolution of the Levanto beach is characterized by a very variable trend, characterized by alternation between erosive and increasing phases. The historical cartography of Matteo Vinzoni (1750) shows a very retreating shoreline. Up to the middle of the XIX century it can be supposed an increasing or stable trend of the Levanto Beach, although the available dataset is not exhaustive. (Fierro et al., 2015). A significant growth of the beach occurred around 1870, due to a massive discharge of anthropic deposits during the built of the railway track. Subsequently, after the end of railway works, a new erosive phase occurred, leading to a retreat up to 20 m. This erosive phase reached the peak around 1920. The erosive trend continued after the end of the Second World War. To prevent the erosive phenomena, three detached breakwaters (one of which is connected to land) were built in the western sector. These coastal structures brought to the generation of a protected sector, causing further erosion of the eastern sector. Between 1960 and 1970, due to the construction of the new motorway, large amounts of nourishment material were also available. During this phase, the Levanto Beach recorded a powerful growth (up to 50 meters) so as to in the western sector the detached breakwaters were reached by the beach increase. The structures were removed in the 70s and were converted into submerged detached breakwaters. Three groins (two in the central sector and one in the extreme eastern side) were built. As a result, the Levanto Beach reached a quite stable equilibrium (with some limited nourishments); only some, but not significant, imbalances were registered (also after the built of new harbour in the western side of the bay) (Fierro et al., 2015).

Chapter 4

Matherials and Methods

4.1 Topographic and bathymetric surveying

4.1.1 2008 LiDAR survey

LiDAR (Light Detection and Ranging) is a surveying method that measures the distance to a target by illuminating the target with pulsed laser light and measuring the reflected pulses with a sensor. The laser uses high-frequency pulses included between 10 and 150 kHz and wavelengths between 1.0 - 1.5 μm are commonly used for morphological studies (Marcoe, 2007). The obtained dataset is a point cloud where the X, Y and Z coordinates are known for each collected point. This data is valuable to realise (through post-processing process) Digital Surface Models (DSM) and Digital Terrain Models (DTM), which are handy analysis tools in several sectors of geosciences. The main feature of this survey tool is the opportunity to obtain (in a relatively short time) an accurate representation of an earth surface area. In this study, we used the LiDAR data of Levanto, provided by Regione Liguria (2008), to obtain an accurate numerical reproduction of the on-land morphology (cliffs and

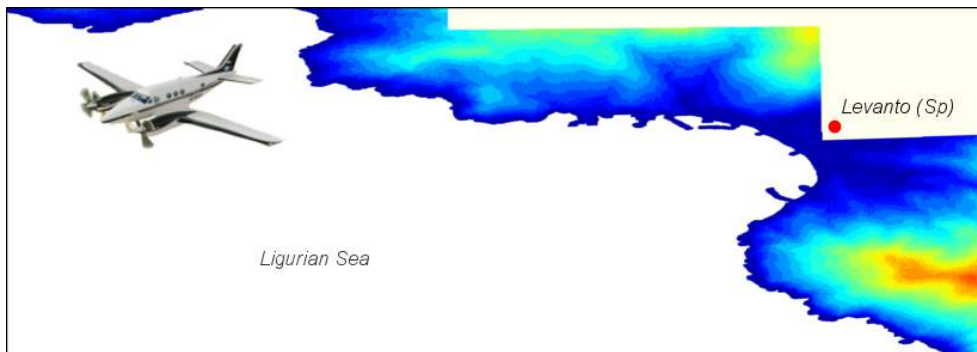headlands) and anthropic structures (seawalls, groins and breakwaters).

Figure 4.1: 2008 LiDAR survey by Regione Liguria.

4.1.2   GPS (Global Positioning System)

The Global Positioning System (commonly known as GPS) is a civilian and military radio navigation system based on a constellation composed by 24 - 32 satellites. GPS is owned by the United States government and operated by the United States Air Force. In summary, the GPS is a positioning system enables to supply the real-time (or pre-recording) position (latitude, longitude, and altitude), and the current time of any GPS receiver in any place of the world. With a GPS device is possible to define an instantaneous position, and thus it can be visualised on the GPS display (by different available coordinates systems). The GPS consists of three major segments: space segment, control segment, and user segment. Space and control segments are developed, maintained and operated by U.S. Air Force. The user segment is composed of hundreds of thousands of military users of the secure GPS Precise Positioning Service, and tens of millions of civil, commercial, and scientific users of the Standard Positioning Service. In this study, we used a GPS device for the topographic beach surveys, and, in detail, we used a GPS Trimble Pathfinder

ProXH with a post-processing correction through GNSS permanent station of Beverino (owned to Regione Liguria). The station is far about 3 km from Levanto beach, and thanks to that we can obtain an error of 0.05 and 0.10 meters on horizontal and vertical respectively. The beach surveys were performed following a predetermined transects series (Figure 4.2).
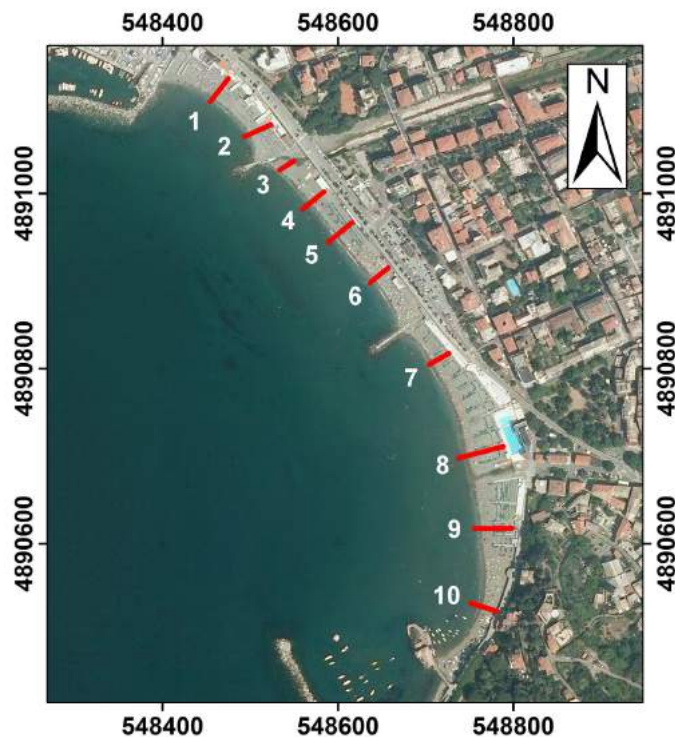

Figure 4.2: Location of the GPS survey transects on the Levanto beach.

4.1.3 Single-beam

A single-beam echo sounder is a tool for coastal bathymetric surveys, and it is generally made up of a transducer-receiver system mounted on the hull of a boat or vessel. The system shoots high-frequency acoustic pulses (30 - 200 kHz) into water column towards the bottom and measures the water depth on the vertical. The acoustic signal is reflected off the sea floor beneath the

receiver. The receiver contains a transmitter, which controls pulse length and provides electrical power at a given frequency. The continuous recording of depth below a moving boat returns a high-resolution depth measurement along the survey transects. It is essential to collect data on the possible measurement errors related to the motion of the boat (such as pitch and roll). The errors can be limited using a Motion Reference Unit (MRU) and performing surveys under flat sea conditions. Another essential information for the correct use of a single-beam echo sounder is the exact position of the collected data, obtainable through the use of Differential Global Positioning Systems (DGPS). In this study, the single-beam survey campaign was performed by means of a single-beam echo sounder (model ODOM) with an accuracy of 0.10 m, and data were collected following pre-determined survey transects (Figure 4.3). The acquired data were subsequently processed by means of GIS software.
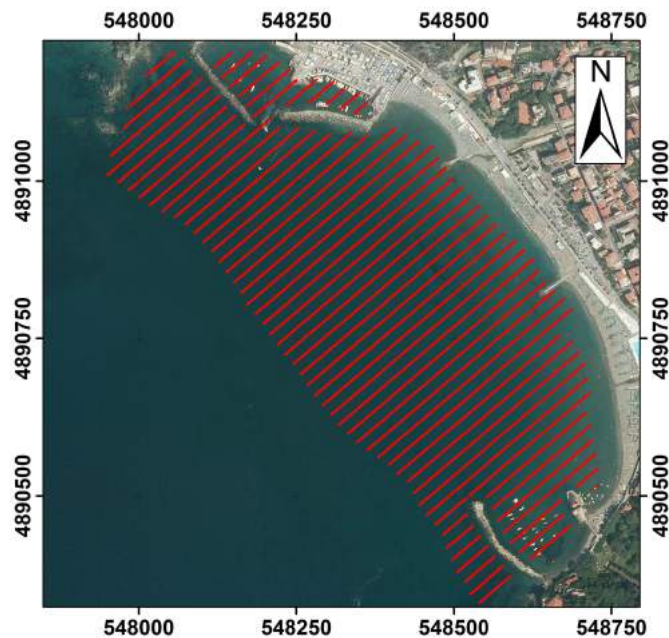

Figure 4.3: Map of the survey transects for single-beam surveys campaigns within the Levanto bay.

4.1.4 Topo-bathymetric surveys: Autumn 2016/Spring 2017

The survey methods described above (section 4.1.2 and 4.1.3) were employed to obtain two topo-bathymetric datasets. The field surveys were performed in October 2016 (before winter) and in March 2017 (after winter) (Figure 4.4) respectively. The data of emerged beach topography and bathymetries were merged and interpolated through a GIS software to obtain an accurate topo-bathymetric representation (pre/post-winter) of the area. The offshore bathymetric dataset, deeper than 12 m, was supplied by the Istituto Idrografico della Marina (2006).
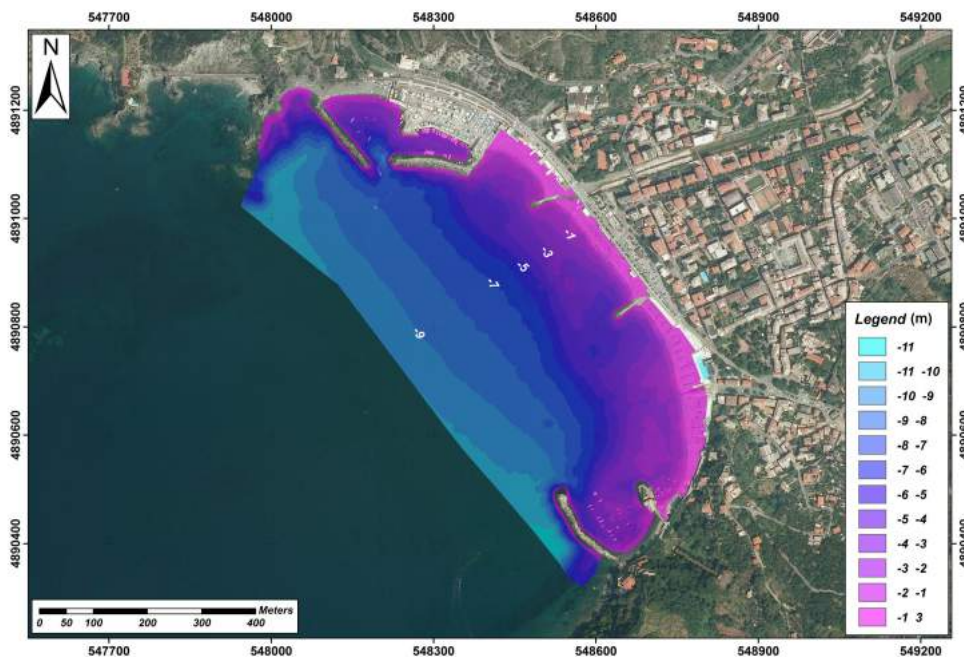

Figure 4.4: Merge and interpolation (through GIS software) of the March 2017 topo-bathymetric dataset.

4.2   Video monitoring system

4.2.1   Beach video monitoring: state of the art

The first beach video monitoring system was developed and built at the beginning of the 1990s by the laboratories of the Oregon State University. This system, known as Argus, is still among the more complete beach monitoring systems today in both of the elaboration images system and for their management. The Argus system guarantees the collection of video data at a gave spatiotemporal scale (decimetres to kilometres and hours to years) and is composed of a dedicated cameras system. The collected images are sent to a server where they are elaborated (in real-time) by a specific software to obtain four image types (Holman and Stanley, 2007): (1) Snapshot, (2) Time exposure, (3) Variance, and (4) Day-timex. Due to evolution in video monitoring technologies, several coastal monitoring systems were developed in the past (Lippmann and Holman, 1989). After the Argus system, several coastal monitoring systems have been installed all around the world (Brignone et al., 2012), and few examples are Coastal Watch, Erdman Video System, Sirena (Nieto et al., 2010), COSMOS (Taborda and Silva, 2012), CoastView project (Davidson et al., 2007), and many others. All these systems were initially based on the Argus system and some used Argus utilities and software (Brignone et al., 2012). A coastal video-monitoring system is generally composed by a fixed number of cameras (or webcams), installed on a set elevation above mean sea level, which collect real-time coastal images (snapshot images) at specified intervals. The snapshot images are often elaborated through specific software (Holman et al., 2003; Alexander and Holman, 2004; Holman and Stanley, 2007; Brignone et al., 2012) to obtain more data regarding the investigated phenomena (Zikra, 2008). According to Brignone et al. (2012) the processed images

are generally classified in:

- Time exposure images (or timex), which are obtained by digitally averaging image intensity over a prefixed acquisition time. These images are obtained by processing and superimposing snapshot images of an acquisition cycle (Brignone et al., 2012). This process eliminates random sea conditions and variability in wave run-up and swash (Salmon et al., 2007). Timex images are therefore an excellent instrument to underline submerged sand bar topography (Lippmann and Holman, 1989; Enckevort and Ruessink, 2001; Ranasinghe et al., 2006), shoreline (Alexander and Holman, 2004; Kroon et al., 2007; Quartel et al., 2006), intertidal beach profile (Plant and Holman, 1997), intertidal beach slope (Madsen and Plant, 2001), morphology formation on beach face (Holland, 1998; Almar et al., 2008), rip currents (Nelko and Dalrymple, 2011; Austin et al., 2012).

- Variance images, derived by digitally averaging image intensity over a prefixed acquisition time and a standard deviation computing on pixel colour intensity, improve the contrasts already achieved by processing timex images (Brignone et al., 2012). They allow to recognize submerged foreshore structures and to highlight regions undergoing some change during acquisition time (a surf zone is brighter than other parts) and unchanged areas (a dry beach is darker than other parts) (Brignone et al., 2012). These images, coupled with timex images, are useful as an additional tool to recognize and study of beach hydro-morphodynamics features.

- Daily time exposure images (or day-timex) are obtained by averaging all images acquired in the whole day (Brignone et al., 2012). This elabora-

tion takes off the effects of tidal variation and the intensity variation of light due to the changing angle of the sun during the day (Morris et al., 2001).

- Time-stack images are created by extracting a line of pixel along a pre-defined array in a video frame (Takewaka and Nakamura, 2001; Salmon et al., 2007; Ojeda et al., 2008; Zhang and Zhang, 2008; Kuo et al., 2009). The same set of pixels is extracted from images of a selected time period and stacked vertically to create an image with time and cross-shore distance on vertical and horizontal axis respectively. These images are useful to gain information on beach morphodynamic features, cross-shore variation, run-up, and swash (Brignone et al., 2012).

A coastal video monitoring network was already developed along the Ligurian coast as part of the ResMar project (2007-2013). Nine commercial webcams previously installed along the coast were selected to compose a coastal video monitoring network (Schiaffino et al., 2013). The images, collected and stored in the central platform, were processed using the Beachkeeper *plus* software (Brignone et al., 2012). The use of commercial webcams is a strategy to obtain a low-cost video monitoring network. The limit of this approach is that the webcams functioning is related to the commercial activities (that mounted the webcams), and proper maintenance is not always guaranteed. Today, thanks to the evolution in video monitoring technologies, the costs to buy and maintain a video monitoring system are low compared to a few years ago. For this reason, a dedicated video monitoring system for coastal research is often a better solution.

4.2.2 Video monitoring system on Levanto Beach

A coastal video monitoring system has been installed on Levanto beach by the local municipality (municipality of Levanto), and it is managed by DISTAV (University of Genova) coastal research group. The monitoring system is composed of three cameras facing three different sectors of the beach (western, central and eastern, depicted in section 3.2.2), installed at an elevation of 25 m above mean sea level. The cameras system have a resolution of 1920×1088 pixels, and the beach sectors captured by each camera are shown in Figure 4.5. A recording device with 2 TB of storage capacity completes the monitoring system. Time recorder and temporal resolution setting are dependent on research purpose. In this case, we set 8 hours/day recorded at 1 second of temporal resolution. This setting is a standard setup for a coastal video monitoring system (Pearre and Puleo, 2009; Archetti and Zanuttigh, 2010; Harley et al., 2011; Taborda and Silva, 2012; Murray et al., 2013).
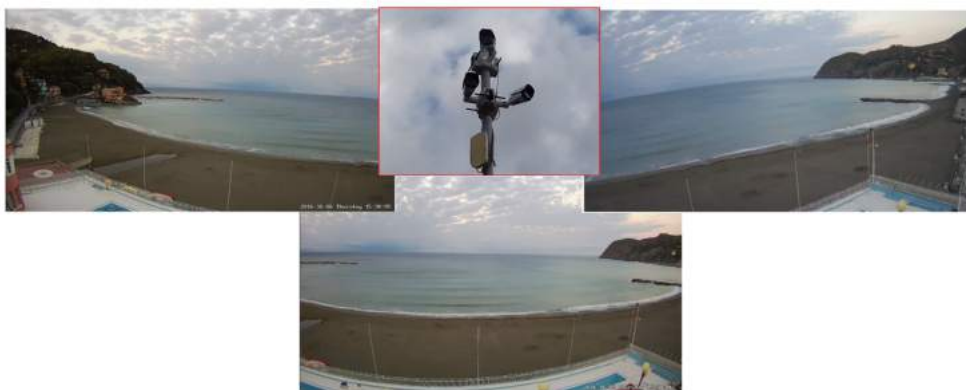

Figure 4.5: The video monitoring system on Levanto beach.

4.2.3 Beach survey for video monitoring

Simultaneously to topo-bathymetric surveys (described in previous sections), we collected the Ground Control Points (GCPs) needed for the geo-rectify pro-

cess and subsequent image processing (Figure 4.6) (Holman et al., 2003; Silva et al., 2009; Vousdoukas et al., 2011; Brignone et al., 2012). The recorded images have been geo-rectified using 27 GCPs, placed in the view area of the cameras. The XY coordinates of the GCPs were acquired using a GPS device with a horizontal and vertical accuracy of 0.05 m and 0.10 m respectively (described in section 4.1.2). The GCPs were selected so that they were visible by cameras, and, for this purpose, we used targets (yellow cones) easily identified in video recorded images. For a better geo-rectified process these targets were located so that they formed a series of triangles to cover the investigated area (Figure 4.6).

Figure 4.6: Example of Ground Control Points (GCPs) triangulation along the eastern sector of the beach.

4.2.4   Image processing

A digital image is a numerical representation (usually binary) of a 2D image. These images are defined as discrete images because they are composed of a

finite number of elements (pixels). An RGB image is coded by means of three primary colour bands (R-red, G-green, B-blue). For example, a digital image a[m, n, i] will be composed by m×n pixels, where m-pixels and n-pixels are pixels along vertical and horizontal axes respectively, whereas "i" is the colour code (red, green or blue). A digital image at 1920×1088 pixels will be composed by 1920 vertical pixels and 1088 horizontal pixels respectively, and each pixel will be characterized by a colour (resulted by superimposition of the primary colour bands). From a mathematical viewpoint, the digital images are matrices, where each pixel is defined by a couple of coordinates (u,v). In our case, a perspective view of littoral was obtained by means of a video monitoring system. The distortion effects, caused by camera location, were deleted through a series of mathematical processes. By means of external orienting parameters, we obtain the camera position in the real space and the geometric relation between image coordinates (u,v) and spatial coordinate (x,y,z) (Figure 4.7). The external geometry of a camera system is defined by three parameters (angular values): azimuth (φ), tilt (τ) and roll (σ) (Figure 4.7).

The relation between image coordinates system and spatial coordinates system is defined by the following equations:

$$u = \frac{L_1 x L_2 y L_3 z L_4}{L_9 x L_{10} y L_{11} z_1}$$

$$v = \frac{L_5 x L_6 y L_7 z L_8}{L_9 x L_{10} y L_{11} z_1}$$

where L1 - L11 are known as Direct Linear Transformation (DLT) coeffi-

cients (Adbel-Aziz, 1971) and they are functions of seven unknowns: φ, τ, σ, [Xc, Yc, Zc] (camera system location) and f (real focal):

$$L = -(x_c m_{31} + y_c m_{32} + z_c m_{33}) \qquad L_6 = \frac{v_0 m_{32} + f m_{22}}{\lambda_v L}$$

$$L_1 = \frac{u_0 m_{31} + f m_{11}}{\lambda_u L} \qquad L_7 = \frac{v_0 m_{33} + f m_{23}}{\lambda_v L}$$

$$L_2 = \frac{u_0 m_{32} + f m_{12}}{\lambda_u L} \qquad L_8 = -(L_8 x_c + L_9 y_c + L_{10} z_c)$$

$$L_3 = \frac{u_0 m_{33} + f m_{13}}{\lambda_u L} \qquad L_9 = \frac{m_{31}}{L}$$

$$L_4 = -(L_1 x_c + L_2 y_c + L_3 z_c) \qquad L_{10} = \frac{m_{32}}{L}$$

$$L_5 = \frac{v_0 m_{31} + f m_{21}}{\lambda_v L} \qquad L_{11} = \frac{m_{33}}{L}$$

where m-coefficients describe the rotation of the camera system in relation to azimuth (φ), tilt (τ) and roll (σ):

$$m_{11} = \cos\phi\cos\sigma + \sin\phi\cos\tau\sin\sigma \qquad m_{23} = \sin\tau\cos\sigma$$

$$m_{12} = -\sin\phi\cos\sigma + \cos\phi\cos\tau\sin\sigma \qquad m_{31} = \sin\phi\sin\tau$$

$$m_{13} = \sin\tau\sin\sigma \qquad m_{32} = \cos\phi\sin\tau$$

$$m_{21} = -\cos\phi\sin\sigma + \sin\phi\cos\tau\cos\sigma \qquad m_{33} = -\cos\tau$$

$$m_{22} = \sin\phi\sin\sigma + \cos\phi\cos\tau\cos\sigma$$

The unknowns can be calculated using a series of control points (GCPs) within the images (as described in section 4.2.3). Image coordinates (u,v) and

spatial coordinates (x,y,z) must be known for at least three GCPs. Finally, having eliminated the distortion effects, the images can be processed through a specific software for pictures analysis. In our case, we used the Beachkeeper *plus* software (Brignone et al., 2012) to obtain Timex and Variance images (described in section 4.2.1) of the study area. Beachkeeper *plus* is a tool specifically developed for coastal video monitoring.
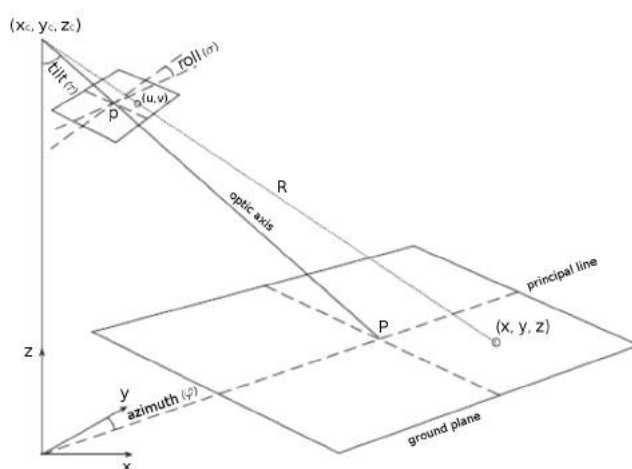

Figure 4.7: Relation between image coordinates (u,v) and real spatial coordinates (x,y,z) (Parlagreco, 2011).

4.3 Sedimentological analysis

The sedimentological characterisation of the area (useful for a better representation of boundary conditions in the modelling process) was obtained through a sedimentological sampling campaign. Sediment samples were collected using a Van Veen Grab Sampler (for the underwater beach) and hand coring (for the on-land beach). The samples were collected based on a pre-constituted sampling grid. The grain size analyses were performed in the sedimentology laboratory through dry sifting at 1/2 phi intervals (Wentworth, 1922), and

statistical parameters were computed following Folk and Ward (1957). The grain size distribution ranges from 0.17 mm to 5.15 mm (2.6 to -2.4 ϕ), and, because of that, Levanto beach can be classified as mixed sand-gravel beach (Jennings and Shulmeister, 2002).
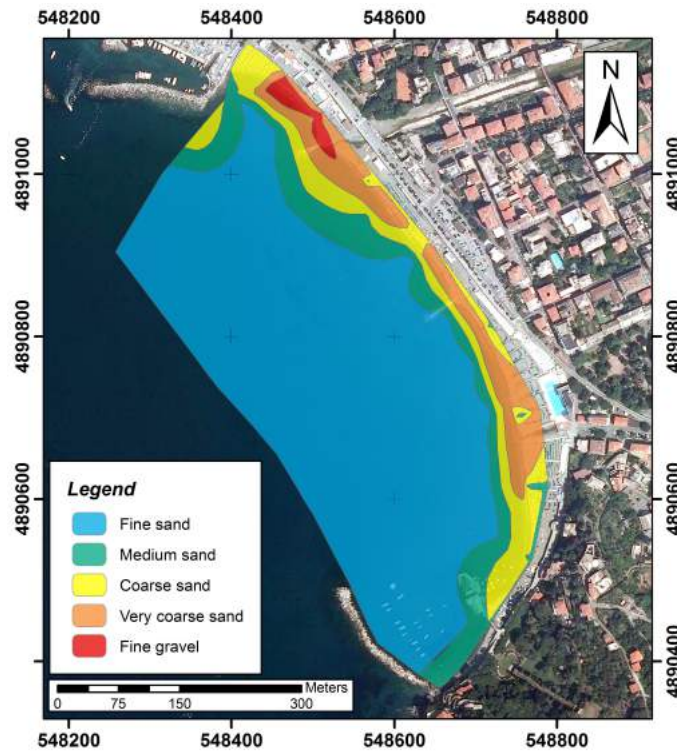

Figure 4.8: Map of the grain size distribution along the Levanto beach.

4.4   Drifter survey

The standard approaches for currents' velocity assessment can be categorised as either Eulerian or Lagrangian techniques (Peynaud and Pijanowski, 1979). The Eulerian approach is characterised by the use of instruments (current meter) located in fixed points. Differently, in the Lagrangian approach, currents' velocity is measured by using tools (drifters) that are in motion with the water

mass.

4.4.1 The lagrangian drifters

A drifter is an oceanographic tool that floats on the ocean surface to investigate ocean currents. The modern drifters are often equipped with a GPS/GNSS receiver for satellite tracking, and they can sample parameters as temperature and salinity (Paduan and Niiler, 1993; Poulain and Zambianchi, 2007; Charria et al., 2013). Following components schematically compose a drifter:

- A sail, which has a "propulsive role", it can be rigid or soft and its main function is that the drifter is in motion with the water mass;

- A float structure, which maintains the drifter on the water surface (and immediately below);

- A GPS/GNSS receiver for satellite tracking;

- A submerged hull, which contains a battery and other electronics devices;

- Sensors for environmental parameters (e.g. temperature and salinity).

On the market, we can find drifters designed for both offshore experiments and coastal experiments. Offshore drifters have a data acquisition time range of hours, days or months, and they are suitable for large scale survey (e.g. ocean circulation). These tools often show a measurement accuracy of hundreds or thousands of meters. Conversely, the coastal drifters show a measurement accuracy of meters (sometimes centimetres), and they have a data collection interval of seconds or minutes. In this project, we used a "homemade Lagrangian drifters system" to obtain field measurements of the surf zone currents. The use of Lagrangian drifters for surf zone currents investigation is a well-known practice in coastal research (Johnson and Pattiaratchi,

2004; MacMahan et al., 2009; Austin et al., 2010, 2012; McCarroll et al., 2014).
However, field measurements of strong and unpredictable currents, such as rip
currents, are logistically difficult to obtain related to their particular hydrody-
namics features (described in section 2.3).

4.4.2   Home-made drifters

As a first attempt, we tested a commercial drifter model and, in details, the
Mini Drifter buoy MD03, produced by Albatros Marine Technologies. This tool
showed a real data acquisition time included between one and five minutes,
related to satellite coverage. Due to its technical features, this instrument has
proved to be unsuitable for the surf zone currents investigation, because the
data recorded were too many averaged on time. Furthermore, the particular
orography of the study area (with mountains close to the coast) is a problem,
due to the effect on daily satellite coverage. Starting with the problem to find
a suitable drifter model, we decided to implement a dedicated "drifter system"
for this thesis work. The purpose was to develop a low-cost drifters system,
coupled with the video monitoring system. Yoon et al. (2014) illustrates a
method to describe the rip currents through the images analysis. In that
case, the analysis was conducted through the tracking of floating tubes in the
video images, converting the image coordinate system into the standard map
coordinate system, and evaluating the Lagrangian velocities. (Yoon et al.,
2014). As a first step, we built some drifters prototypes to define the better
design. The target was to obtain a floating device that it was visible in the
video images. After some field test, we chose the design showed in Figure
4.9. The obtained result is a tool visible by the video monitoring system, and
suitable to follow the water mass in the surf zone. An important feature is a low
susceptibility to the wind (which often blow on the study area). Each drifter is

composed of materials that cost approximately 10 euros (wood, plastic, floating material, steel wire, paint).

Figure 4.9: Design of the home-made drifters for the nearshore currents investigation.
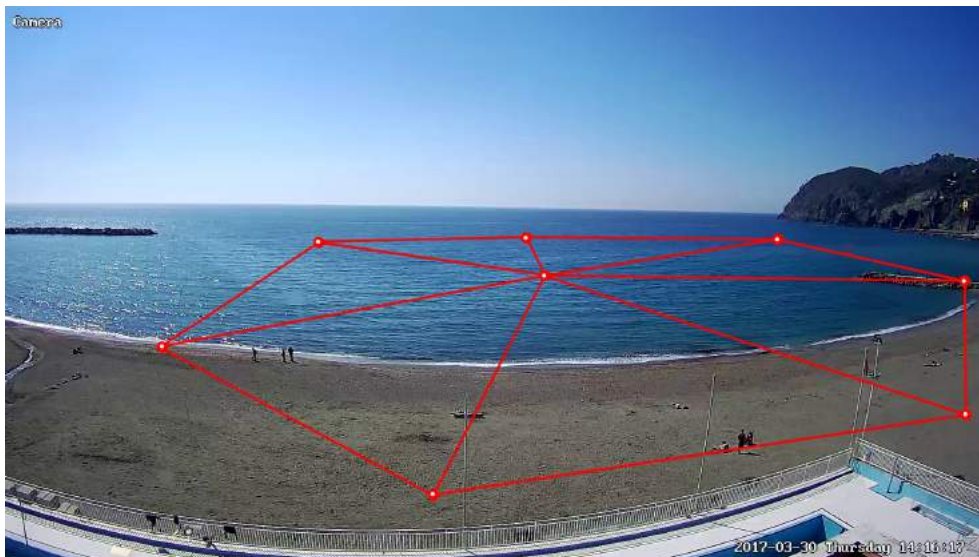

Figure 4.10: Ground Control Points (GCPs) and their triangulation in the surfzone.

As a second step, we collected a set of GCPs in the surf zone (Figure 4.10). The survey campaign was performed by a GPS Trimble Pathfinder ProXH (described in section 4.1.2) mounted on a small boat and under flat sea conditions. The geo-rectify process (as described in section 4.2.3) was only performed for the central camera, which shows better orientation features. The obtained method is a video-drifters coupled system, which allows tracking (XY coordinates and time) of the drifter locations. The subsequently drifters locations are imported in GIS software, where Lagrangian velocities can be computed through an easy equation of velocity. The spatial drifters' location is affected by a maximum error of some ten of centimetres.

4.5 Coastal modelling

4.5.1 The models: state of the art

The models can be defined as a formalised representation of reality (Roelvink, 2011). Represented phenomena are often very complex, and simplification processes are necessary to obtain reliable models, suitable for real technical applications. An overly complicated model (which take into account an excessive number of variables) will show an excessive computing time, and the real model applicability will be compromised. However, the lack of data is one of the significant problems for the models' users, and this is particularly relevant when complex phenomena, with complex boundary conditions, are modelled. In this regard, coastal dynamics is a clear example of very complex phenomena influenced by several boundary factors. The models can be classified into two macro-categories: (1) physical models, and (2) mathematical models. The physical models are scale representations of investigated phenomena (e.g. a physical scale representation of a port basin). The mathematical models

are mathematical representations, where the several parameters and variables (that caused phenomena) are linked through equations (more or less complicated). Mathematical models can be furthermore classified into physics-based models and conceptual models. The physics-based models are based on a detailed physical description of phenomena and process that play a role in them. They are commonly expressed through differential equations which describe the physics phenomena (e.g. equations of motion, etc.). In the conceptual models, we do not find a detailed physical description, but they are expressed by equations that describe only the interaction among considered parameters. It can be maintained that (in general) a more complex model is not always better, but the reliability and usefulness of a model is dependent by available dataset, computing time, costs, and required results. However, the classification between conceptual models and physics-based models is not always clear, and the physics-based models are often integrated by conceptual models to solve problems of lack of data, or to simplification needs. The models can also be classified in deterministic models and stochastic models. Clear cause-effect relationships characterise deterministic models, and the implemented input (dataset) lead to a univocal solution. A statistical approach conversely characterises stochastic models, and phenomena are described through a series of aleatory variables and their probability distributions. These models do not show univocal solutions, but they produce a series of scenarios that they will be assessed by statistical analysis. Based on their spatial representation features, the models can also be classified into four class:

- Zero-dimensional models,

- One-dimensional models (1D),

- Two-dimensional models (2D),

- Three-dimensional models (3D).

The zero-dimensional models describe a physics phenomena on the space. The description is expressed in terms of average values, or through hypothesis that makes homogenous the interested physical quantities. The classification between one-dimensional models and two-dimensional models concerns the only formal characteristics of the dimensional representation. Two-dimensional models are not only suitable to describe plan motions, but they can be suitable to represent a not uniform distribution of a variable (e.g. the not uniform distribution of a water surface levels in a coastal basin with irregular bathymetry). In general, the zero-dimensional models are described as "lumped parameter models", whereas the 1D, 2D, and 3D models are known as "distributed parameter models". The analytic solutions are feasible for physics-based models in the only cases characterised by low geometric complexity degree. This operative limit is exceeded thanks to numerical methods to solve the complex equations. In the case of a continuous system, the numerical methods are based on their discretised representation (referred to a computational grid). The numerical methods supply approximated solutions through numerical values. These solutions are referred to the initial conditions provided (model input), they are located in a discrete set of points in the computational grid, and (in case of phenomena which evolved on time) in a finite number of the time step. The terms "numerical model" (commonly used) is referred to as the coupling between mathematical models and numerical methods to solve equations that characterise them. The numerical methods are generally implemented in a calculation code (written through a programming language), and the numerical model is provided in a software format. The numerical models can be suitable tools for engineering and environmental design, and their costs are (generally) lower if compared with physical models. However, it is always important to

remember that the numerical models cannot remedy possible lack of data or lack in knowledge of physics phenomena. For these reasons, a critical analysis of results is always necessary to obtain reliable results.

4.5.2 The coastal models

A coastal model (software format) is a numerical model that contains ideas about hydraulics, waves, sediment transport, and sediment conservation that are captured in formulations (Roelvink, 2011). Three types of models are traditionally considered: (1) coastal profile models, where the focus is on cross-shore processes, and the longshore variability is neglected (Roelvink and Brøker, 1993; Schoonees and Theron, 1995), (2) coastline models, where the cross-shore profiles are assumed to retain their shape even the coast advances or retreats (Szmytkiewicz et al., 2000), (3) coastal area models, where variations in both horizontal dimensions are resolved (de Vriend° et al., 1993; Nicholson et al., 1997). Coastal profile models are generally applied for two main purposes: evaluation of storm impacts on a coastal profile, and evaluation of longer-term behaviour of sandbars and nourishment schemes (on the beach and the shoreface) (Roelvink, 2011). Coastline models assume gradually varying flow conditions and approximately parallel depth contours (Roelvink, 2011). These models are mainly applied for large-scale applications, over alongshore distances of many kilometres (Dean, 1992; Szmytkiewicz et al., 2000; Buijsman et al., 2001). However, these models can be coupled with 2D wave models to predict nearshore wave climates and, thanks to that, they can be applied at relatively small-scale phenomena (Roelvink, 2011). Coastal area models are applied where a separation between longshore and cross-shore scales is not possible, and they are applicable at a range of scales, from small-scale coastal engineering problems to macro-scale evolution of tidal basins (Roelvink, 2011).

In this thesis, we applied the XBeach model (Roelvink et al., 2009), which is a coastal area model. For this reason, we will bring our attention to this type of models. These models are further subdivided into two-dimensional horizontal (2DH) models, which use depth-averaged equations (Roelvink, 2011), and three-dimensional (3D) models (Lesser et al., 2004), which resolve the vertical variations in flow and transport (Roelvink, 2011). In general, when we are talking about the difference between 2DH, Q3D (Quasi-3D), and 3D, we are talking about the flow model, the sediment transport model, and the bed update model. The wave models are generally 2DH models based on the spectral wave action balance (Roelvink, 2011). The models can be classified by their wave drivers into wave-averaged models, which consider wave field averaged over both individual waves and wave groups, and into short-wave (but not wave group) averaged models, which resolve variations at wave group time scale (Roelvink, 2011). Models as Delft3D and XBeach have both these modules. The flow models (2DH) are based on the depth-averaged shallow water equations, and this feature often means that the sediment transport direction is the same as the depth-averaged flow direction (although sometimes the mean return flow is considered) (Roelvink, 2011). Regarding the sediment transport, in most models, it is subdivided into bed load transport and suspended load transport. Bed load transport is always considered a direct function of the bed shear stress or near-bed velocity. The suspended transport is generally solved using the advection-diffusion equations (in 2DH or 3D). However, in some models, it is still only a function of the local flow and waves conditions (Roelvink, 2011). The computing grid represents a fundamental models component, and models can use either structured grids or unstructured grids. The structured grids can be rectilinear or curvilinear and are used in finite difference methods; the unstructured grids are typically built up from triangles (sometimes from a

combination of triangles and quadrilaterals) and are used in finite element or finite volume methods. Traditionally, finite difference methods are considered relatively easy to understand and relatively fast per grid cell. These methods are commonly used in coastal morphology. Conversely, finite element methods are much more complicated mathematically, and they are much slower per grid cell (Roelvink, 2011). The models can use implicit schemes (Delft3D, Mike21) or explicit schemes (XBeach). Implicit methods imply that the equation systems are set up so that they relate to state variables (e.g. velocities, water level) at the next time step to each other. Conversely, explicit methods imply that the state variables at the next time step are directly solved as a function of the values at the previous time step. Regarding the computing time, implicit models need to more time for each timestep, but they can use much bigger timestep because there is no hard stability limit. Differently, explicit methods take little effort for each timestep but have to keep to a strict time step criterion (Roelvink, 2011).

4.5.3 The XBeach model

XBeach (Roelvink et al., 2009) is an open-source model for coastal morphodynamics. The model was initially designed to assess the coastal erosion during extreme events such as storms and hurricanes (Roelvink et al., 2009, 2015), but it can also be applied for small-scale coastal engineering problems (Roelvink, 2011). In the last years, XBeach has also been used for long-term modelling (Bart, 2017) and, in detail, to determine the morphological change on the time-scale of years (Pender and Karunarathna, 2013; Wang et al., 2015). The model is classified as a Coastal Area Model (Roelvink, 2011) and includes the hydrodynamic processes of short waves transformation (refraction, shoaling and breaking), long waves (infragravity wave) transformation (generation,

propagation and dissipation), wave-induced setup and unstable currents, as well as overwash and inundation. The morphodynamic processes include bed load and suspended sediment transport, dune face avalanching, bed update, and breaching. Furthermore, the effects of vegetation and hard structures can be included (Roelvink et al., 2015). XBeach uses a coordinate system where the x-axis is always oriented towards the coast (approximately perpendicular to the coastline), and the y-axis is alongshore (Figure 4.11). The model uses
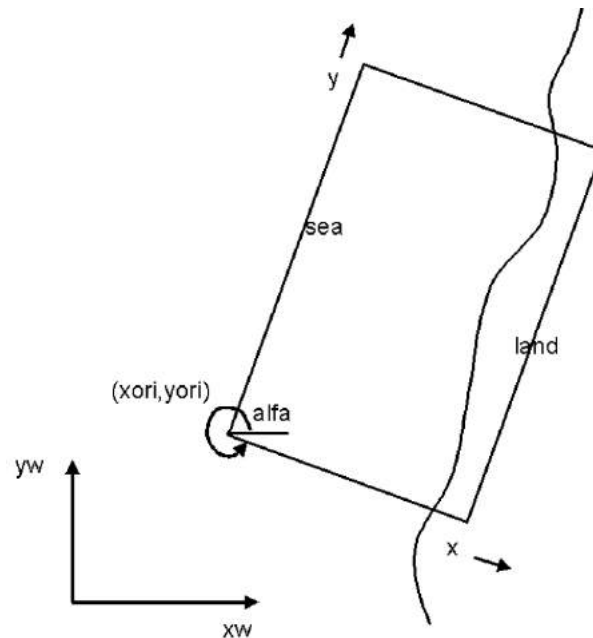
Figure 4.11: XBeach model grid definitions (Roelvink et al., 2015).

a structured computing grid (rectilinear or curvilinear) defined in the world coordinates system (WGS84). XBeach contains three different hydrodynamics options, i.e.: (1) stationary wave mode, (2) surfbeat (instationary) mode, and (3) non-hydrostatic mode. The stationary wave mode is efficiently solving wave-averaged equations but neglecting infragravity waves, in the surfbeat mode the short wave variations on the wave group scale (short wave envelope) and the long waves associated with them are resolved, and finally the non-

hydrostatic mode is characterised by a combination of the non-linear shallow water equations with a pressure correction term (Roelvink et al., 2015). Regarding the short wave action balance, the wave forcing in the shallow water momentum equation is obtained from a time-dependent version of the wave action balance equation (equation 4.1) similar to Delft University's (stationary) HISWA model (Holthuijsen et al., 1989). The directional distribution of the action density is taken into account, whereas a frequency, best represented by the spectral parameter $f_{m-1,0}$, represents the frequency spectrum. The wave action balance is then given by:

$$\frac{\partial A}{\partial t} + \frac{\partial c_x A}{\partial x} + \frac{\partial c_y A}{\partial y} + \frac{\partial c_\theta A}{\partial \theta} = -\frac{D_w + D_f + D_v}{\sigma} \tag{4.1}$$

Where the wave action A is calculated as:

$$A(x, y, t, \theta) = -\frac{S_w(x, y, t, \theta)}{\sigma(x, y, t)} \tag{4.2}$$

In which θ is the angle of incidence with respect to the x-axis, S_w is the wave energy density in each directional bin, and σ represents the intrinsic wave frequency. The intrinsic frequency σ and group velocity c_g is obtained from the linear dispersion relation. The intrinsic frequency is for example obtained with:

$$\sigma = \sqrt{gk \tanh kh} \tag{4.3}$$

The wave action propagation speeds in x, y and directional space are given by:

$$c_x(x, y, t, \theta) = c_g \cos(\theta)$$

$$c_y(x, y, t, \theta) = c_g \sin(\theta) \tag{4.4}$$

$$c_\theta(x, y, t, \theta) = \frac{\sigma}{\sinh 2kh} \left(\frac{\partial h}{\partial x} \sin \theta - \frac{\partial h}{\partial y} \cos \theta \right)$$

Where h is the local water depth and k is the wave number. The intrinsic wave frequency σ is obtained without considering the wave-current interaction, which means it is equal to the absolute radial frequency ω. As regards the dissipative phenomena, three several dissipation processes are considered in XBeach: wave breaking (D_w), bottom friction (D_f), and vegetation (D_v) (not considered in this study). Five different wave breaking (D_w) formulations are implemented in XBeach:

- Roelvink (1993a) (instationary waves)

$$\overline{D}_w = 2 \frac{\alpha}{T_{rep}} Q_b E_w \tag{4.5}$$

In which

$$Q_b = 1 - exp\left(-\left(\frac{H_{rms}}{H_{max}}\right)^n\right) \qquad H_{rms} = \sqrt{\frac{8E_w}{\rho g}}$$

$$H_max = \gamma(h + \delta H_rms) \qquad E_w(x,y,t) = \int_0^{2\pi} S_w(x,y,t,\theta)d\theta$$

Q_b is a fraction of breaking waves, α is a wave dissipation coefficient, T_{rep} is the representative wave period, E_w is the wave energy, H_{rms} is the-root-mean square wave height, H_{max} is the maximum wave height, γ is a breaker index, ρ is the water density, and g is the gravitational constant.

- Roelvink (1993a) extended (instationary waves)

$$\overline{D}_w = 2\frac{\alpha}{T_{rep}}Q_b E_w \frac{H_{rms}}{h} \tag{4.6}$$

The main difference with the original formulation is that wave dissipation is proportional to H^3/h instead of H^2.

- Daly et al. (2010) (instationary waves)

In this formulation, waves are entirely breaking if the wave height exceeds a threshold (γ) and stop breaking if the wave height falls below another threshold (γ_2).

$$\begin{cases} Q_b = 1, & \text{if } H_{rms} > \gamma h \\ Q_b = 0, & \text{if } H_{rms} > \gamma_2 h \end{cases} \tag{4.7}$$

- Baldock et al. (1998) (stationary waves)

$$\overline{D}_w = \frac{1}{4}\alpha Q_b \rho g f_{rep}\left(H_b^2 + H_{rms}^2\right) \tag{4.8}$$

In which

$$Q_b = exp\left(-\left(\frac{H_b^2}{H_{rms}^2}\right)\right) \qquad H_b = \frac{0.88}{k}\tanh\left[\frac{\gamma kh}{0.88}\right]$$

α is a wave dissipation coefficient, f_{rep} represents a representative intrinsic frequency, and γ is a calibration factor.

In this breaking formulation, the waves breaking fraction Q_b and breaking wave height H_b are calculated differently compared to the breaking formulations used for a non-stationary situation.

- Janssen and Battjes (2007) (stationary waves)

$$\overline{D}_w = \frac{3\sqrt{\pi}\alpha f_{rep}\rho g H_{rms}^3}{16}Q_b \tag{4.9}$$

In which

$$Q_b = 1 + \frac{4}{3\sqrt{\pi}}\left(R^3 + \frac{3}{2}R\right)exp\left(-R^2\right) - erf\left(R\right) \qquad R = \frac{H_b}{H_{rms}}$$

This formulation represents a revision of Baldock's formulation.

Finally, in both the instationary and stationary case the total wave dissipation is distributed proportionally over the wave directions with following formulation:

$$\overline{D}_w(x,y,t,\theta) = \frac{S_w(x,y,t,\theta)}{E_w(x,y,t)}\overline{D}_w(x,y,t) \tag{4.10}$$

The short-wave dissipation phenomena (D_f) due to the bottom friction is modelled as:

$$\overline{D}_f = \frac{2}{3\pi}\rho f_w \left(\frac{\pi H_{rms}}{T_{m01}\sinh kh} \right)^3 \tag{4.11}$$

Where f_w is the short-wave friction coefficient. This value only affected the wave action equation and is unrelated to bed friction in the flow equation. The hydro-morphodynamic processes in the surf zone, due to the action of wave motion and swash phenomena, are very complex phenomena and their numeric representation is possible through several modules (numeric methods) implemented in XBeach software.

4.5.4 XBeach grid setup

XBeach bed level is based on the combined bathymetric and topographic data survey (described in section 4.1). The all topo-bathymetric data were merged and interpolated into a regular grid (with a resolution of 3 m) through GIS software, to obtain a Digital Terrain Model (DTM) of the study area (Figure 4.12). Digital Terrain Model was exported (thanks to GIS tools) in an XYZ file, necessary to create the several XBeach layers.
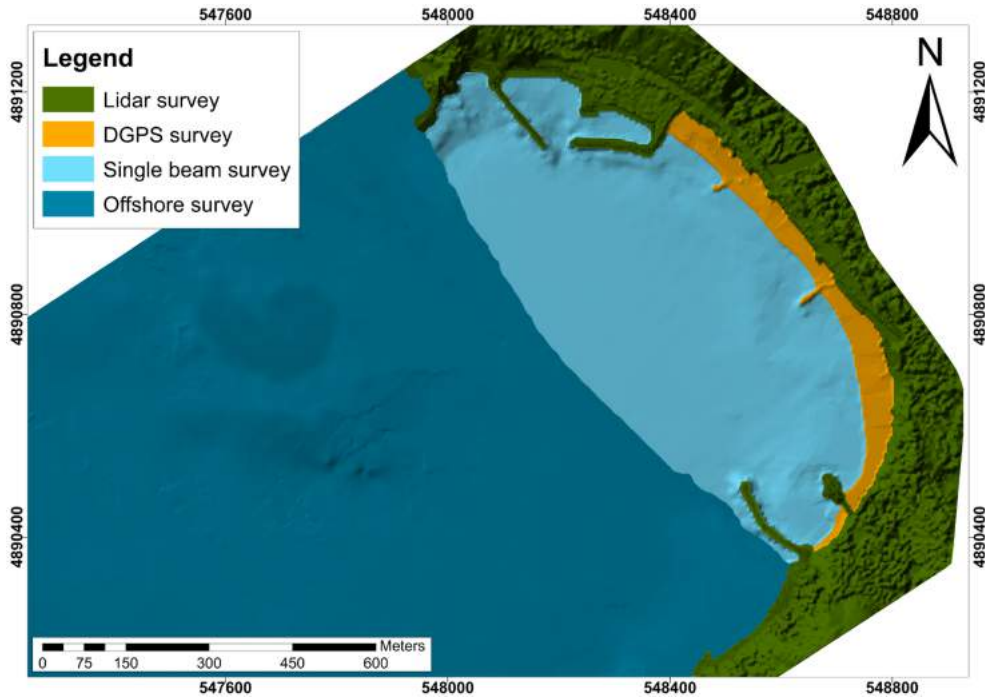
Figure 4.12: Digital Elevation Model of Levanto Bay, obtained through merge and interpolation of the topo-bathymetric dataset.

The computational grid was created through "RGFGRID" tool of the Delft3D software suite. We obtained a structured computational grid characterised by a higher resolution on the surf zone (5 m) and a lower resolution in the offshore area (30 m) (Figure 4.13). This solution is useful to obtain a reduction of model runtime, necessary to launch many model run test (indispensable to the model setting process). The XYZ files (bed level and non-erodible structures) have been re-interpolated on the computational grid to obtain XBeach layers (Figure 4.13). This last interpolation process was performed by the "QUICKIN" tool of the Delft3D software suite.
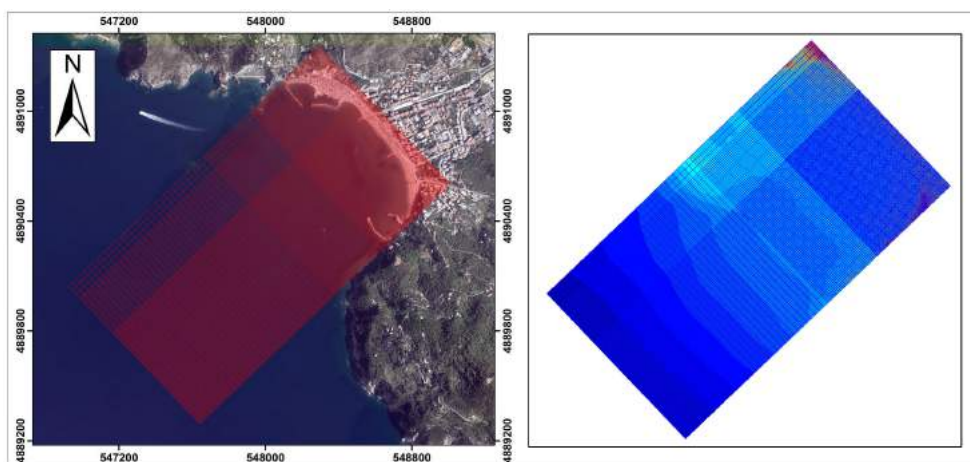
Figure 4.13: The geographical area included within the computing grid (left panel), and grid Interpolation through the QUICKIN tool (right panel).

4.5.5   XBeach parameters setup

An accurate model setting is essential to obtain a reliable representation of investigated phenomena, and the main modified parameters (than default setting) will be illustrated in this section.

- MPI parameters

  When running XBeach in parallel mode, the model domain is subdivided into submodels, and each submodel is then computed on a separate core. This process will increase the model computational speed. The MPI parameters (keyword: *mpiboundary*) determine how the model domain is subdivided. In *auto* mode (default) the model domain is subdivided such that the internal boundary is smallest. In *man* mode (our case) the model domain is manually subdivided using the values specified with the *mmpi* and *nmpi* keywords. This setting is useful to optimise the computational speed of model (related to available computing power).

parameter	unit	default value	setting value
mpiboundary	-	auto	man
mmpi	-	2	1
nmpi	-	4	3

Table 4.1: MPI parameters setting.

- Physical processes

  XBeach supports several physical processes, and each process can be switched on or off. Differently, than default mode, we switched on the short wave run-up (keyword: *swrunup*) and Snell's law for wave refraction (keyword: *snells*). The short wave run-up plays a key role in surf zone dynamics (Short, 1999) and could play an important role in rip currents dynamics.

parameter	unit	default value	setting value
swrunup	-	0	1
snells	-	0	1

Table 4.2: Physical processes setting.

- Sediment input

  The sediment input determines the composition of the bed and the detail in which processes related to sediment sorting are resolved. In this case, the values of $D50$ and $D90$ have been set based on the results of the sedimentological analysis.

parameter	unit	default value	setting value
D50	m	0.0002	0.0017
D90	m	0.0003	0.0006

Table 4.3: Sediment input setting.

- Grid parameters

  XBeach supports Delft3d grids created with RFGRID tools (As described in section 4.5.4) and, in this study, we have chosen this option. The use of RFGRID tools interface allows a relatively easy grid building.

parameter	unit	default value	setting value
gridform	-	XBeach	Delft3d

Table 4.4: Grid form setting.

- <u>Morphology parameters</u>

  In XBeach there are several available parameters which help us to obtain a good description of morphological features and processes. In particular, we highlight the use of the non-erodible layer (keyword: *struct*) to represents details of the hard structures present on the beach (e.g. groynes).

parameter	unit	default value	setting value
struct	-	0	1

Table 4.5: non-erodible layer setting.

4.5.6   Wave input

Offshore wave dataset has been supplied by the DICCA hindcast database (MeteOcean research group, www.dicca.unige.it/meteocean) (Figure 4.14). This dataset is the result of numerical simulations of the wavewatchIII (WWIII) model (Komen et al., 1996; Tolman et al., 2009), and of the weather research and forecasting models (WRF-ARW) (Skamarock and Klemp, 2008) in the Mediterranean sea from 01/01/1979 - 31/12/2017 (Mentaschi et al., 2013, 2015). Five swell events have been considered in this study; three events for rip currents modelling (13th - 14th October 2016, 09th - 11th November 2016, 05th March 2017), and two events for model validation process (09th February 2017, and 23rd March 2018). The wave climate of these events is depicted in table 4.6.
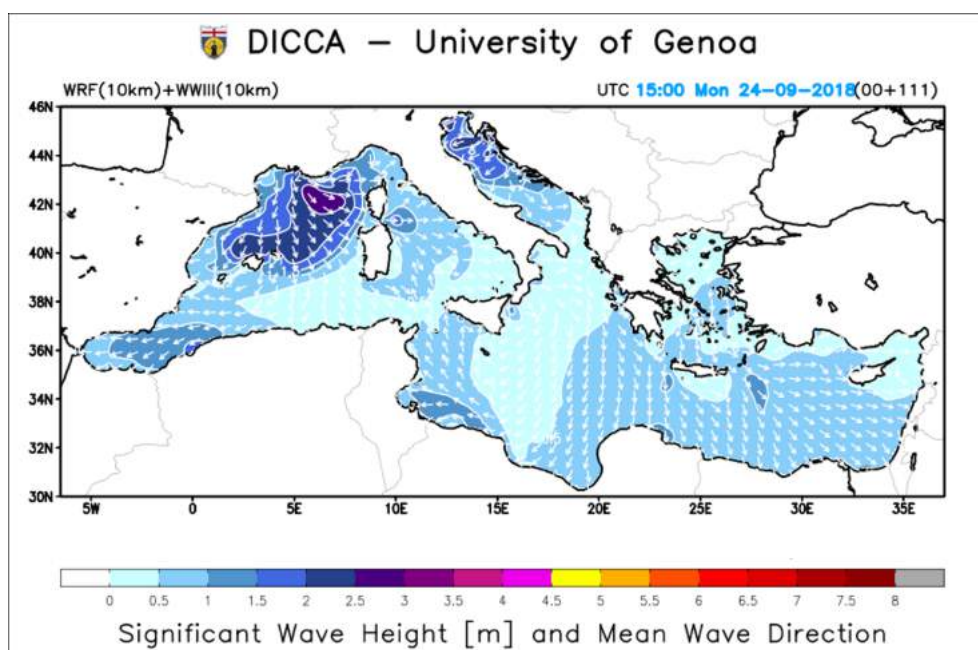
Figure 4.14: WavewatchIII (WWIII) model by MeteOcean research group, www.dicca.unige.it/meteocean.

Event	Hs (m)	Tm (s)	Direction (°N)	Purpose
13th - 14th October 2016	2.02	6.10	152	rip modeling
09th - 11th November 2016	1.70	7.48	225	rip modeling
09th February 2017	1.24	3.97	209	validation
05th March 2017	2.91	7.92	225	rip modeling
23rd March 2018	0.40	4.08	223	validation

Table 4.6: offshore wave data.

The events have been described through a spectral approach ($JONSWAP$ model), and details are displayed below.
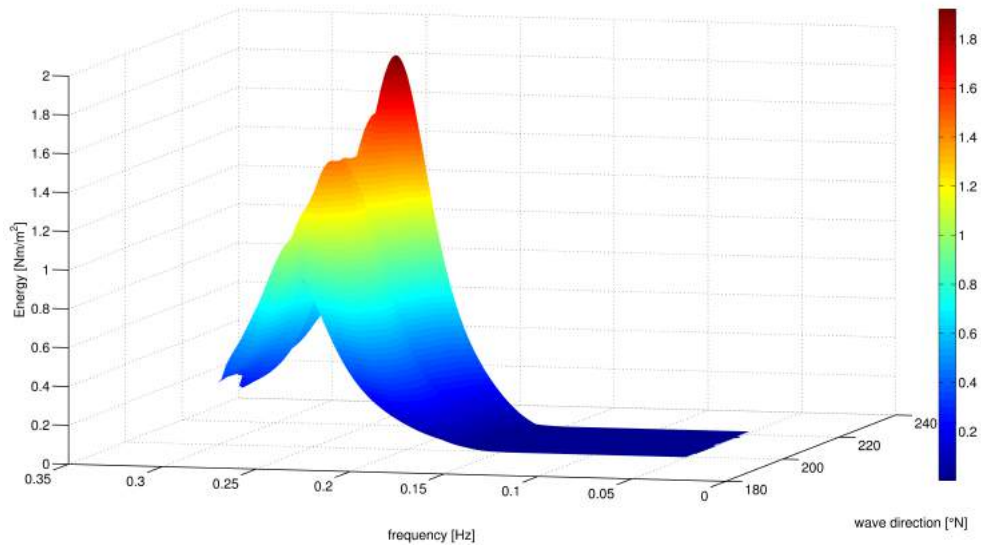
- **13th - 14th October 2016**
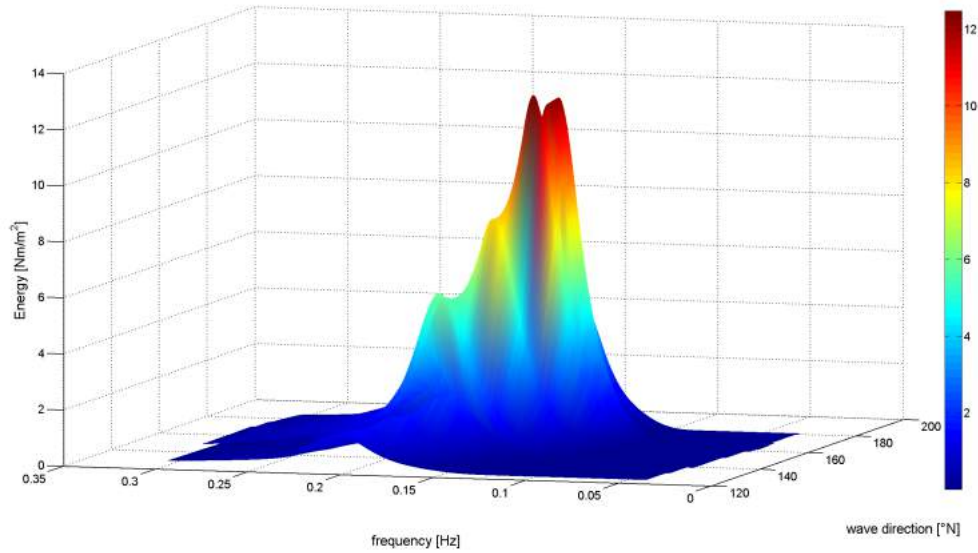
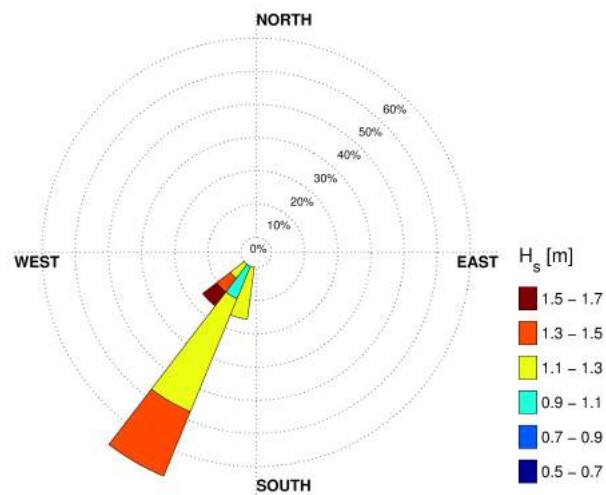**Figure 4.15:** Directional wave spectra ($JONSWAP$).
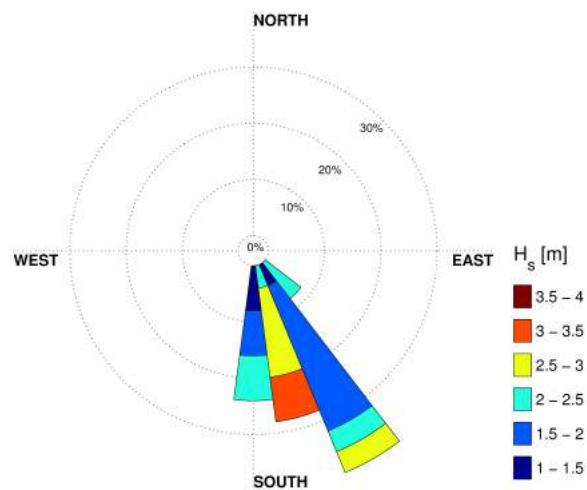
Figure 4.16: Directional wave rose. The significant wave height (Hs) associated with the various directions are illustrated by the different colours.
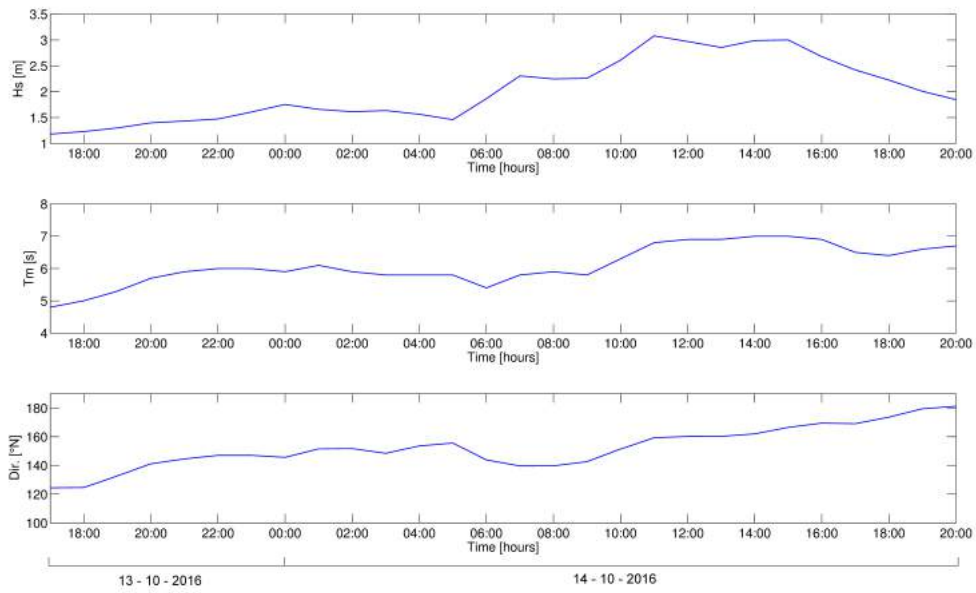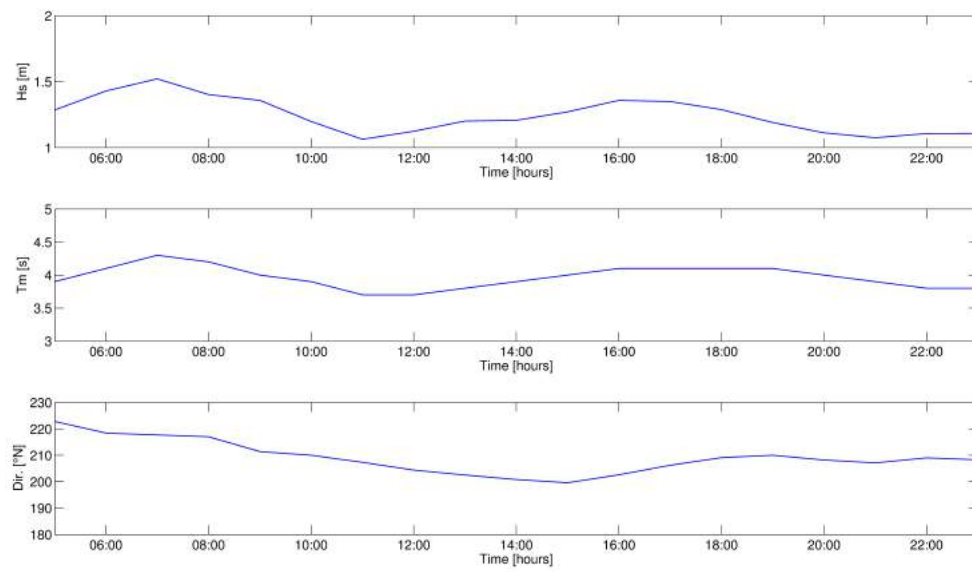
Figure 4.17: Wave parameters: significant wave hight (Hs), mean period (Tm) and wave direction (Dir.).

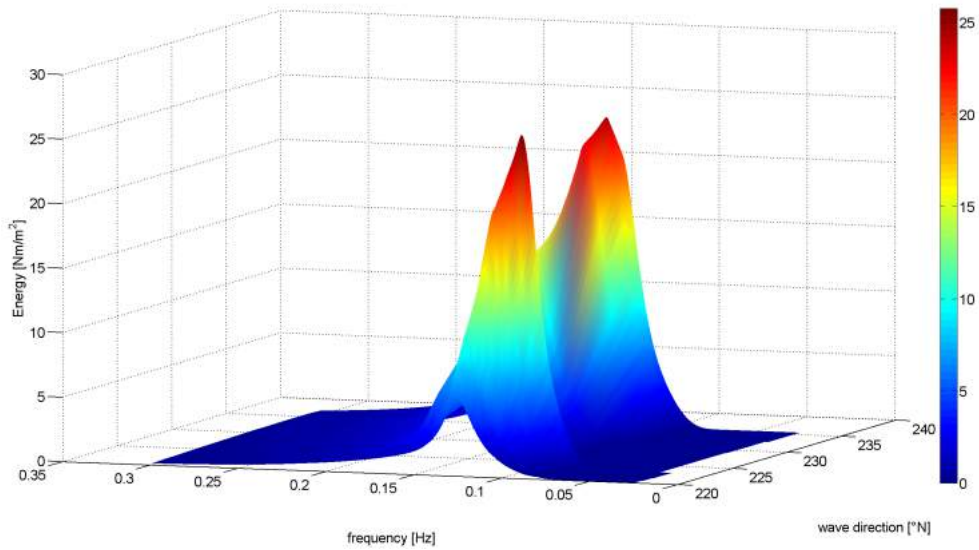• **9th - 11th November 2016**
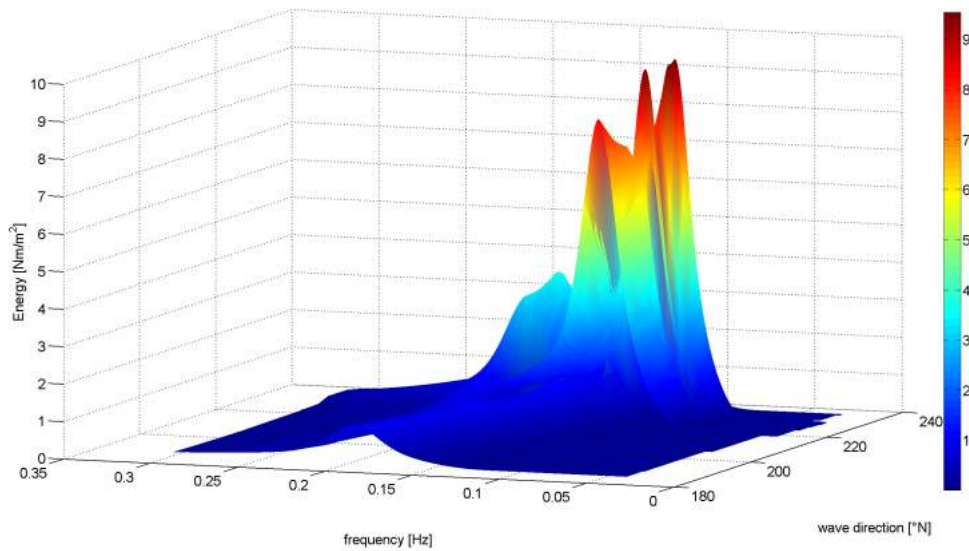
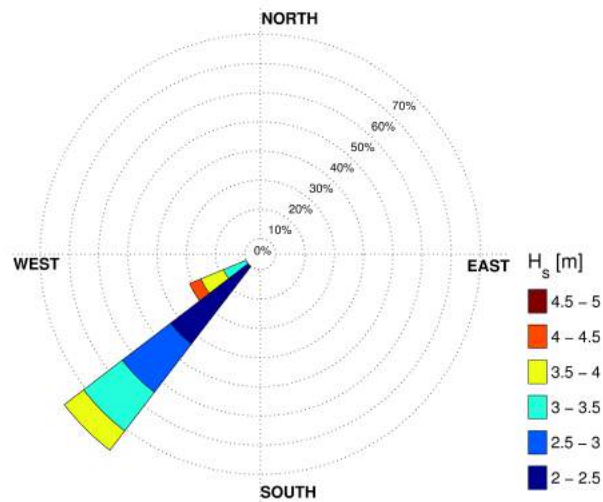**Figure 4.18:** Directional wave spectra ($JONSWAP$).
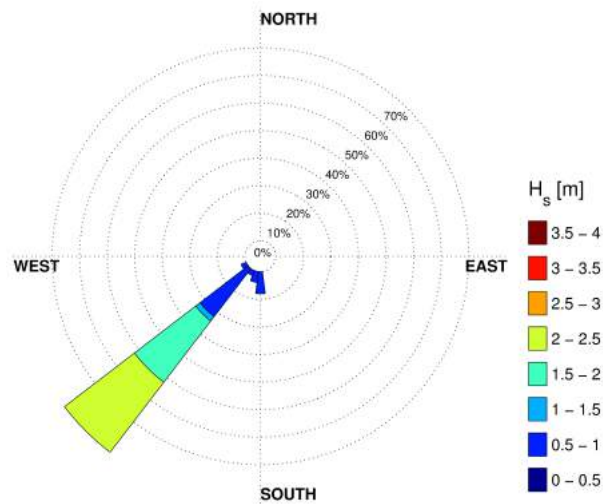
Figure 4.19: Directional wave rose. The significant wave height (Hs) associated with the various directions are illustrated by the different colours.
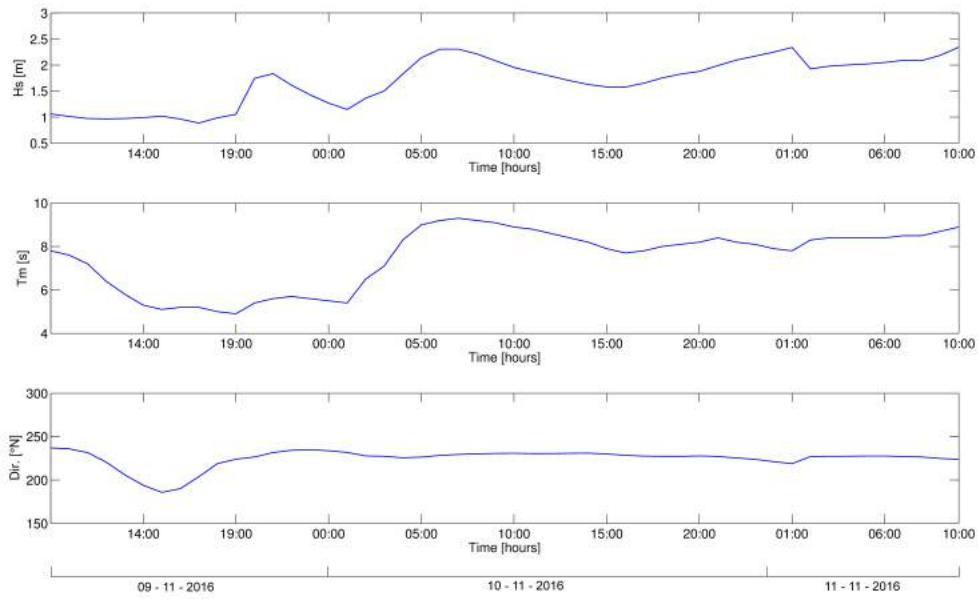
Figure 4.20: Wave parameters: significant wave hight (Hs), mean period (Tm) and wave direction (Dir.).

- **9th February 2017**

Figure 4.21: Directional wave spectra ($JONSWAP$).

Figure 4.22: Directional wave rose. The significant wave height (Hs) associated with the various directions are illustrated by the different colours.
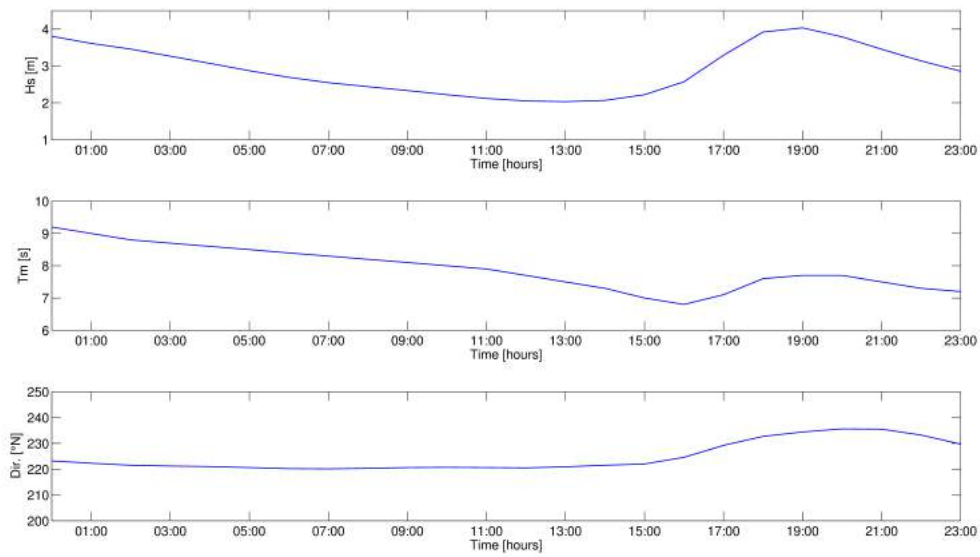
Figure 4.23: Wave parameters: significant wave hight (Hs), mean period (Tm) and wave direction (Dir.).

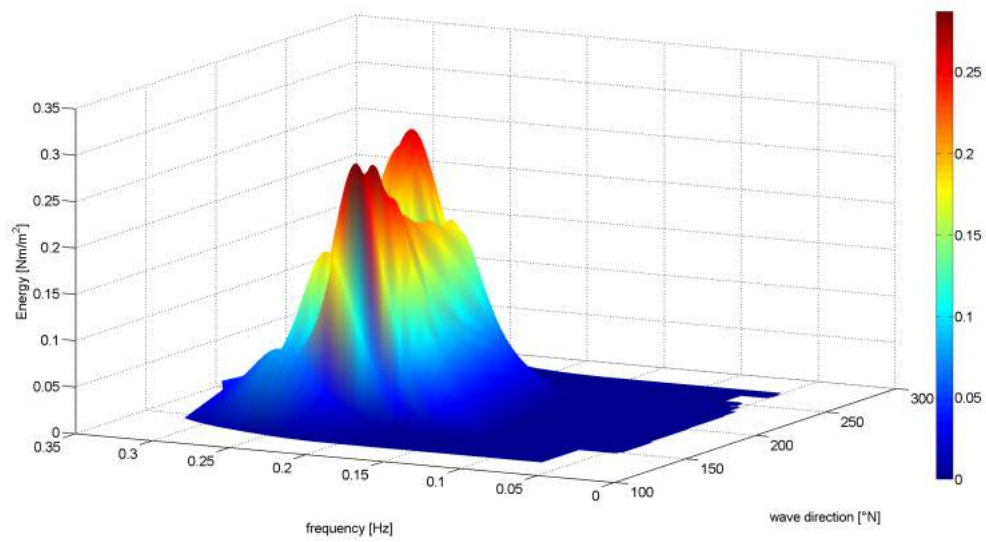- 5th **March 2018**

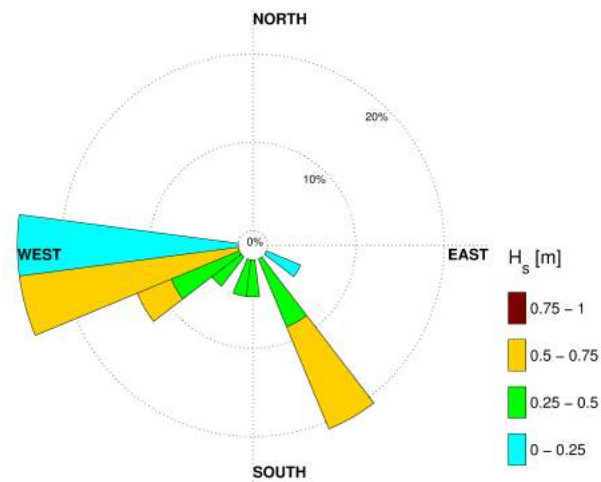**Figure 4.24:** Directional wave spectra ($JONSWAP$).

Figure 4.25: Directional wave rose. The significant wave height (Hs) associated with the various directions are illustrated by the different colours.

Figure 4.26: Wave parameters: significant wave hight (Hs), mean period (Tm) and wave direction (Dir.).

- **23th March 2018**

Figure 4.27: Directional wave spectra ($JONSWAP$).

Figure 4.28: Directional wave rose. The significant wave height (Hs) associated with the various directions are illustrated by the different colours.
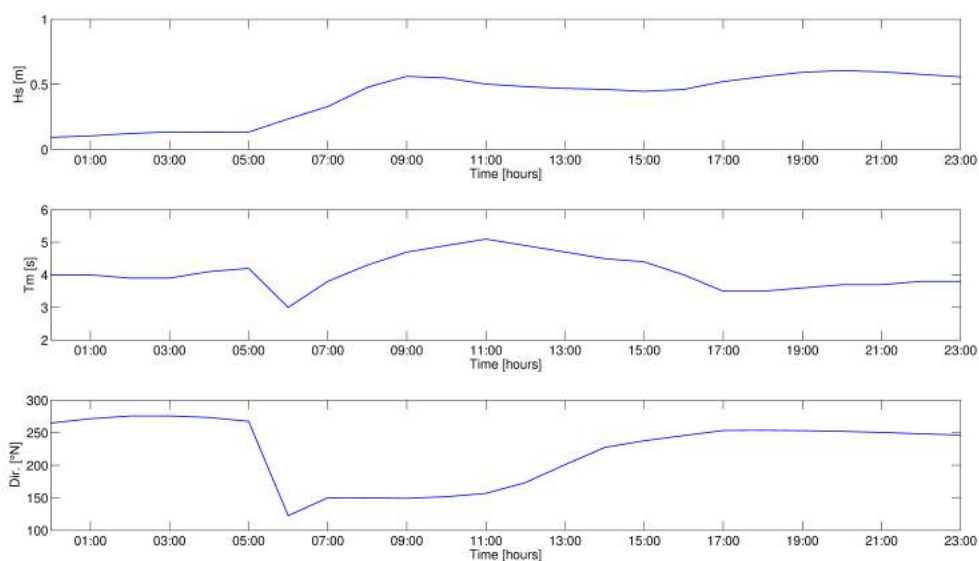
Figure 4.29: Wave parameters: significant wave hight (Hs), mean period (Tm) and wave direction (Dir.).

4.5.7   Sea-level (LSL) projections

Sea level changes are a key factor affecting the evolution and management of coastal environments (Marcos et al., 2012). To quantify SLR in the study area, we used projections to the year 2100 in Genoa (Kopp, 2015). We modelled SLR under the RCP 4.5 scenario (Meinshausen et al., 2011) which corresponds to a likely global mean temperature increases in 2081 - 2100 of 2.0-3.6 °C above 1850-1900 levels (IPCC, 2013). RCP 4.5 corresponds to a moderate scenario of gases mitigation policy (Meinshausen et al., 2011). From Kopp (2015), we extracted median (0.43 m) and 0.5^{th}, 5th. 95th and 99.5^{th} percentiles for the Genoa tide gauge, and used them as SLR scenarios (Figure 5.46 and Table 4.7).
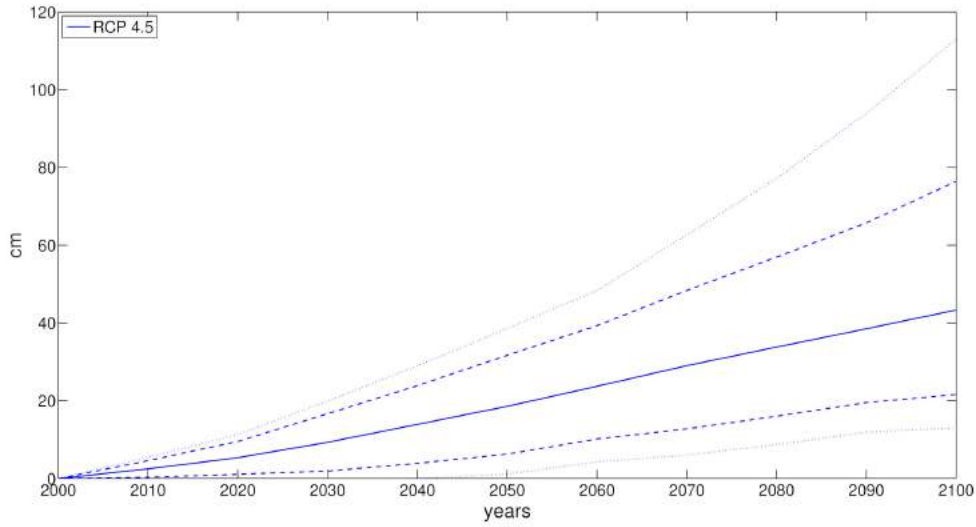
Figure 4.30: Local Sea Level (LSL) projection in Genoa by 2100 (Kopp, 2015), based on RCP 4.5 (Meinshausen et al., 2011). Heavy = median, dashed = 5th - 95th percentile; dotted = 0.5^{th} - 99.5^{th} percentiles.

.

Scenarios	LSL (m)
S1 (today)	0
S2	0.13
S3	0.21
S4	0.43
S5	0.76
S3	1.13

Table 4.7: Several LSL rise computing scenarios.

The event of 09th-11th November 2016 was considered to evaluate the rip currents behaviour in higher sea level scenarios. This event has been selected

(among the several investigated events) because it is characterised by a significant development over time (some days) and by a clear rip currents development pattern. The model setting was maintained, changing only the interval time of output (parameter keyword: tintg) to reduce the computational time. This change has been useful due to the high number of necessary model simulations.

4.5.8 XBeach model validation

The model validation was performed through two different approaches, i.e. comparing model results with data collected through video monitoring and drifter surveys. The video monitoring validation was obtained comparing the rip currents generation points, whereas drifters validation was accomplished through an error statistics analysis. Due to the difficulty to obtain field measurements of the rip currents, two drifter surveys were achieved in dates of 09th February 2017, and 23rd March 2018 and the collected data have been compared with the model simulations of the same events. According to Austin et al. (2012), the error statistics analysis was performed through the evaluation of the scatter index (SCI) and relative bias (Rel. bias).

Parameter	Formula*	Description
SCI	$\frac{RMS_{(c-m)}}{max(RMS_m|\langle m \rangle|)}$	This is a relative measure of the scatter between model and data. The error is normalized with the maximum of the RMS of the data and the absolute value of the mean of the data; this avoids strange results for data with small mean and large variability
Rel. bias	$\frac{\langle c-m \rangle}{max(RMS_m|\langle m \rangle|)}$	This is a relative measure of the bias, normalized in the same way as the SCI. This parameter relates the variance of the difference between data and model to the variance of the data.

Table 4.8: error parameters (* m = measured, c = computed).

Chapter 5

Results

5.1 Seabed morphological analysis

A seabed morphological analysis was performed through spatial analysis tools in GIS environment. The analysis allowed characterisation of the morpho-sedimentary trends inside the considered time range (October 2016/March 2017). In details, it was calculated the differences between the topo-bathymetric data of March 2017 and October 2016 (Figure 5.1). This methodology allowed depiction of the beach hydro-morphodynamic responses during winter, and some significant morphological features, related to rip currents dynamics, were identified. In details, three rip channels were identified (Figure 5.1). The more evident rip channel is identified on the east side of the groyne between the central and eastern sectors of the beach. Two other rip channels were identified on the west side of the groyne and in the central area of the beach eastern sector. It is essential highlights that the development of rip channels is related to the dominant wave boundaries conditions, and with sea conditions before the second survey campaign (March 2017) in particular. However, the obtained results are proof of the crucial role played by the cross-shore dynamics along
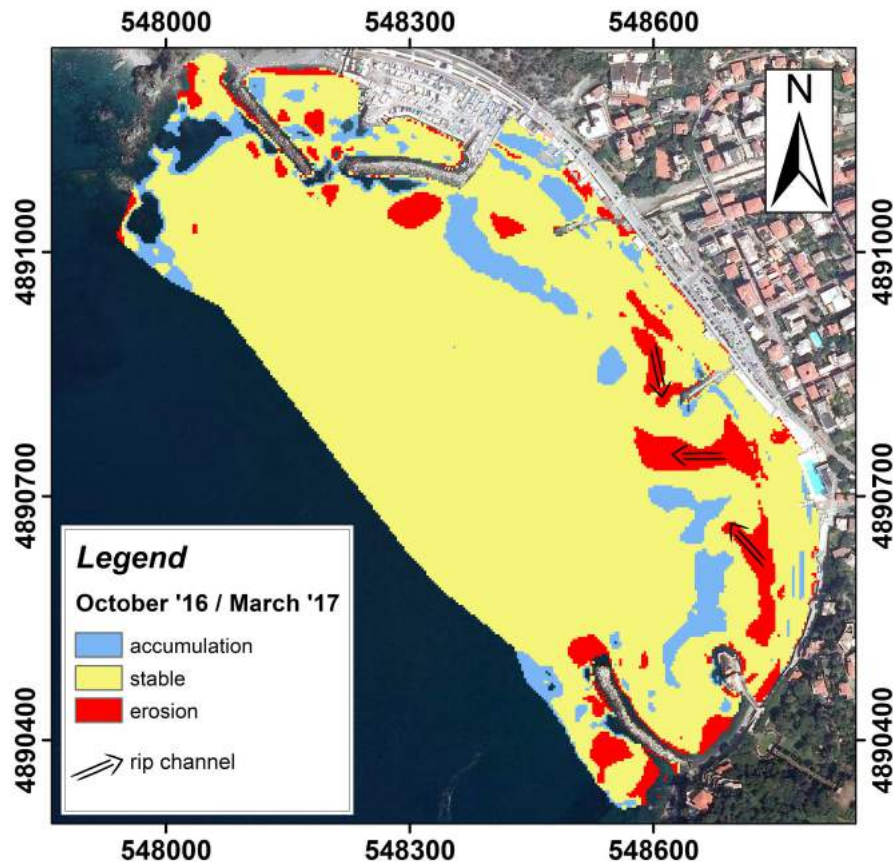
the Levanto beach.

Figure 5.1: Map of the morphodynamic trend between October 2016 and March 2017 (GIS elaboration), arrows show the rip channels.

5.2 Video monitoring results

Rip currents individuation through coastal video monitoring is a well-known approach in the field of coastal research (Nelko and Dalrymple, 2011; Austin et al., 2012; Murray et al., 2013). In details, during this research project, several rip currents were recorded by means of a video monitoring system, and they are shown in this section. Image processing, through the Beachkeeper *plus* software, was performed to supports the rip currents individuation. Time exposure images (timex) and variance images were obtained through processing of snapshot images sampled every 5 seconds (related to features of the observed phenomena).

5.2.1 13th -14th October 2016

Several rip currents were observed during the October event. In detail, two rip currents were identified on the down-wave and up-wave sides of the groyne, between central and eastern sectors of the beach (Figure 5.2, 5.3). In Figure 5.2 we notice the rip current development in the lee of the groyne. In this case, rip current behaviour is evident due to the sea foam, which is wiped out by water flow. The second rip current was observed on the west side of the groyne. This rip phenomenon is very evident (Figure 5.3), and its behaviour is well depicted by suspended sediment. In this particular situation, water turbidity works like a coloured tracer.
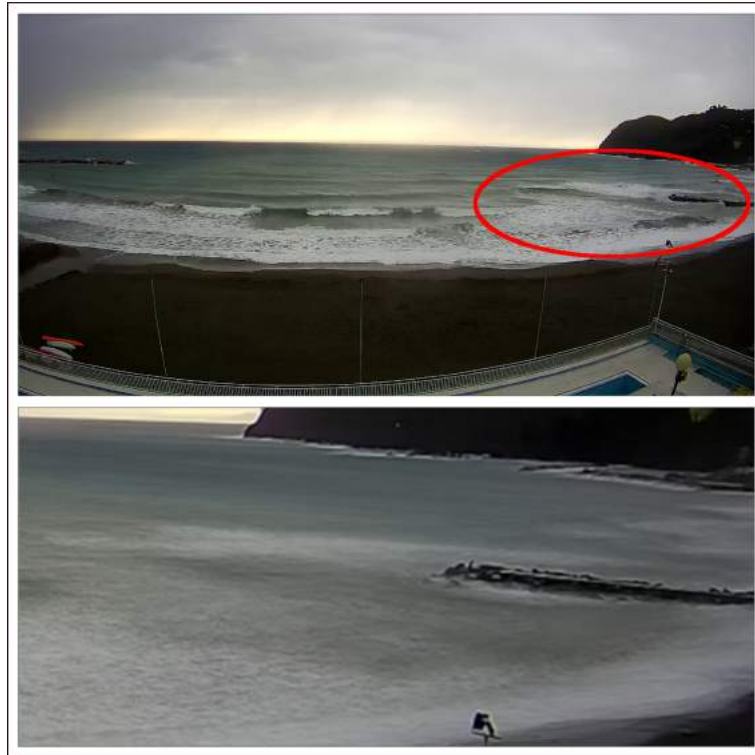
Figure 5.2: Rip current development in the lee of the groyne. (Top panel) snapshot of a rip current generation process (red circle). (Bottom panel) rip current behaviour analysed through timex processing.

Figure 5.3: Rip current development on the west side of the groyne (timex image). Rip behaviour is traced by water turbidity.

5.2.2 09th -11th November 2016

Several rip currents characterise this event and different rip currents type were recorded by the monitoring system (Figure 5.4, 5.5, 5.6, 5.7). Two rip currents were identified on the sides of groyne between central and eastern sectors of the beach (Figure 5.4).

Figure 5.4: Rip currents on the sides of groyne between central and eastern sector of the beach (variance image).

In Figure 5.5, we observe a snapshot image of a rip current in the central area of the beach eastern sector. Furthermore, a more clear phenomenon identification was obtained through timex and variance elaborations (Figure 5.6). Moreover, also a series of small rip currents, associated with cuspidate morphologies, were recorded by the monitoring system. These phenomena are shown in Figure 5.7, where we notice their quite limited spatial development (if compared to others observed rip currents).

Figure 5.5: Rip current development (red circle) in the central sector of beach eastern sector.

Figure 5.6: Rip current development in the central sector of beach eastern sector. (Top to bottom) timex and variance images.

Figure 5.7: Rips associated with cuspidate morphologies along the beach eastern sector (central camera). (Top panel) timex image. (Bottom panel) rip details (zoomed snapshot).

5.2.3 05th March 2017

Several rip currents were also recorded during the storm event of March 2017 and, in details, two rip current phenomena appeared very evident. A first rip was observed in the central area of the beach eastern sector (Figure 5.8). A second rip current was observed on the east side of the groyne, between central and eastern sectors of the beach (Figure 5.9). As well as for other considered storm events, we used image processing techniques as support in rip currents individuation process (Figure 5.8, 5.9).

Figure 5.8: Rip current development in the central sector of the beach eastern sector. (Top to bottom) snapshot image (rip current in red circle) and timex image (zoomed).

Figure 5.9: Figure 5.8: Rip current on the east side of groyne. (Top to bottom) snapshot image (rip current in red circle) and timex image (zoomed).

5.3   XBeach model results

In this section, we describe the results of the XBeach model simulations. Rip currents behaviour, under several wave boundary conditions, is described through XBeach 2D output and diagrams of velocities. In order to evaluate the rip currents intensity, we considered the x-component of the Eulerian velocity (ue). ue values (positive or negative) are based on the XBeach grid orientation. Model grid is oriented orthogonal to the coast, and ue negative values highlight the presence of cross-shore currents. For this reason, we will use the ue values to define the rip currents behaviour. In details, more negative values of ue shows more strong rip currents.

5.3.1 Model validation

As described in section 4.5.8, the model validation was obtained through two different approaches and results of the validation process are described in this section. The XBeach results are georeferenced and, thanks to that, it was possible to compare the rip currents generation points in the model with rip locations recorded by the video monitoring system. Moreover, also the structures on the beach (e.g. groynes) are reference points to define the rip currents location clearly. The correspondence between the rip currents generation points was observed for each modelled event and examples are shown in Figure 5.10, 5.11 and 5.12. The data comparison was only possible for the rip currents in the filmed area and the visibility of the rip currents also depends by external variables (e.g. presence of foam, suspended sediments). For example, the event of 13th-14th October 2016 is characterised by moderate sea conditions (than other considered cases) and, consequently, by the lesser presence of foam. However, thanks to the suspended sediments (tracer effect), the correspondence between video data and model results are evident for the rip on the west side of the groyne (Figure 5.10). For each investigated event at least one clear correspondence was observed, and, for this reason, the video validation process can be considered accomplished. Moreover, an error statistics analysis between modelled data and Lagrangian data allowed obtaining a quantitative model validation. The analysis has been conducted comparing the Lagrangian data, collected during survey campaign in date 09th February 2017 and 23rd March 2018, with the model results (model implemented on the same events). In details, the Relative Bias (Rel. Bias) and Scatter Index (SCI) have been calculated, obtaining the following results: SCI = 0.34, Rel. bias = 0.14 for the event of 09th February 2017; SCI = 1.09, Rel. bias = 0.66 for the event of 23rd March 2018 (Figure 5.13). The results support the reliability of the

model, also from a quantitative viewpoint. The values of the considered currents, observable in Figure 5.13, are moderate, and it is related to the fact that drifter surveys have been only possible under calm sea conditions. However, according to Austin et al. (2012), obtained results can be considered satisfying, and the model is validated.
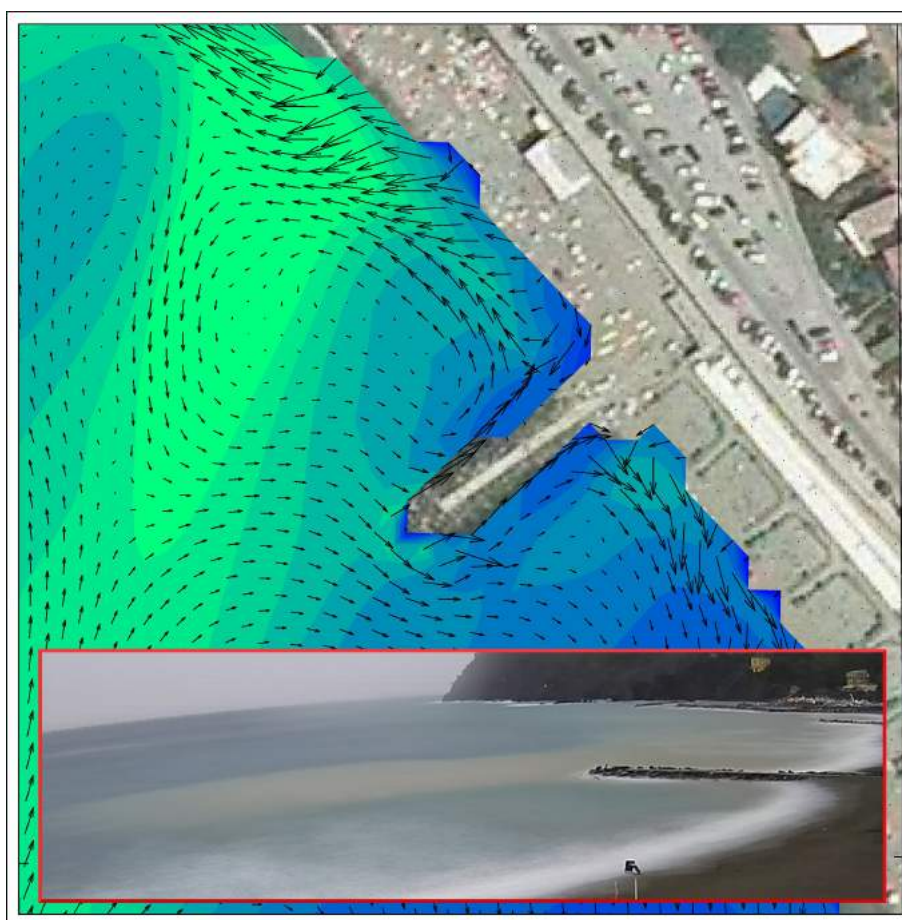

Figure 5.10: Correspondence between video data (red frame) and model results for the event of 13th-14th October 2016. The correspondence between video data and model results is evident (see rip current on the west side of the groyne), and the video validation process is accomplished.
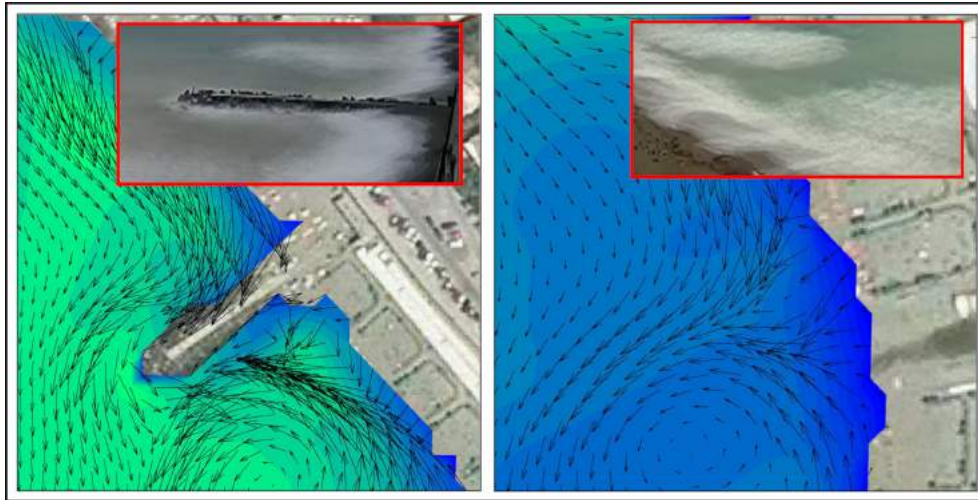
Figure 5.11: Correspondence between video data (red frames) and model results for the event of 09th-11th November 2016. Left panels: correspondence for the rip currents on sides of the groyne. Right panel: rip current in the central sector of the beach eastern sector. The video validation process is accomplished.
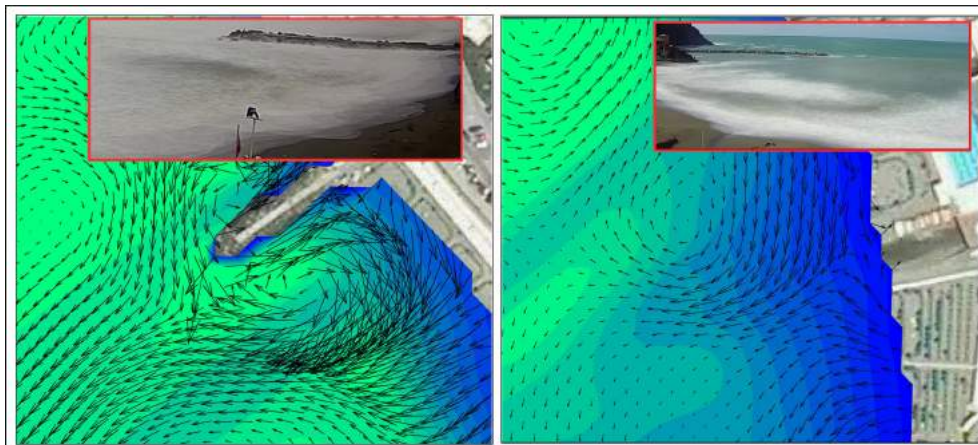

Figure 5.12: Correspondence between video data (red frames) and model results for the event of 05th March 2017. Left panels: correspondence for the rip current on the east side of groyne. Right panel: rip current in the central sector of the beach eastern sector. The video validation process is accomplished.
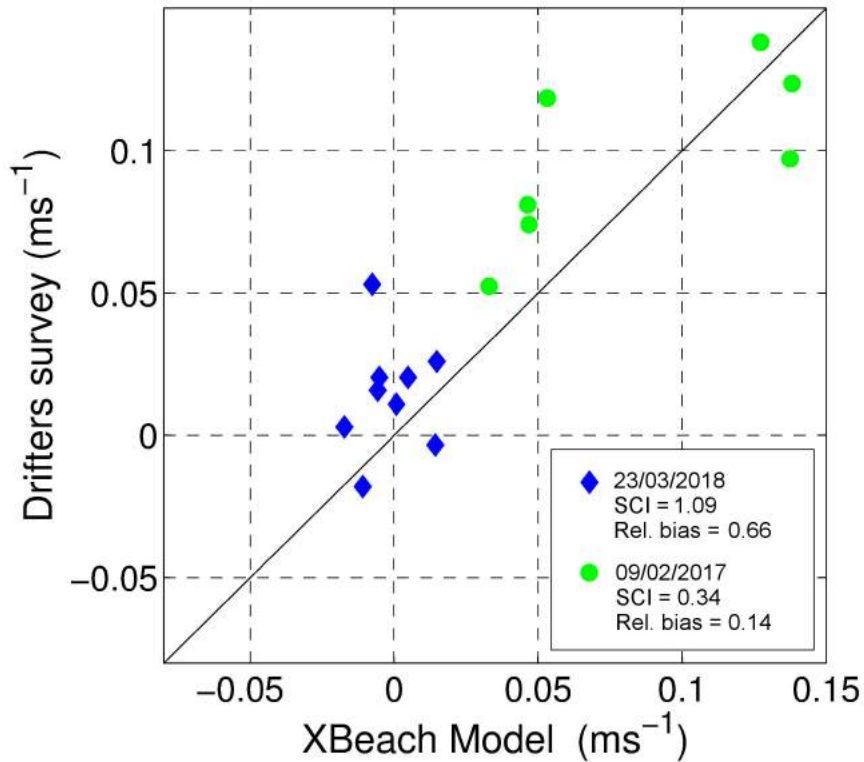
Figure 5.13: The image shows comparison between observed current intensity values and modelled current intensity values. The positive and negative values show the flow direction referred to the model grid orientation (negative = offshore, positive = onshore).

5.3.2 13th-14th October 2016

As described in section 4.5.6, this storm is characterised by waves direction from SE, and waves propagation, with rip currents generation sectors, are depicted in Figure 5.14. Observing waves propagation within Levanto bay, we notice the presence of a protected sector in the eastern sector of the beach. This fact is due to the presence of the Punta Mesco promontory (at the East of the Levanto bay), which defends the eastern sector of the beach. Bringing

attention on the beach sectors where rip currents occur, we notice that the rip phenomena occur in western and central sectors of the beach (near groynes in particular) (S.1 and S.2 in Figure 5.14), and in the central area of the beach eastern sector (S.3 in Figure 5.14). Model results show that rip phenomena do not occur in the more protected stretch of the beach.
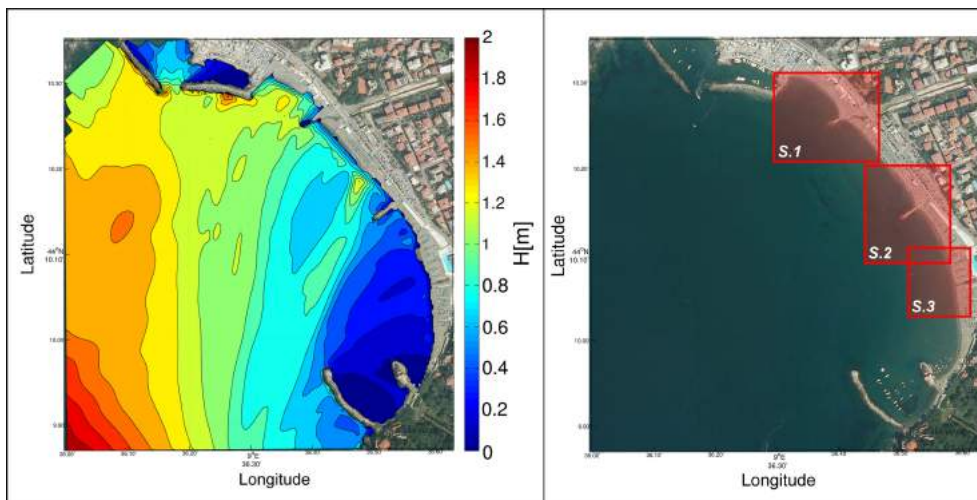

Figure 5.14: Left panels: waves propagation within the Levanto bay. Right panel: Beach sectors (S.1, S.2, S.3) where rip currents occur.

From West to East, between western and central sectors of the beach, we find the first rip currents generation sector (S.1) (Figure 5.15), where two rip currents occur on both sides of the groyne. Moreover, a wave height decrease concomitant with the rip current flow is evident on the West side of the groyne (Figure 5.15).
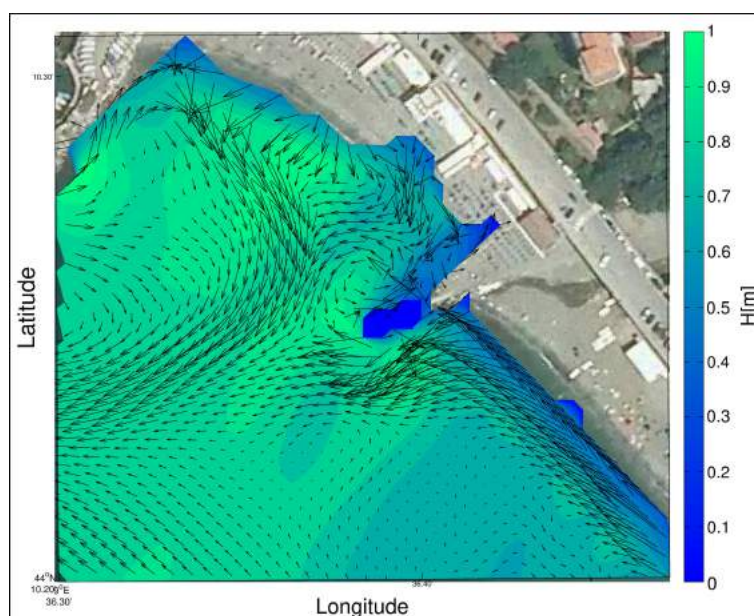

Figure 5.15: Rip currents development in sector 1 (S.1 in Figure 5.14). Results obtained through XBeach model simulation.

Figure 5.16 shows the rip current behaviour on the west side of the groyne. Model results highlight the rip current development between 12:45 and 16:45 on 14th October, with an average velocity of 0.25 ms^{-1} and peak values around 0.5 ms^{-1}. The behaviour of the rip current on the east side of the groyne is shown in Figure 5.17. The development of this other phenomenon is more persistent over time, and the rip current flow is evident around 11:00 and persists throughout the day. This rip current is characterised by an average velocity of 0.53 ms^{-1} and by peak values around 0.7 ms^{-1} (Figure 5.17).
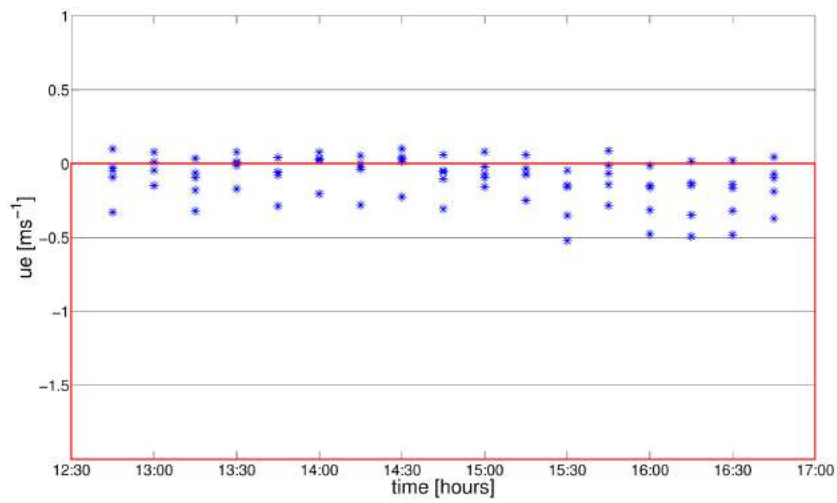
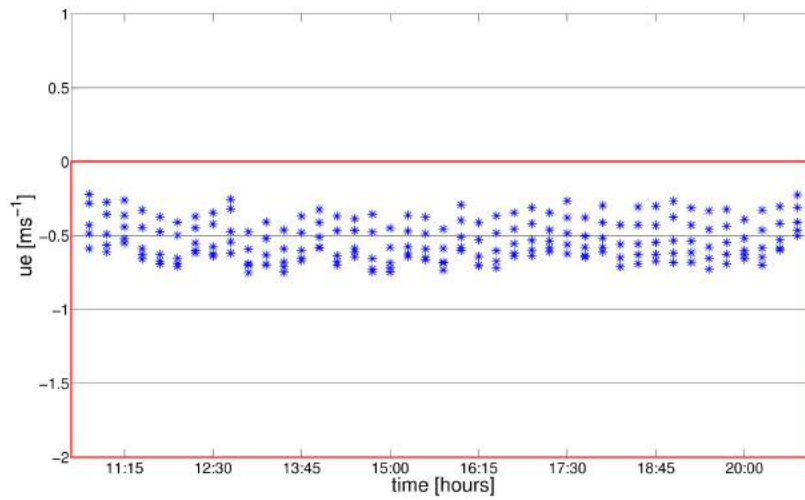**Figure 5.16:** Rip current behaviour on the west side of the groyne, rip generation sector 1 (S.1).

Figure 5.17: Rip current behaviour on the east side of the groyne, rip generation sector 1 (S.1).

Proceeding towards the East, near the groyne between the central and eastern sectors of the beach, we find the rip currents generation sector 2 (Figure 5.18). Rip currents occur on both sides of the groyne, but they are not very close to the hard structure (Figure 5.18). Rip current on the west side of the groyne occurs between 10:15 and 20:45, showing an average velocity of 0.17 ms^{-1} and peak values of 0.4 - 0.5 ms^{-1} (Figure 5.19). Rip current on the east side of the groyne shows a similar behaviour, with a comparable development over time, an average velocity of 0.25 ms^{-1} and peak values around 0.5 ms^{-1} (Figure 5.20).
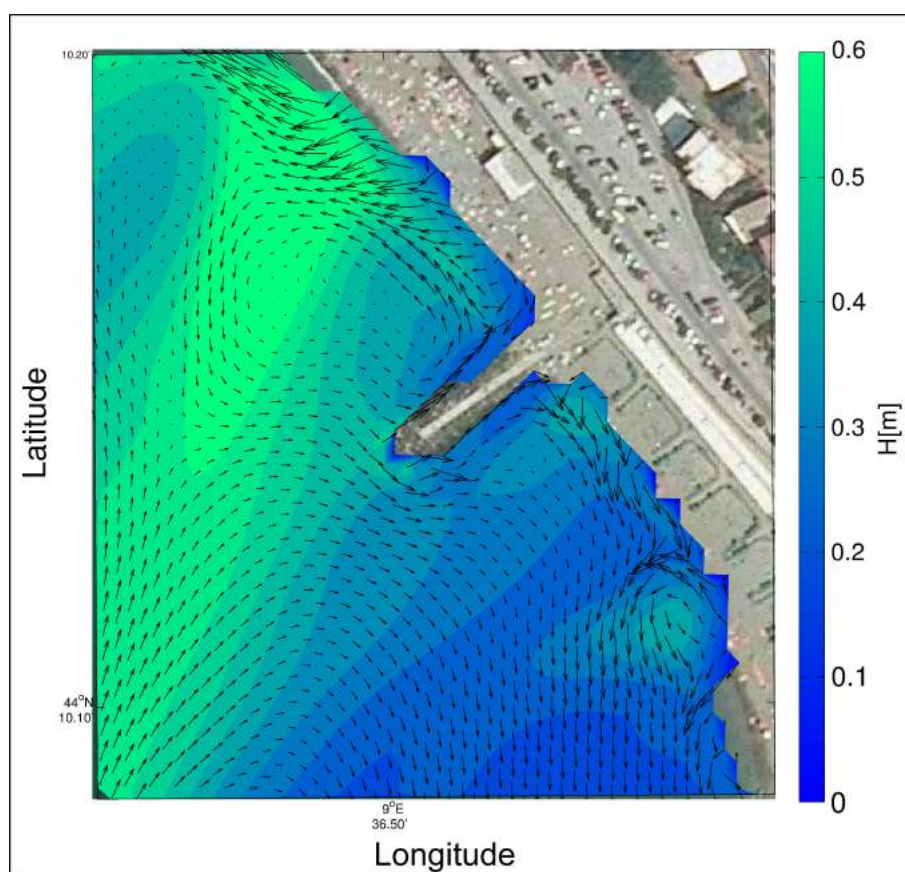

Figure 5.18: Rip currents development in sector 2 (S.2 in Figure 5.14). Results obtained through XBeach model simulation.
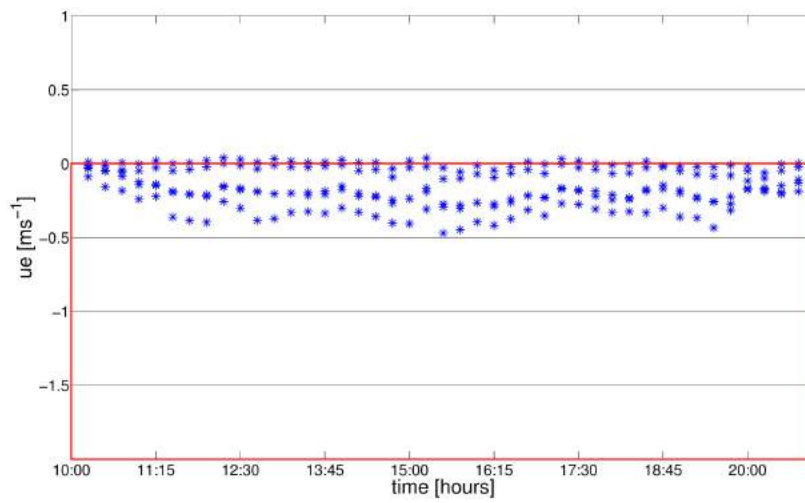
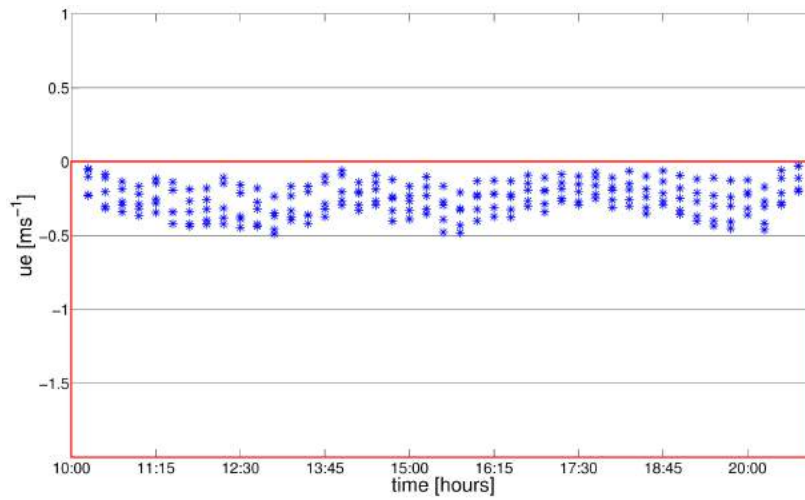**Figure 5.19:** Rip current behaviour on the west side of the groyne, rip generation sector 2 (S.2).

Figure 5.20: Rip current behaviour on the east side of the groyne, rip generation sector 2 (S.2).

Finally, in the central area of the eastern sector, we observe an evident wa-
ter flow rotation close to the shoreline, which highlights the last rip phenomena
of this model simulation (Figure 5.21). In this last case, the rip current de-
velopment is not associated with the presence of hard structures (differently
to phenomena described above), and occurs between 11:15 and 20:30, has an
average velocity of 0.15 ms^{-1} and peak values around 0.35 ms^{-1} (Figure 5.22).
Furthermore, a wave height decrease occurs in concomitance with the rip flow
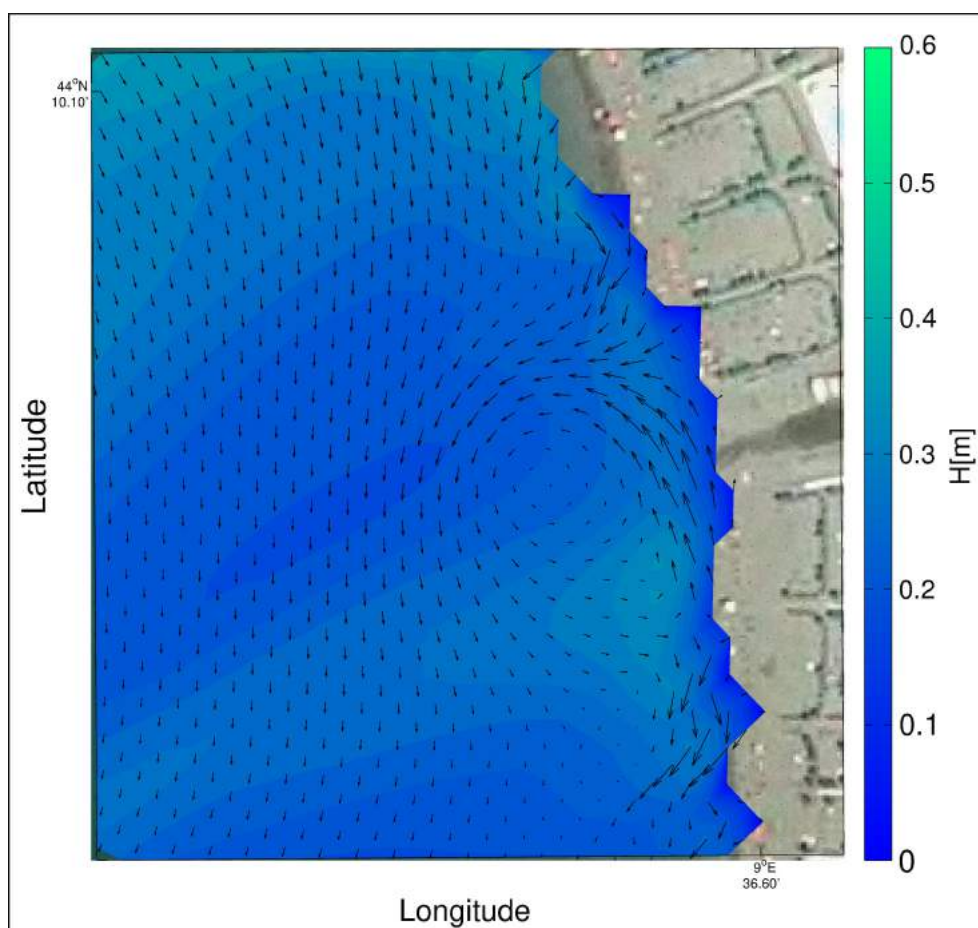(Figure 5.21).

Figure 5.21: Rip currents development in sector 3 (S.3 in Figure 5.14). Results
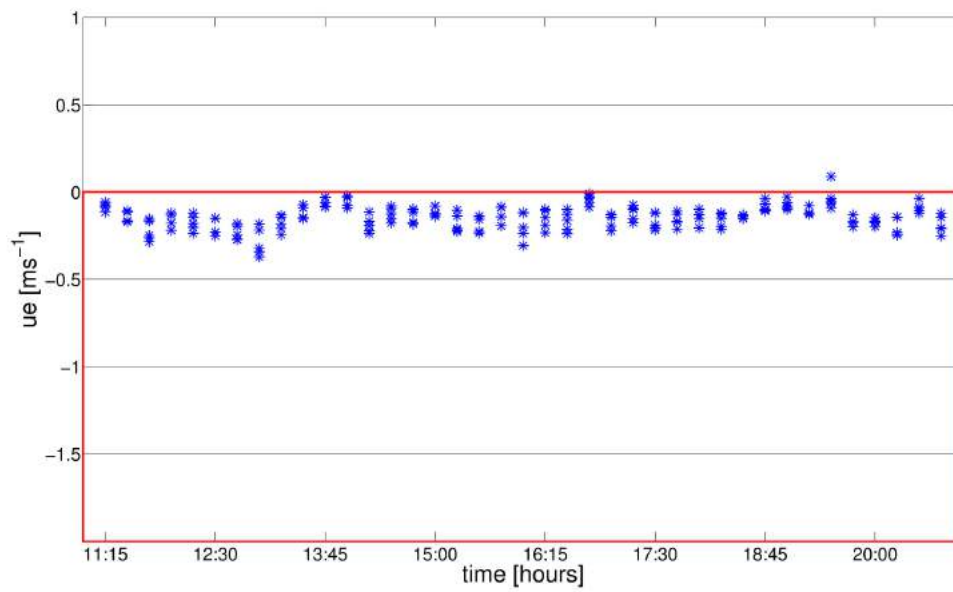obtained through XBeach model simulation.

Figure 5.22: Rip current behaviour in rip generation sector 3 (S.3).

5.3.3 09th-11th November 2016

Conversely to the event described in the previous paragraph, this storm is characterised by waves direction from SW (section 4.5.6) and, for this reason, the beach is more exposed. In Figure 5.23, we notice the absence of protected sectors (conversely to what described in the previous section). Rip currents occur in four rip current generation sectors (depicted in Figure 5.23). From West to East, the first three rip generation sectors (S.1, S.2, and S.3 in Figure 5.23) are superimposable with sectors described for the October event. A further rip generation sector (S.4) is located at the extreme border of the beach eastern sector (Figure 5.23).
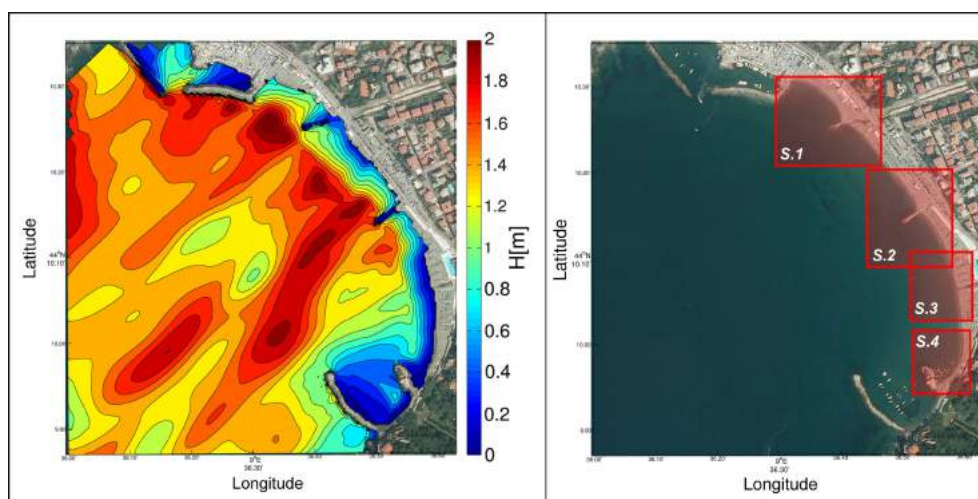

Figure 5.23: Left panels: waves propagation within Levanto bay. Right panel: Beach sectors (S.1, S.2, S.3, S.4) where rip currents occur.

Two rip currents occur on both sides of the groyne in sector 1 (Figure 5.24), and their flow determines an incident waves height decrease (in front of groyne head) (Figure 5.24). Rip current on the west side of the groyne shows an extended development over time, between 11:15 on 09th November and 10:30 on 10th November, with a stasis period between around 14:30 and 19:30 on 09th November. This rip is characterised by an average velocity of 0.31 ms^{-1} and peak values around 1.2 ms^{-1} (Figure 5.25). Conversely, rip current on the east side of the groyne occurs over a more limited time range; between 13:35 and 21:30 of 09th November. This phenomenon is characterised by an average velocity of 0.31 ms^{-1} (as the rip on the west side of the groyne) and peak values around 0.6 ms^{-1} (Figure 5.26).

Figure 5.24: Rip currents development in sector 1 (S.1 in Figure 5.23). Results obtained through XBeach model simulation.
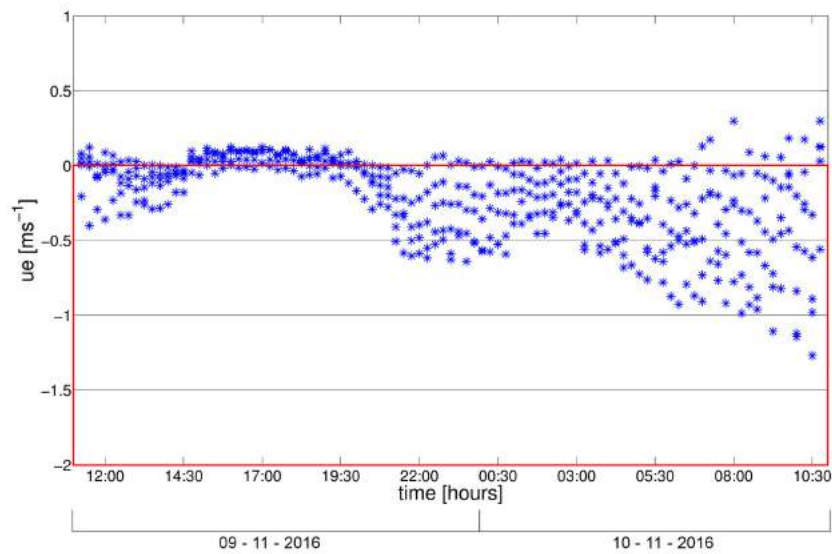
Figure 5.25: Rip current behaviour on the west side of the groyne, rip generation sector 1 (S.1).

Figure 5.26: Rip current behaviour on the east side of the groyne, rip generation sector 1 (S.1).

Proceeding towards the East, we find the rip generation sector 2 (Figure 5.27). Here, again, two rip currents occur on both sides of the groyne, determining an incident waves hight decrease in concomitance to their flow. Rip current on the west side of the groyne is characterised by a highly extended development over time. This rip occurs between 20:00 on 09th November and 11:45 on 11th November, showing an intensity increase after 07:00 on 10th November. This rip current shows an average velocity of 0.59 ms^{-1} and peak values around 1.5 - 1.7 ms^{-1} (Figure 5.28). Also, the rip on the east side of groyne shows a behaviour characterised by a persistent development over time (between 20:00 on 09th November and 11:45 on 11th November) (Figure 5.29). This rip shows an average velocity of 0.62 ms^{-1} and peak values around 1.4 ms^{-1}.
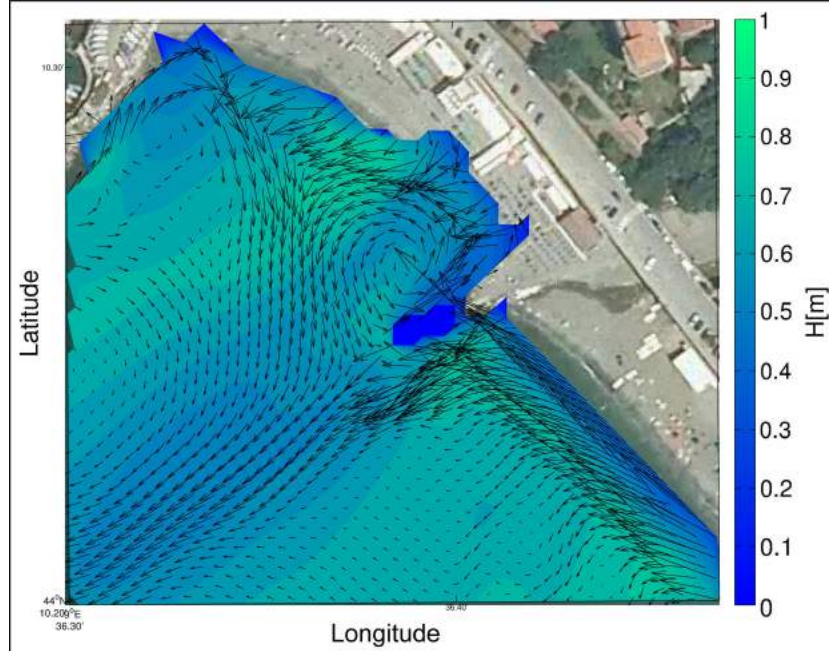

Figure 5.27: Rip currents development in sector 2 (S.2 in Figure 5.23). Results obtained through XBeach model simulation.

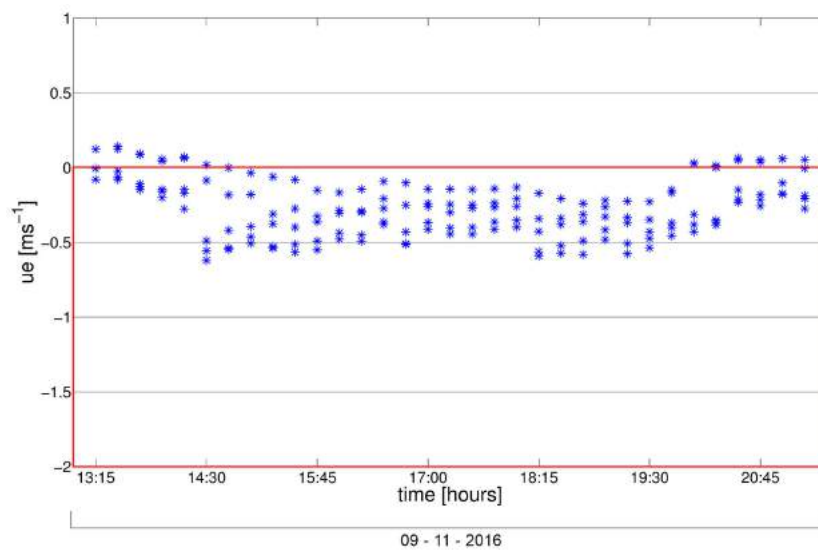**Figure 5.28:** Rip current behaviour on the west side of the groyne, rip generation sector 2 (S.2).
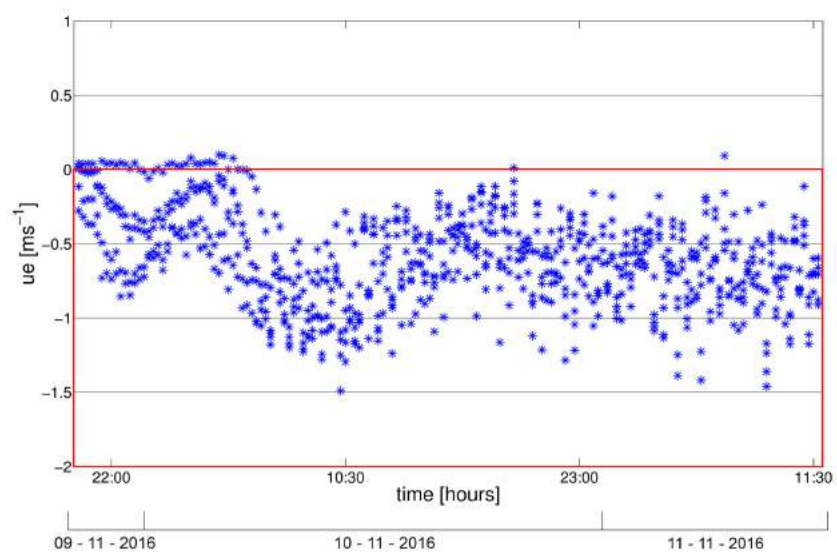
Figure 5.29: Rip current behaviour on the east side of the groyne, rip generation sector 2 (S.2).

Figure 5.30 shows the development of a rip current in sector 3, where hard structures (e.g. groynes) are not present. The flow rotation close to the shoreline is evident, as well as a wave height decrease in concomitance with the rip flow. The rip current generation occurs in the time range between 11:45 on 09th November and 05:30 on 10th November, with a stasis period between 14:30 and 19:15 on 09th November. The rip flow is characterised by an average velocity of 0.28 ms^{-1} and by peak values around 0.7 ms^{-1} (Figure 5.31).

Figure 5.30: Rip currents development in sector 3 (S.3 in Figure 5.23). Results obtained through XBeach model simulation.
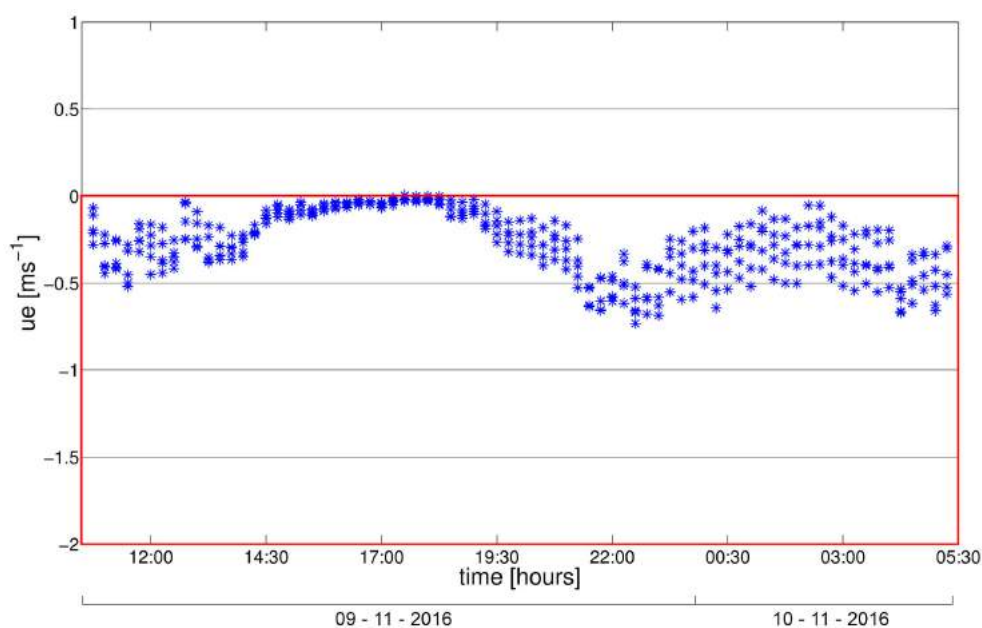
Figure 5.31: Rip current behaviour in rip generation sector 3 (S.3).

The last observed rip current is depicted in the Figure 5.32. This rip phenomenon is located in the rip generation sector 4, close to the hard structure known as "La Pietra". This phenomenon shows a persistent development over time, between 21:45 on 09th November and 11:45 on 11th November. Their flow is characterised by an average velocity of 0.28 ms^{-1} (with an increasing trend over time) and by peak values between 0.8 - 1.2 ms^{-1} (Figure 5.33).
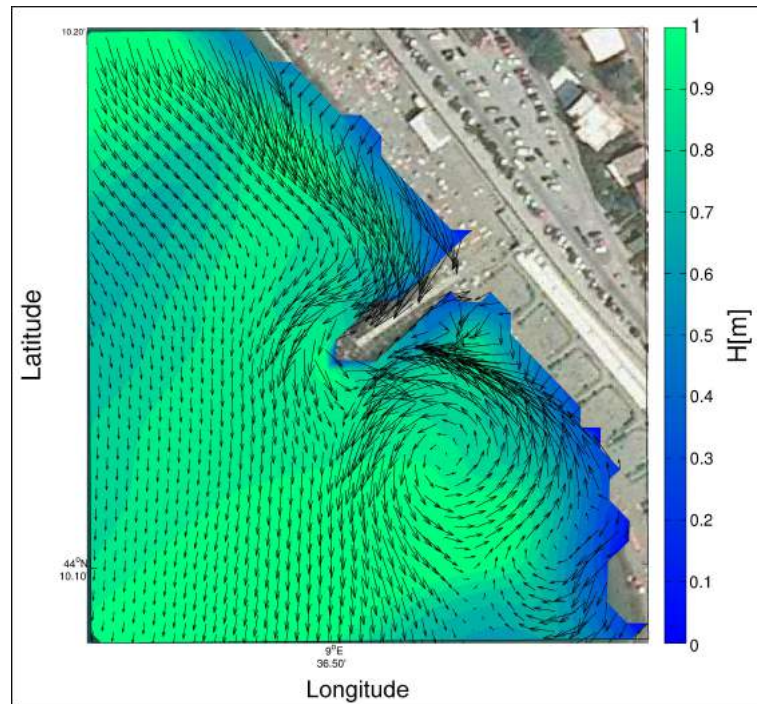
Figure 5.32: Rip currents development in sector 4 (S.4 in Figure 5.23). Results obtained through XBeach model simulation.
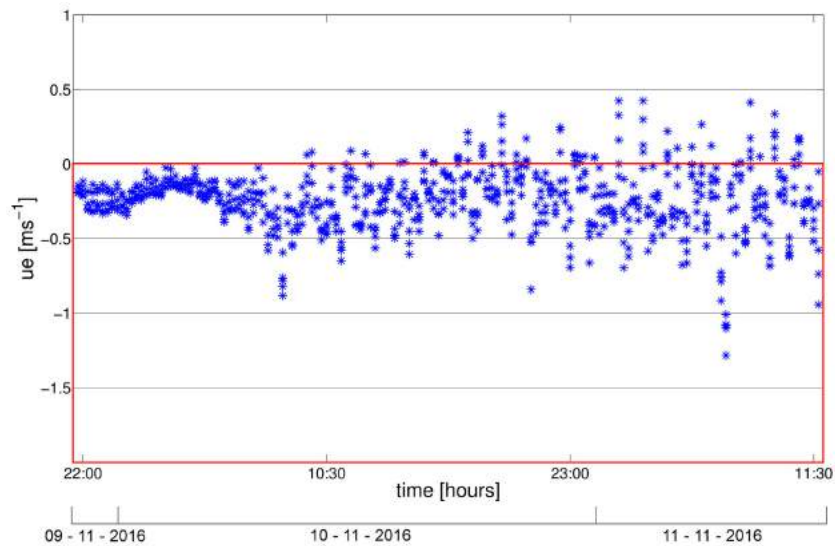
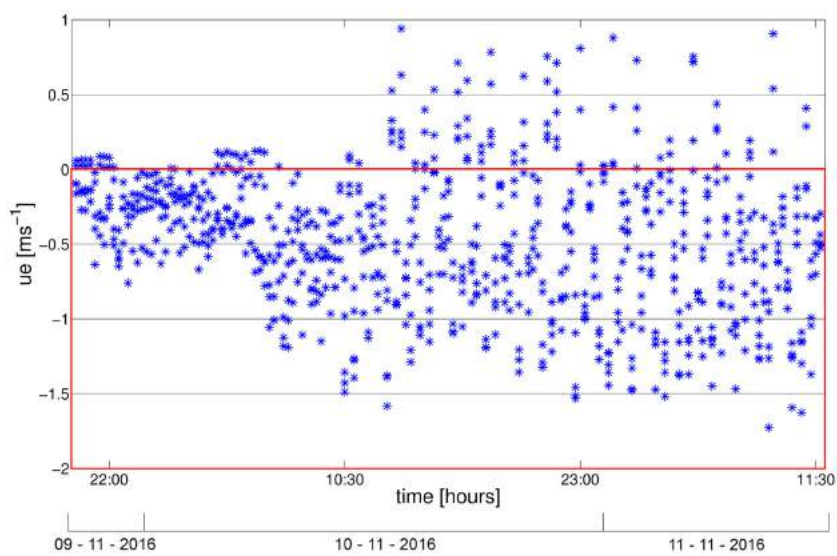**Figure 5.33:** Rip current behaviour in rip generation sector 4 (S.4).

5.3.4   05th March 2017

This last modelled event is characterised by waves direction from SW (section 4.5.6) and it is the most energetic event among those considered. The waves propagation within the bay (Figure 5.34) is comparable with waves propagation observed for November storm. The entire extension of the beach is exposed to incident waves, and the rip currents generation sectors (Figure 5.34) are superimposable with rip sectors observed throughout the November event.
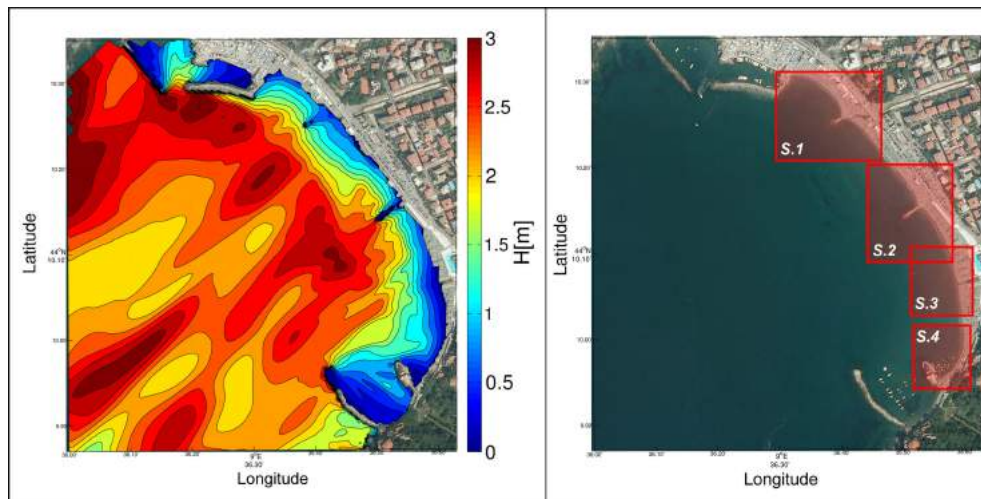
Figure 5.34: Left panels: waves propagation within Levanto bay. Right panel: Beach sectors (S.1, S.2, S.3, S.4) where rip currents occur.

Two rip currents occur in sector 1, on both sides of the groyne (Figure 5.35). Rip current on the west side of groyne develops between 01:00 and 23:00, showing a persistent development over time. This rip phenomenon is characterised by an average velocity of 0.57 ms^{-1}, and by peak values around 1.5 ms^{-1} (Figure 5.36). Rip current on the east side of groyne (Figure 5.37) shows somewhat different behaviour. This rip current occurs between 07:00 and 17:00, showing a limited development over time (if compared to the phenomenon on the other side of the groyne), and its average velocity is 0.38 ms^{-1}, with peak values around 1 ms^{-1}.
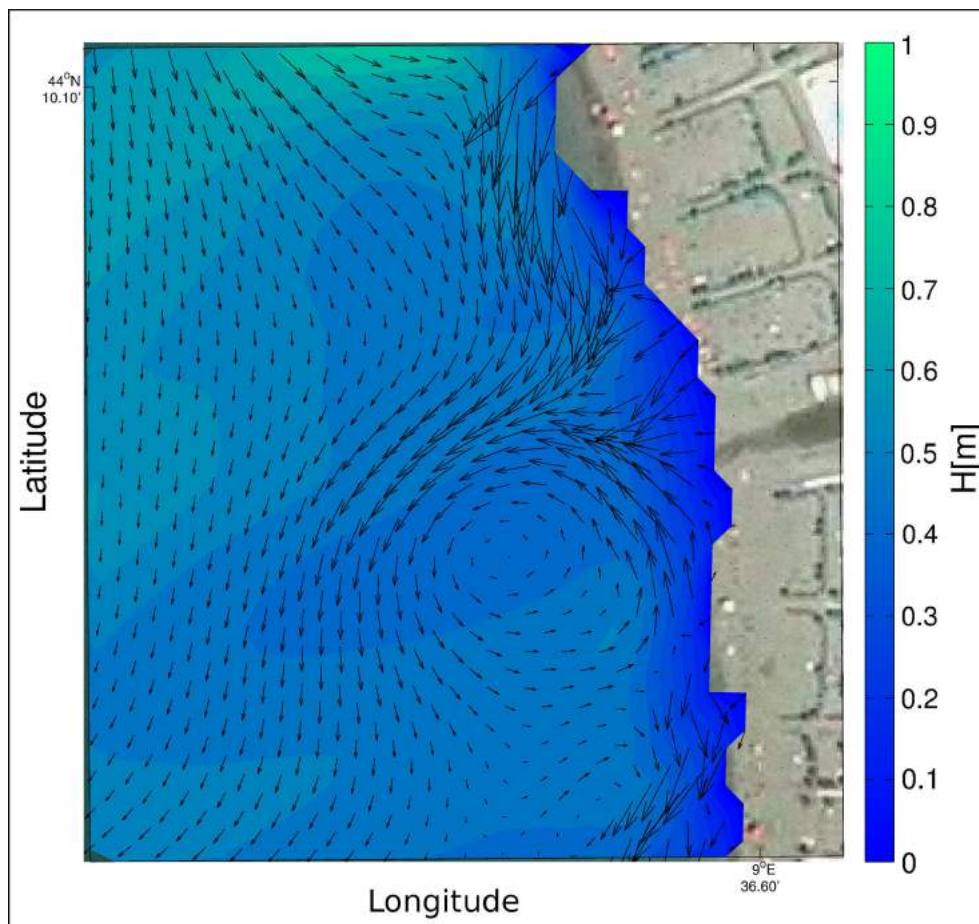

Figure 5.35: Rip currents development in sector 1 (S.1 in Figure 5.34). Results obtained through XBeach model simulation.

**Figure 5.36:** Rip current behaviour on the west side of the groyne, rip generation sector 1 (S.1).
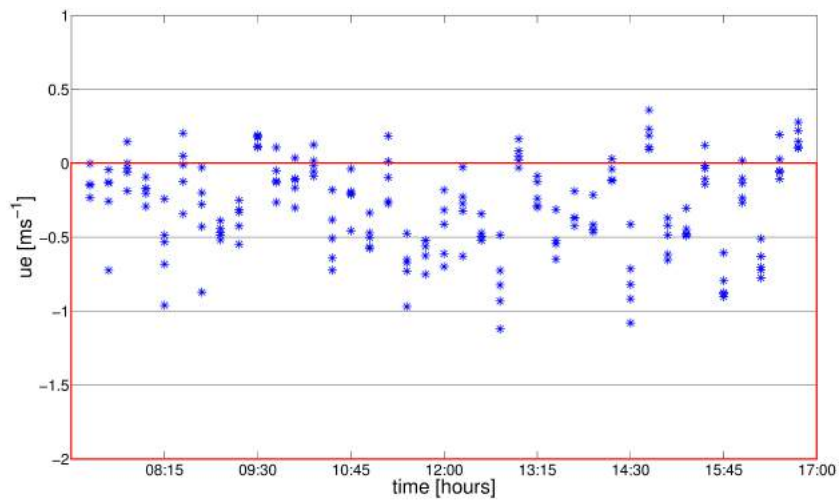
Figure 5.37: Rip current behaviour on the east side of the groyne, rip generation sector 1 (S.1).

Proceeding towards the East, we find sector 2, where two rip currents occur
on both sides of the groyne (Figure 5.38). Moreover, a waves height decrease,
associated with rip currents flow, is evident (Figure 5.38). Rip current on the
west side of groyne occurs between 00:00 and 14:00, and it is characterised by
an average velocity of $0.50 \, \mathrm{ms^{-1}}$ and peak values around $1.5 \, \mathrm{ms^{-1}}$ (Figure 5.39).
Differently, rip current on the east side of the groyne shows a more extended
development over time (Figure 5.40). This phenomenon occurs between 00:00
and 23:00 and, between 09:00 and 14:30, shows a significant decrease in its
intensity. This rip current is characterised by an average velocity of $0.60 \, \mathrm{ms^{-1}}$
and peak values around 1.3 - $1.5 \, \mathrm{ms^{-1}}$ (Figure 5.40).
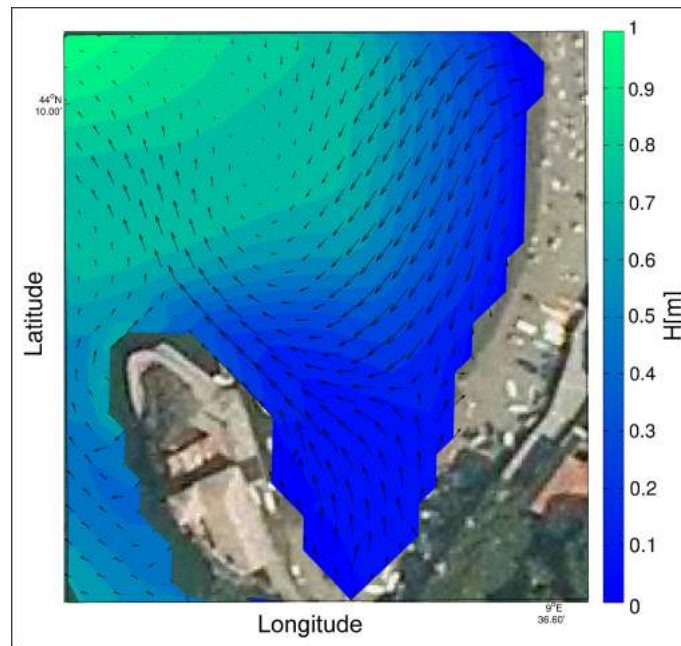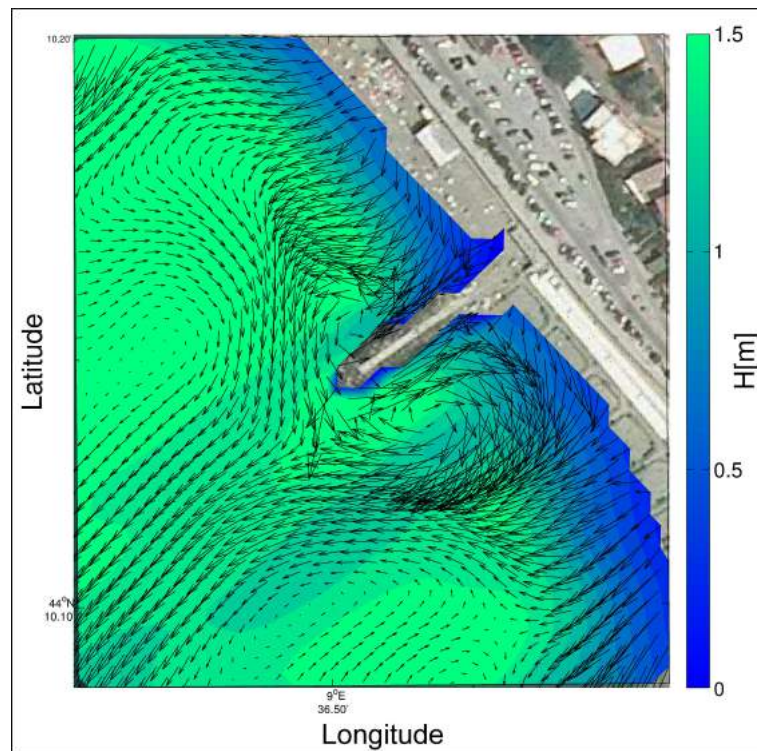

Figure 5.38: Rip currents development in sector 2 (S.2 in Figure 5.34). Results
obtained through XBeach model simulation.
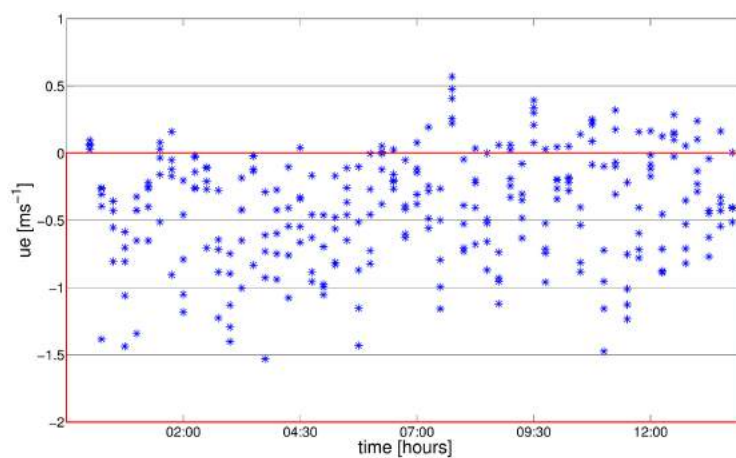
Figure 5.39: Rip current behaviour on the west side of the groyne, rip generation sector 2 (S.2).
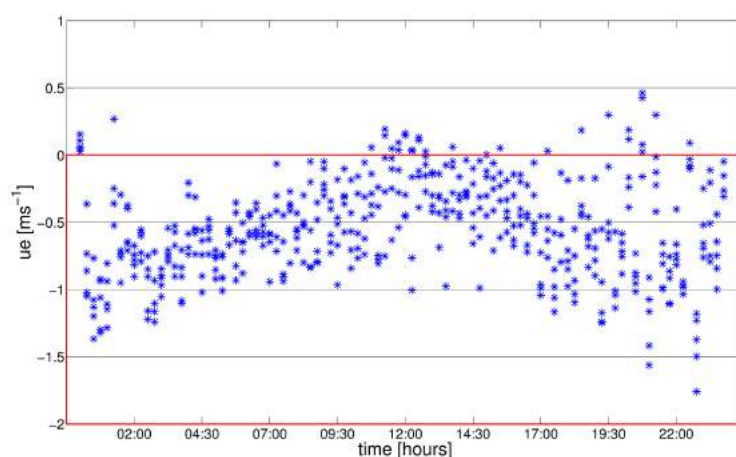
Figure 5.40: Rip current behaviour on the east side of the groyne, rip generation sector 2 (S.2).

Advancing towards the East, we observe the rip generation sector 3 (Figure 5.41), where the absence of rigid boundaries characterises the rip currents development (as observed in the other simulated events, sections 5.3.2 and 5.3.3). In this sector, both the flow rotation near the shoreline and the incident waves height decrease (related to rip current flow) is evident (Figure 5.41). The

observed rip current is characterised by an average velocity of 0.51 ms^{-1} and peak values around 1.3 ms^{-1} (Figure 5.42).
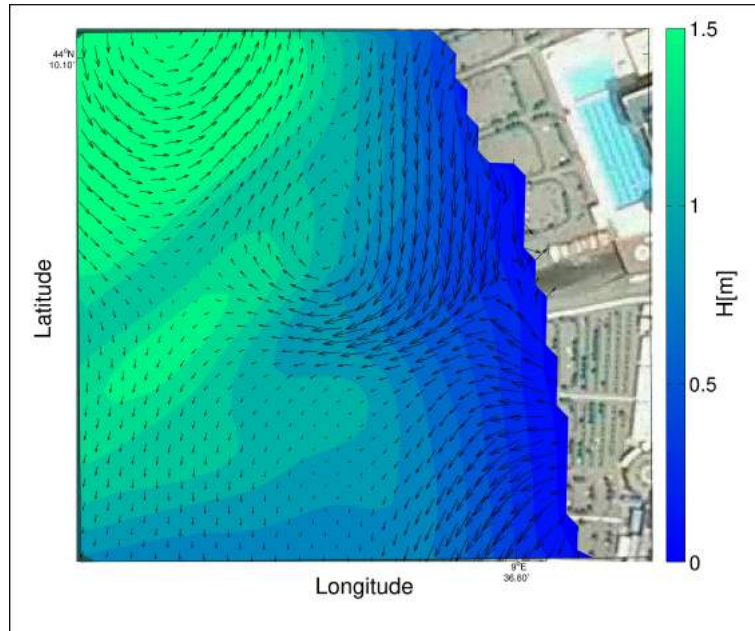
Figure 5.41: Rip currents development in sector 3 (S.3 in Figure 5.34). Results obtained through XBeach model simulation.
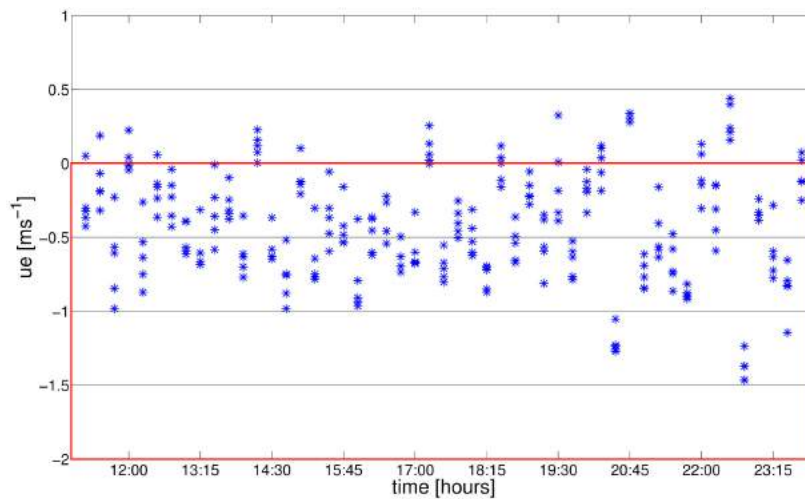
Figure 5.42: Rip current behaviour in rip generation sector 3 (S.3).

Finally, in the easternmost sector of the beach, we find the rip generation sector 4 (Figure 5.43). A rip current is evident close to the hard structure known as "La Pietra" (as described for November event, section 5.3.3) (Figure 5.43). This rip current occurs between 12:00 and 23:15, showing a significant velocity increase after 17:00 (Figure 5.44). This rip shows an average velocity of 0.46 ms^{-1} and peak values around 1.5 - 2 ms^{-1} (Figure 5.44).
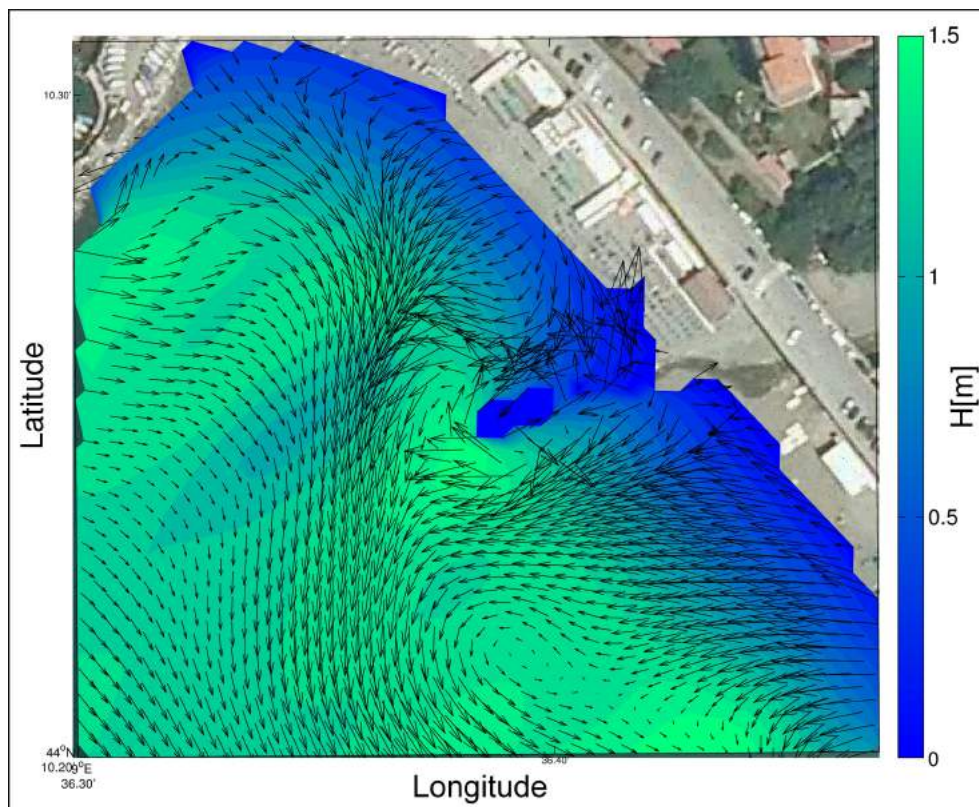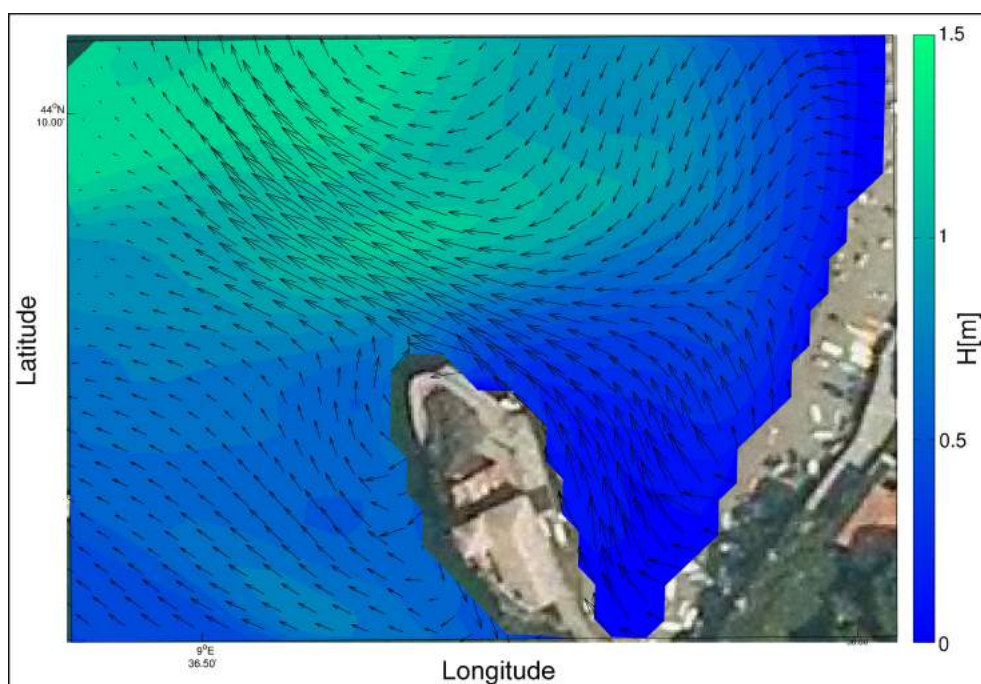

Figure 5.43: Rip currents development in sector 4 (S.4 in Figure 5.34). Results obtained through XBeach model simulation.
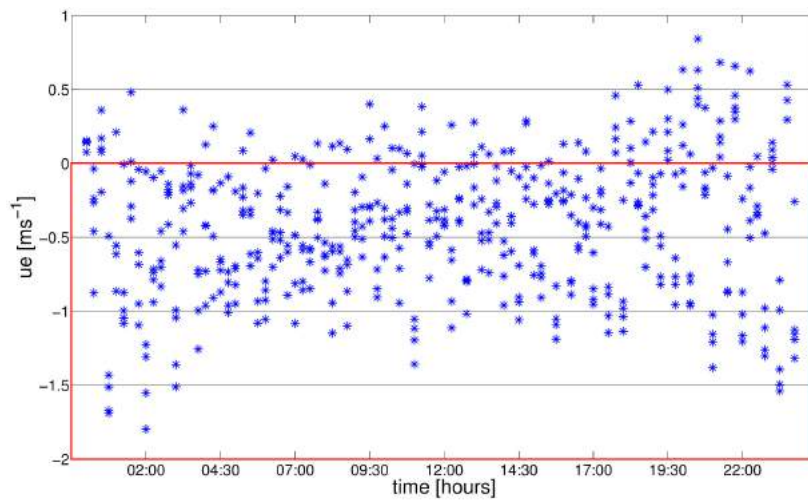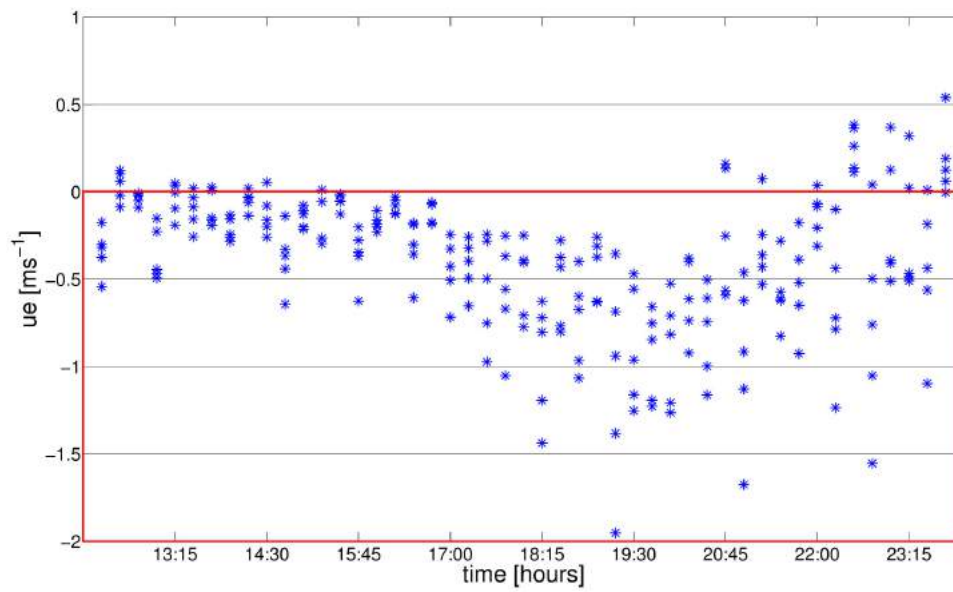
Figure 5.44: Rip current behaviour in rip generation sector 4 (S.4).

5.3.5 Sea-level change and rip response

As described in section 4.5.7, we used wave boundary conditions of the event on 09th-11th November 2016 to evaluate the possible SLR role on rip currents dynamics.
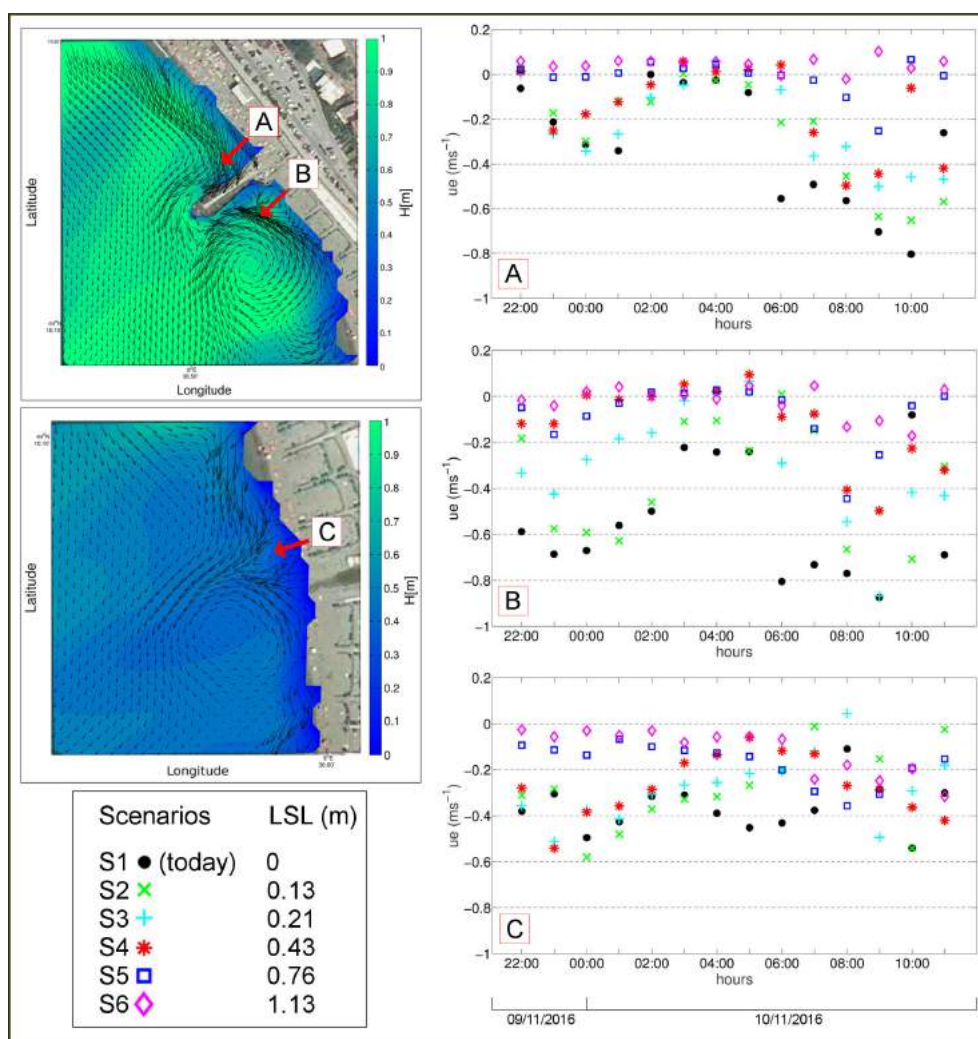
Figure 5.45: Sea-level (LSL) projections and effects on rip currents behaviour. Left panels (top to bottom): rip currents generation and location under present sea-level conditions (S1), and list of LSL scenarios (S1, S2, S3, S4, S5, S6). Right panels: Rip currents intensity change in several LSL scenarios.

When SLR is factored into the models rip currents change (compare *ue* values of considered rip currents under different SLR scenarios, Figure 5.45). A rip currents intensity decrease is depicted clearly in Figure 5.45, and it is evident under higher sea-level scenarios (S5 and S6). In Figure 5.46, we show the difference between the average *ue* calculated across the entire simulations with *ue* as calculated in S1 (modern sea level). This elaboration shows that the considered rip currents have not only a different intensity, but they are also characterised by a significant difference in their spatial pattern. In maps of differences (Figure 5.46), we can observe that rip current at point *a* show a clear decrease (around to 0.30 ms^{-1}) in its intensity for LSL scenarios S5 and S6 (Figure 5.46, panels E and F). Rip current at *b* show a velocity decrease for each sea level rise scenario (Figure 5.46, panels B, C, D, E, F), with decrease values from $\approx$ 0.10 ms^{-1} (in scenario S2, Figure 5.46, panel B) to $\approx$ 0.37 ms^{-1} (in S6 scenario, Figure 5.46, panel F). Rip current at point *c* show the lesser effects of sea level rise on its dynamics, and these are presents in scenarios S5 and S6 with decrease values of $\approx$ 0.08 and $\approx$ 0.17 ms^{-1} respectively.
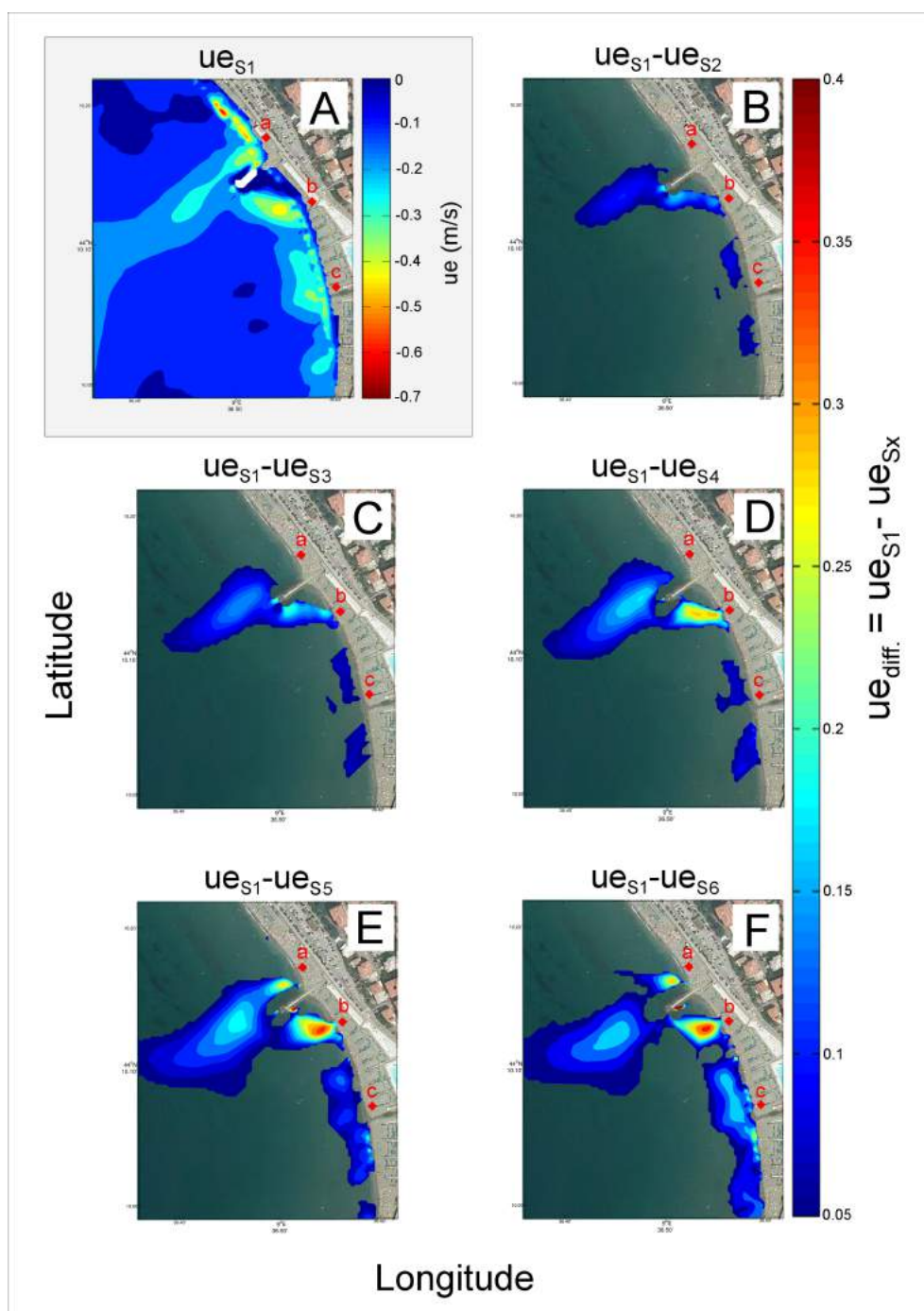
Figure 5.46: Panel A. Average values of *ue* in scenario 1 (S1). panels B, C, D, E, F. Difference between *ue* magnitude in scenario 1 (S1) and *ue* magnitude under sea-level change scenarios (S2, S3, S4, S5, S6).

Chapter 6

Discussion

6.1 Morphological analysis

The interdependence between water motion and bottom morphology is a key factor of coastal dynamics (Short, 1999). For this reason, we executed a seabed morphological analysis to understand the local dynamics, and to evaluate the role of rip currents in it. In details, morphological analysis was performed through GIS analysis by applying spatial analysis tools. Our idea was to compare the beach morphology before and after winter, to identify morphological features related to rip currents development. The comparison allows the identification of some interesting features and, in particular, three erosion areas have captured our attention. These erosive phenomena show a cross-shore development and are located on both sides of the groyne between the central and eastern sector of the beach, and in the central area of the beach eastern sector. This fact is important because the relation between submarine morphologies and rip currents development is a well-known character (Sonu et al., 1967; Bowen, 1969; Sonu, 1972; Hino, 1974; Noda, 1974; Dalrymple and Lozano, 1978; Wright and Short, 1984; Lippmann and Holman, 1990; Chen

117

et al., 1999; Short, 1999). So, according to cited bibliography, we can describe the observed erosive phenomena as "rip channels", well-known morphologies associated to rip currents development. Moreover, the presence of structures, such as groynes, is a recognised rip currents trigger mechanism (Castelle et al., 2016; Scott et al., 2016). Thus, the presence of erosive channels on both sides of the groyne is an ulterior support to describe these morphological forms as "rip channels". Moreover, according to Castelle et al. (2016), the rip channel recognised in the central area of the beach eastern sector is probably associated with the development of a bathymetrically-controlled rip. Also, the results of the morphological analysis are conforming to results of coastal monitoring and coastal modelling. In conclusion, it can be said that the rip currents are amongst the driving forces in the morphodynamic processes within Levanto bay.

6.2   Video monitoring

Coastal video monitoring was used in this study for the rip currents identification along the beach of Levanto. Also, the rip currents individuation process was supported by image processing through application of BeachKeeper *plus* (Brignone et al., 2012), which is a dedicated software for beach video monitoring. As described in the results section, within the time interval included between October 2016 and March 2017, three events were selected. Several rip currents were observed during the considered storms and, based on the rip currents classification of Castelle et al. (2016), several rip currents types were recognised. Some rip currents, classifiable as boundary-controlled rip currents, were clearly identified during the events on 13th - 14th October 2016, 09th - 11th November 2016 and 05th March 2017. This rip currents type is often triggered

by the presence of hard structures (e.g. groynes), and this is confirmed by the individuation of rip currents on both sides of the groyne between the central and eastern sector of the beach. Another rip current, which could be classified as a bathymetrically-controlled rip (due to its fixed location during different events), was identified during the events on 09th - 11th November 2016 and 05th March 2017. The classification of the phenomenon was possible thanks to its fixed location during the several considered storm. In general, the rip currents are identified observing the contrast of intense white foam (due to the waves breaking) versus the flat, "dark" waters of the rip currents flow. Most of the observed rip currents were identified through this feature. However, during the event of 13th - 14th October 2016, we noticed a "tracer effect" caused by the suspended sediment, which highlights the rip current development on the west side of the groyne. Moreover, during the event of November 2016, we observed a series of small rip currents on the eastern sector of the beach. These phenomena are characterised by a development imposed on cuspidate morphologies, forced by the swash dynamics. Based on observed data, we can classify these phenomena as mini-rips (Russell and McIntire, 1965) or swash rips (Dalrymple et al., 2011). Thanks to coastal video monitoring we were able to select storm events for this research project. However, during work, some issues concerning the rip currents video monitoring emerged. The rip currents are evident when they are highlighted by foam, or in case of "tracers" (e.g. suspended sediment). In absence of foam or "tracers", rip currents can be invisible to the video monitoring system. Moreover, it is necessary to remember that the rip currents individuation, even in the case where foam is present in the surf zone, is not always univocal. For example, rip currents are sometimes characterised by an area with flat "dark" waters across the foam of the surf zone (Castelle et al., 2016), and, in other cases, by the seaward foam transport (Murray,

2004). Furthermore, rip currents individuation is uncertain during extreme storm events, where rip development can be hidden by the chaotic state of the surf zone. Despite these issues, the video monitoring remains a reliable method for rip currents monitoring. In particular, Timex and Variance images have proved to be a reliable support in the rip currents individuation process, solving several cases of uncertain identification. Moreover, in our study site, the rip monitoring through direct methods (e.g. fixed current meters) is harder, due to operative and logistic problems. For example, Levanto beach has a very high tourist vocation and from April to September/October the beach is very crowded. In autumn and winter, the beach is frequented by surfers and fishers (both anglers and spearfishers) operating in the surf zone. For these reasons, fixed tools located in the surf zone could be subject to damages (volountary or not). Also, the presence of hard structures (e.g. the structure of a current meter) could be a hazard source for bathers (possible hits). Understandably, these problems are not present with video monitoring. In our study case, the video monitoring system allows the collection of a large amount of data (video data), allowing the clear identification of several rip currents phenomena.

6.3   Model results

6.3.1   Rip currents dynamics

Coastal modelling is commonly used for coastal research activities (Roelvink, 2011) and, in this study, we used the XBeach model (Roelvink et al., 2009) for the evaluation of rip currents development in the case of several wave boundary conditions. The field measurements of rip currents are logistically difficult to obtain (Brander and MacMahan, 2011), both for the surf zone dynamic features (described in section 2.3) and for operative issues (as described in

the previous section). For these reasons, we chose the coastal modelling as a tool for rip currents assessment within Levanto bay. The modelled events include one event with wave direction from SE (13th - 14th October 2016) and two events from SW (09th - 11th November 2016, 05th March 2017). These waves boundaries conditions are common along the Ligurian coasts, and, for this reason, they can be considered as representative cases. As the first step, we consider the waves propagation within Levanto bay, which is an essential component for the rip currents generation. Starting by the event on 13th - 14th October 2016, we observe that the Punta Mesco Promontory (at the East of the Levanto Bay) determines the presence of a protected stretch in the easternmost sector of the beach. Comparing the beach sectors where rip currents occur, it is evident the absence of rip currents along the more protected stretch of the beach (see Figure 5.14 in section 5.3.2). Conversely, during the SW storm, rip currents also occur in the easternmost sector of the beach eastern sector (see Figure 5.23 in section 5.3.3 and Figure 5.34 in section 5.3.4). Given the different wave boundary conditions, we focus our attention on the rip currents development and, according to the rip currents classification of Castelle et al. (2016), on their possible classification. Starting from the western border of the beach, we find the beach western sector: a littoral portion included between a small harbour (at West) and a groyne (at East), and where a rip current occurs during the all simulated events. This sector could be described as a little artificial embayed (or pocket) beach, where rigid boundaries dominate the coastal circulation. According to Castelle et al. (2016), the observed rip can be classified as an embayed-cellular rip, triggered by a combination of several factors, such as "shadowing, deflection, and channelisation to various degrees, together with the alongshore circulation within the embayment being additionally constrained by the alongshore embayment length" (Castelle

et al., 2016). This rip currents type is often described as common under storm wave conditions (Loureiro et al., 2012), and due to their large spatial scales, they are defined as "mega-rip" (Loureiro et al., 2012; Wright and Thom, 1977; Short, 2007). In our case, it is interesting to note that the rip occurs in a small "anthropic embayed beach". The results show that this phenomenon occurs in all modelled events, but with different intensities. During the events of 09th - 11th November 2016 and 05th March 2017, the rip shows highest velocity values, whereas, during the event of 13th - 14th October 2016, shows lower values. This circumstance is easily explained through the different wave boundary conditions (storm events of November and March are more energetic than October event). Moving on the east side of the groyne, but remaining into rip sector S.1, we encounter another rip phenomenon occurred during all model simulations. The presence of the groyne, according to Castelle et al. (2016), make possible to classify this phenomenon as a boundary-controlled rip current. Moreover, about the October event, we can also classify this rip current as a shadow rip. Due to the incidence waves angle, this further classification is only suitable for the October event where rip current occurs on the upwave side of the groyne. Conversely, other modelled storms are characterised by waves direction from SW, with wave fronts approaching parallel to the coast. According to Nelko and Dalrymple (2011), this rip current shows the highest intensities during the March event (which is the stronger event), whereas, during the events of October and November, velocity values are similar. This last point is interesting because the wave heights in the area where the rip current occurs are different for the two storm events. Modelling of the October storm shows lower wave heights than November simulation. This difference is caused by the different interaction between the coast and incident waves, in turn, triggered by the different incident waves directions. Then, we

can deduce that rip currents with the same intensity can also occur under different wave boundary conditions, and this point must be considered in terms of rip forecasting. Shifting attention on the second rip generation sector (S.2), we find the genesis of other two rip phenomena. This sector, located inside the video monitoring area, is characterised by the presence of a groyne. In details, two rip currents on both sides of the groyne were observed and, according to (Castelle et al., 2016), these phenomena are classifiable as boundary-controlled rips. These rip currents show a similar behaviour under wave boundary conditions of November and March. This point is interesting because the events show the same waves direction, but the March storm is stronger than November storm. Therefore, we can suppose a "superior limit" in rip currents intensity, caused by the local boundary conditions (both hydrodynamical and morphological). These phenomena were also observed in the model simulation of the October event. In this situation, the rip currents velocities are lower, and this is probably related to the lower wave heights into the surf zone. Furthermore, observing the incidence wave angles of October event, the rip current on the west side of the groyne (downwave side) can be defined as a deflection rip (Castelle et al., 2016). Conversely, the rip current on the east side of the groyne (upwave side) is different. It is not very close to the groyne, and its behaviour does not appears strictly related to the structure itself. According to Castelle et al. (2016), this rip could be classified as a channel-flash rip but, its classification is uncertain, and we do not exclude its development is related to the groyne. In the central area of the beach eastern sector, always inside the video monitoring area, we observed another rip phenomenon (sector S.3). According to Castelle et al. (2016), and based on its features, this rip current can be classified as a bathymetrically-controlled rip. This classification is also supported by results of the morphological analysis (which highlights a

rip channel at the same spot), and by results of the video monitoring (which has documented a rip phenomenon in the same spot). As widely described in literature (Nelko and Dalrymple, 2011; Loureiro et al., 2012), the velocities of this rip current are related to the wave boundary conditions. In details, we observed the highest values for the March event, intermediate values for the November event and lowest values for the October event. Because of its behaviour, this rip can be indicated as the "more classical rip" observed in this study. Finally, in the easternmost area of the beach eastern sector (sector S.4), we find the last observed rip current of this study. This rip phenomenon was observed under November and March wave boundary conditions and did not occur under October wave boundary conditions. This feature is easily explained with the fact that this littoral portion is protected from SE storms. Through the coastal video monitoring, we also identified rip phenomena classifiable as mini-rips or swash rips (section 6.2). Due to their limited extension, intensity, and irregular development, these phenomena were not reproducible through coastal modelling. Moreover, because of their limited extension, the highest resolution of the computational grid would be necessary, however the model operability would result compromised by a too dense resolution of the computational grid. As aforementioned, we can affirm that the rip currents are an essential component of the coastal dynamics within Levanto bay, and the beach of Levanto can be considered as dominated by cross-shore phenomena. Also, this consideration is based on what observed through coastal video monitoring and seabed morphological analysis. Moreover, the observed results lead the attention on the rip currents role in micro-tidal environments, such as along the Mediterranean coasts. This aspect is a key point because the Mediterranean rips are commonly considered "less important" than rip currents along the oceanic coasts. Most of the observed rip currents were classified

based on the rip currents classification proposed by Castelle et al. (2016), and this is an important link between Mediterranean rip and oceanic rip. The boundary-controlled rip currents showed peak velocities around 1 - 1.5 ms^{-1}, and they are the strongest observed phenomena. These values are comparable with those developping in oceanic environments (Short, 1999), and highlight issues concerning the rip hazard and beach safety. For example, Levanto beach has a very high touristic vocation, with thousands of bathers during the summer season. All these people are potentially exposed to rip hazard, then it is evident how risk is often underestimated.

6.3.2   Sea-level (LSL) projections and rip responses

Sea-level changes are the major effect of climate change (Mimura, 2013), and they are a crucial factor for the future coastal areas management and protection (Marcos et al., 2012). The local sea-level projections (Kopp et al., 2014) are an essential tool to understand sea-level changes local implications, and to organise proper action planning. About coastal environments, we can affirm that the sea-level changes will lead to changes in the local coastal dynamics, and rip currents are among the most important phenomena that characterise the near-shore circulation. Also, they play an important role in coastal ecosystems (Shanks et al., 2010; Fujimura et al., 2014). In this study, we introduced a numerical approach to evaluate sea-level change effects on the rip currents behaviour along a Mediterranean beach. To achieve this goal, we considered the rip currents occurred under wave boundary conditions on 09th - 11th November 2016. We selected only one event, among those considered in this study, due to the computational time needed for each sea-level scenario. November event was chosen in reason of its wave boundary conditions. Levanto beach is not protected by SW storms (whereas beach is partially protected by the SE storms,

e.g. October event) and wave boundary conditions of November event are less
extreme than in March event (a less intense event allow a better point of view
on the rip currents behaviour under different sea-level scenarios). Finally, to
maintain a good degree of the model reilability, our attention was focused on
the rip currents inside the video monitoring area. Results showed that rip cur-
rents behaviour change under different sea-level scenarios, showing a general
decrease in their intensity (in response to a sea-level increase). Boundary-
controlled rips (close to the groyne) showed stronger responses under several
sea-level change scenarios, with very visible effects under extreme sea-level
rise scenarios (LSL rise $\geq$ 0.43 m). Boundary-controlled rips are triggered by
the presence of natural (e.g. headlands) or anthropogenic (e.g. groynes) rigid
structures (Scott et al., 2016), and its development is always characterised by
a very fixed location (physical boundaries exert a lateral bathymetric control
on the rip flow adjacent to them) (Castelle et al., 2016). These features in
their trigger mechanism are probably related to their strong responses under
different sea-level scenarios. Moreover, between the two considered boundary-
controlled rips (on the west and east side of the groyne), the rip current on the
east side shows a more pronounced response to sea-level change. Conversely,
to what observed for rip current on the west side of the groyne, this rip phe-
nomenon shows a clear response also under sea-level increase < 0.43 m. The
different response can be related to a different interaction, on the two sides
of the groyne, between the incident waves and the morphological boundaries.
However, this point is quite uncertain and worthy of further attention. More-
over, also the bathymetrically-controlled rip in the central area of the beach
eastern sector shows a response to sea-level change. The rip current behaviour
changes under extreme sea-level rise scenarios (LSL $\geq$ 0.76 m), while the rip
response under moderate sea-level rise scenarios is limited and almost negli-

gible under smaller sea-level rise scenario. The different response is probably related to its different trigger mechanisms. These rips are relatively persistent in space and time (Castelle et al., 2016), but their development is not "fixed and stable" like for the boundary-controlled rips (controlled by rigid boundaries). The results of this study showed that under gradual sea-level rise scenarios, rip currents show a generalised decrease in their intensity. The major sea-level rise effects on rip currents dynamics were recorded under extreme sea-level change scenarios (LSL $\geq$ 0.76 m). These responses can be caused by a change in the local hydrodynamic regime, coupled with a different morphodynamic response. The beach of Levanto is characterised by a very high anthropization degree (groynes, piers, and seawall), and this feature restricts the natural morphodynamic response of the beach. Moreover, it is possible that the sea-level rise determines a series of cascade effects, interrelated among them, leading to the disappearance of the geomorphologic forms that trigger (and support) the rip currents themselves. However, we must highlight some "issues" that emerged throughout this research project. The main problem is the significant difference between the time scale of the investigated phenomena (sea-level rise and rip currents). This huge difference makes very hard to understand the relations between phenomena, and further studies would be necessary for the better understanding of the hydro-morphodynamic forces driving the rip responses under sea-level change scenarios. Finally, it is important to highlight that the changes in the rip current development may be a severe problem for the coastal environment, due to the essential role played by these phenomena. For example, a generalised decrease of the rip currents intensity along a physiographic unit will produce an important change in the sedimentary dynamics, with possible side effects on local ecosystems. Also, it should not be underestimated the rip currents role in the larval recruitment, nutrient transport,

pollutants transport and heat exchange between coastal and offshore areas.

Chapter 7

Conclusions

In this thesis, we proposed an accurate study on the rip currents dynamics within a micro-tidal embayed beach of the eastern Liguria. Research activity was conducted through an integrated application between several research methodologies. This approach allowed to obtain an accurate description and analysis of the investigated phenomena. In details, we illustrate in this section the main conclusions of the PhD project.

According to the results, the cross-shore currents are driving processes within the Levanto bay. In details, rip currents were identified through coastal video monitoring, and they were reproduced through coastal modelling. Moreover, evidences of the rip currents development were also observed through the seabed morphological analysis, thanks to the identification of some rip channels. Some modelled rip currents showed velocity values comparable with those in oceanic environments (around 1.5 ms^{-1}), and this feature highlights their role along the considered stretch of coast. For example, the presence of these phenomena will be considered for the annual beach nourishments planning, in order to avoid seaward sediments transport. Furthermore, due to the

well-known rip currents role in nutrients transport, pollutants dispersion, heat exchange and larval recruitment (Shanks et al., 2010; Fujimura et al., 2014), we can also affirm that the presence of cross-shore phenomena influence the local ecosystems. All these points will be essential and will be considered for the correct application of an integrated strategy for coastal management.

Remaining on the velocity data, we can also conclude that the rip phenomena in micro-tidal environments were often underestimated also from the beach safety point of view. We observed rip currents velocities around 1.5 ms^{-1}, and this is a clear evidence to understand how the rip current hazard is often underestimated along the Mediterranean coast. Moreover, Levanto beach is a recognised destination for seaside tourism, with thousands of people potentially exposed to the rip current hazard. Therefore, this thesis is a solid starting point to work on a rip currents forecasting method for the rip currents risk prevention and management.

The rip currents observed in this work have been described and classified using the rip currents classification proposed for oceanic environments. However, sometimes, the rip currents classification as proposed was difficult to apply, and this may be related to the different boundary conditions that characterise the Mediterranean environments and the oceanic environments. For this reason, an important point of this research is that of a possible (further) classification of the Mediterranean rip currents. This would also be useful for the rip currents forecasting process and risks prevention.

Forecasting of the sea-level change effects is one of the main future challenges for coastal scientists. In this project, we applied coastal modelling to

evaluate the future sea-level change effects on the cross-shore dynamics within Levanto bay. Results showed that, based on the sea-level projection to 2100, the rip currents behaviour could be modified, and a generalised decrease in the rip currents intensity was observed (under high sea-level scenarios in particular). This point might have significant impacts on coastal ecosystems. For example, due to the rip currents role in the larval recruitment process, a change in the rip development pattern might modify (or also compromise) the reproductive success of any marine species. These effects could also be transferred at superior levels, causing a series of cascading effects up to the whole coastal ecosystems. Moreover, in the case of fish species of commercial interest, the sea-level change effects might also be perceived by local coastal communities. These points might be considered for the correct future planning of the coastal zone management policies.

For what concerns the investigation methodologies, the use of coastal video monitoring allowed the collection of a considerable amount of data, counterbalancing the well-known issues in the rip currents field measurements. Moreover, also the seabed morphological analysis supported the video monitoring data. About the coastal modelling, XBeach model was a useful tool for rip currents investigation. The model was validated in the study area, and it allowed an accurate modelling, description and analysis of the rip currents phenomena in a Mediterranean context. In conclusions, the methodological approach used has proven suitable for the rip currents investigation, showing its usefulness in any context along the Mediterranean coasts.

References

Aagaard, T. and Masselink, G. (1999). The surf zone. In *Handbook of beach and shoreface morphodynamics*, pages 72–118. IEEE Computer Society Press.

Aagaard, T. and Vinther, N. (2008). Cross-shore currents in the surf zone: rips or undertow? *Journal of Coastal Research*, 24(3):561–570.

Abbate, E. (1969). *Geologia delle Cinque Terre e dell'entroterra di Levanto (Liguria Orientale). Memorie della Societa' Geologica Italiana*. Societa' Geologica Italiana.

Abbate, E., Fanucci, F., Benvenuti, P. B., Cipriani, N., Falorni, P., Fazzuoli, M., Morelli, D., Pandeli, E., Papini, M., Sagri, M., Reale, V., and Vannucchi, P. (2005). *Note Illustrative della CartaGeologica dItalia alla scala 1: 50.000, Foglio 248, La Spezia*. Regione Liguria, Dipartimento Ambiente Edilizia e Lavori Pubblici, Servizio Politiche dell'Assetto Territoriale, Genova.

Adbel-Aziz, Y. (1971). Direct linear transformation from comparator coordinates into object space coordinates in close-range photogrammetry. In *Proceedings of the Symposium on Close-Range Photogrammetry (American Society of Photogrammetry), 1971*, pages 1–18.

Alexander, P. and Holman, R. (2004). Quantification of nearshore morphology based on video imaging. *Marine geology*, 208(1):101–111.

Almar, R., Coco, G., Bryan, K. R., Huntley, D. A., Short, A. D., and Senechal, N. (2008). Video observations of beach cusp morphodynamics. *Marine geology*, 254(3-4):216–223.

Archetti, R. and Zanuttigh, B. (2010). Integrated monitoring of the hydro-morphodynamics of a beach protected by low crested detached breakwaters. *Coastal Engineering*, 57(10):879–891.

Austin, M., Scott, T., Brown, J., Brown, J., MacMahan, J., Masselink, G., and Russell, P. (2010). Temporal observations of rip current circulation on a macro-tidal beach. *Continental Shelf Research*, 30(9):1149–1165.

Austin, M. J., Scott, T., Russell, P. E., and Masselink, G. (2012). Rip current prediction: development, validation, and evaluation of an operational tool. *Journal of coastal research*, 29(2):283–300.

Bagnold, R. A. (1940). Beach formation by waves: some model experiments in a wave tank. (includes photographs). *Journal of the Institution of Civil Engineers*, 15(1):27–52.

Bart, L. J. C. (2017). Long-term modelling with xbeach: combining stationary and surfbeat mode in an integrated approach.

Benassai, G., Aucelli, P., Budillon, G., De Stefano, M., Di Luccio, D., Di Paola, G., Montella, R., Mucerino, L., Sica, M., and Pennetta, M. (2017). Rip current evidence by hydrodynamic simulations, bathymetric surveys and uav observation. *Natural Hazards and Earth System Sciences*, 17(9):1493–1503.

Bowen, A. J. (1969). Rip currents: 1. theoretical investigations. *Journal of Geophysical Research*, 74(23):5467–5478.

Brander, R. W. and MacMahan, J. H. (2011). Future challenges for rip current research and outreach. *Rip Currents, Beach Safety, Physical Oceanography and Wave Modeling, edited by: Leatherman, S. and Fletemeyer, J., CRC Press, Boca Raton, FL*, pages 1–29.

Brander, R. W. and Scott, T. (2016). Science of the rip current hazard. *The science of beach lifeguarding: principles and practice. CRC Press, Boca Raton*, pages 67–86.

Brandolini, P. L., Cortemiglia, G. C., Firpo, M., Piccazzo, M., Queirolo, C., and Terranova, R. (2002). Dinamica e caratteri evolutivi della spiaggia di levanto (liguria orientale). *Atti Associazione Italiana Oceanologia e Limnologia*, 15:147–162.

Brignone, M., Schiaffino, C. F., Isla, F. I., and Ferrari, M. (2012). A system for beach video-monitoring: Beachkeeper plus. *Computers & geosciences*, 49:53–61.

Buijsman, M. C., Ruggiero, P., and Kaminsky, G. M. (2001). Sensitivity of shoreline change predictions to wave climate variability along the southwest washington coast, usa. In *Coastal Dynamics' 01*, pages 617–626.

Carey, W. and Rogers, S. (2005). Rip currents - coordinating coastal research, outreach and forecast methodologies to improve public safety. In *Solutions to Coastal Disasters 2005*, pages 285–296.

Castelle, B., Marieu, V., Bujan, S., Splinter, K. D., Robinet, A., Sénéchal, N., and Ferreira, S. (2015). Impact of the winter 2013–2014 series of severe western europe storms on a double-barred sandy coast: Beach and dune erosion and megacusp embayments. *Geomorphology*, 238:135–148.

Castelle, B., Scott, T., Brander, R. W., and McCarroll, R. J. (2016). Rip current types, circulation and hazard. *Earth-Science Reviews*, 163:1–21.

Charria, G., Lazure, P., Le Cann, B., Serpette, A., Reverdin, G., Louazel, S., Batifoulier, F., Dumas, F., Pichon, A., and Morel, Y. (2013). Surface layer circulation derived from lagrangian drifters in the bay of biscay. *Journal of Marine Systems*, 109:S60–S76.

Chen, Q., Dalrymple, R. A., Kirby, J. T., Kennedy, A. B., and Haller, M. C. (1999). Boussinesq modeling of a rip current system. *Journal of Geophysical Research: Oceans*, 104(C9):20617–20637.

Cobianchi, M., Galbiati, B., and Villa, G. (1994). Stratigraphy of the palombini shales in the bracco unit (northern apennine). *Ofioliti*, 19(2A):193–216.

Cook, D. O. (1970). The occurrence and geologic work of rip currents off southern california. *Marine Geology*, 9(3):173–186.

Cortesogno, L., Galbiati, B., and Principi, G. (1987). *Note alla "carta geologica delle ofioliti del Bracco" e ricostruzione della paleogeografia giurassico-cretacea*. Edizioni ETS.

Cowell, P. J. and Thom, B. G. (1994). *Morphodynamics of coastal evolution*. Cambridge University Press, Cambridge, United Kingdom and New York, NY, USA.

da F. Klein, A. H., Santana, G. G., Diehl, F. L., and De Menezes, J. T. (2003). Analysis of hazards associated with sea bathing: results of five years work in oceanic beaches of santa catarina state, southern brazil. *Journal of Coastal Research*, 35:107–116.

Dalrymple, R. A. and Lozano, C. J. (1978). Wave-current interaction models for rip currents. *Journal of Geophysical Research: Oceans*, 83(C12):6063–6071.

Dalrymple, R. A., MacMahan, J. H., Reniers, A. J. H. M., and Nelko, V. (2011). Rip currents. *Annual Review of Fluid Mechanics*, 43:551–581.

Davidson, M., Van Koningsveld, M., de Kruif, A., Rawson, J., Holman, R. A., Lamberti, A., Medina, R., Kroon, A., and Aarninkhof, S. (2007). The coastview project: Developing video-derived coastal state indicators in support of coastal zone management. *Coastal Engineering*, 54(6-7):463–475.

Davies, J. L. (1958). *Wave refraction and the evolution of shoreline curves.* Birbeck College.

Davis, W. M. (1925). The undertow myth. *Science*, 61(1573):206–208.

de Vriendº, H. J., Zyserman, J., Nicholson, J., Roelvinkº, J. A., and Pechon, P. (1993). Medium-term 2dh coastal area modelling. *Coastal engineering*, 2(1):193–224.

Dean, R. G. (1992). Beach nourishment: design principles. *Design and Reliability of Coastal Structures, short course during the 23rd ICCE in Venice.*

Decandia, F. A. and Elter, P. (1972). *La "zona" ofiolitifera del Bracco nel settore compreso fra Levanto e la Val Graveglia (Appennino ligure).* Mem.Soc.Geol.It.

Drønen, N., Karunarathna, H., Fredsøe, J., Sumer, B. M., and Deigaard, R. (2002). An experimental study of rip channel flow. *Coastal Engineering*, 45(3-4):223–238.

Dronkers, J. (2005). *Dynamics of coastal systems*. World Scientific Publishing Co. Pte. Ltd.

Enckevort, I. M. J. v. and Ruessink, B. G. (2001). Effect of hydrodynamics and bathymetry on video estimates of nearshore sandbar position. *Journal of Geophysical Research: Oceans*, 106(C8):16969–16979.

Evans, O. F. (1938). The undertow. *Science*, 88(2282):279–281.

Faria, A. F., Thornton, E. B., Lippmann, T. C., and Stanton, T. P. (2000). Undertow over a barred beach. *Journal of Geophysical Research: Oceans*, 105(C7):16999–17010.

Fierro, G., Berriolo, G., and Ferrari, M. (2010). *Le spiagge della Liguria occidentale-analisi evolutiva*. Regione Liguria.

Fierro, G., Berriolo, G., and Ferrari, M. (2015). *Le spiagge della Liguria orientale-analisi evolutiva*. Regione Liguria.

Finkl, C. W. (2004). Coastal classification: systematic approaches to consider in the development of a comprehensive scheme. *Journal of Coastal Research*, 20(1):166–213.

Folk, R. L. and Ward, W. C. (1957). Brazos river bar [texas]; a study in the significance of grain size parameters. *Journal of Sedimentary Research*, 27(1):3–26.

Fuell, K. K., Olson, K., and Schott, T. (2005). Rip current training for coastal forecasters. In *Preprints AMS Forum: Living in the Coastal Zone, AMS J.*, volume 1.

Fujimura, A. G., Reniers, A. J. H. M., Paris, C. B., Shanks, A. L., MacMahan, J. H., and Morgan, S. G. (2014). Numerical simulations of larval transport

into a rip-channeled surf zone. *Limnology and Oceanography*, 59(4):1434–1447.

Gensini, V. A. and Ashley, W. S. (2010). An examination of rip current fatalities in the united states. *Natural Hazards*, 54(1):159–175.

Grant, W. D. and Madsen, O. S. (1979). Combined wave and current interaction with a rough bottom. *Journal of Geophysical Research: Oceans*, 84(C4):1797–1808.

Grant, W. D., Williams III, A. J., and Glenn, S. M. (1984). Bottom stress estimates and their prediction on the northern california continental shelf during code-1: the importance of wave-current interaction. *Journal of Physical Oceanography*, 14(3):506–527.

Harley, M. D., Turner, I. L., Short, A. D., and Ranasinghe, R. (2011). Assessment and integration of conventional, rtk-gps and image-derived beach survey methods for daily to decadal coastal monitoring. *Coastal Engineering*, 58(2):194–205.

Hartmann, D. (2006). Drowning and beach-safety management (bsm) along the mediterranean beaches of israela long-term perspective. *Journal of Coastal Research*, 22(6):1505–1514.

Hino, M. (1974). Theory on formation of rip-current and cuspidal coast. *Coastal Engineering in Japan*, 17(1):23–37.

Holland, K. T. (1998). Beach cusp formation and spacings at duck, usa. *Continental Shelf Research*, 18(10):1081–1098.

Holman, R. A. and Stanley, J. (2007). The history and technical capabilities of argus. *Coastal engineering*, 54(6-7):477–491.

Holman, R. A., Stanley, J., and Ozkan-Haller, T. (2003). Applying video sensor networks to nearshore environment monitoring. *IEEE Pervasive Computing*, 2(4):14–21.

Holthuijsen, L. H., Booij, N., and Herbers, T. H. C. (1989). A prediction model for stationary, short-crested waves in shallow water with ambient currents. *Coastal Engineering*, 13(1):23–54.

Inman, D. L. and Brush, B. M. (1973). The coastal challenge. *Science*, 181(4094):20–32.

Inman, D. L. and Quinn, W. H. (1951). Currents in the surf zone. *Coastal Engineering Proceedings*, 1(2):3.

IPCC (2013). *Climate Change 2013: The Physical Science Basis. Contribution of Working Group I to the Fifth Assessment Report of the Intergovernmental Panel on Climate Change*. Cambridge University Press, Cambridge, United Kingdom and New York, NY, USA.

Istituto Idrografico della Marina, I. I. M. (2006). Carta Nautica (Nautical Chart) da Portofino a San Rossore. foglio no. 3, scala 1:100000.

Jennings, R. and Shulmeister, J. (2002). A field based classification scheme for gravel beaches. *Marine Geology*, 186(3-4):211–228.

Johnson, D. and Pattiaratchi, C. (2004). Transient rip currents and nearshore circulation on a swell-dominated beach. *Journal of Geophysical Research: Oceans*, 109(C2).

Johnson, D. W. (1919). *Shore processes and shoreline development*. John Wiley & Sons, Incorporated.

Komen, G. J., Cavaleri, L., Donelan, M., Hasselmann, K., Hasselmann, S., and Janssen, P. A. E. M. (1996). Dynamics and modelling of ocean waves. *ISBN 0521577810. Cambridge, UK: Cambridge University Press*, page 554.

Kopp, R. E. (2015). [https://github.com/bobkopp/localizesl/releases].

Kopp, R. E., Horton, R. M., Little, C. M., Mitrovica, J. X., Oppenheimer, M., Rasmussen, D. J., Strauss, B. H., and Tebaldi, C. (2014). Probabilistic 21st and 22nd century sea-level projections at a global network of tide-gauge sites. *Earth's Future*, 2(8):383–406.

Kroon, A., Davidson, M. A., Aarninkhof, S. G. J., Archetti, R., Armaroli, C., Gonzalez, M., Medri, S., Osorio, A., Aagaard, T., Holman, R. A., et al. (2007). Application of remote sensing video systems to coastline management problems. *Coastal Engineering*, 54(6-7):493–505.

Kuo, C. A., Hwung, H. H., and Chien, C. H. (2009). Using time-stack overlooking images to separate incident and reflected waves in wave flume. *Wave Motion*, 46(3):189–199.

LeBlond, P. H. (1979). An explanation of the logarithmic spiral plan shape of headland-bay beaches. *Journal of Sedimentary Research*, 49(4):1093–1100.

Lesser, G. R., Roelvink, J. A., Van Kester, J. A. T. M., and Stelling, G. S. (2004). Development and validation of a three-dimensional morphological model. *Coastal engineering*, 51(8-9):883–915.

Lippmann, T. C. and Holman, R. A. (1989). Quantification of sand bar morphology: A video technique based on wave dissipation. *Journal of Geophysical Research: Oceans*, 94(C1):995–1011.

Lippmann, T. C. and Holman, R. A. (1990). The spatial and temporal variability of sand bar morphology. *Journal of Geophysical Research: Oceans*, 95(C7):11575–11590.

Longuet-Higgins, M. S. and Stewart, R. W. (1964). Radiation stresses in water waves; a physical discussion, with applications. In *Deep Sea Research and Oceanographic Abstracts*, volume 11, pages 529–562. Elsevier.

Loureiro, C., Ferreira, Ó., and Cooper, J. A. G. (2012). Extreme erosion on high-energy embayed beaches: influence of megarips and storm grouping. *Geomorphology*, 139:155–171.

Lushine, J. B. (1991). A study of rip current drownings and related weather factors. In *Natl. Wea. Dig.* Citeseer.

MacMahan, J., Brown, J., and Thornton, E. (2009). Low-cost handheld global positioning system for measuring surf-zone currents. *Journal of Coastal Research*, 25(3):744–754.

MacMahan, J. H., Thornton, E. B., and Reniers, A. J. H. M. (2006). Rip current review. *Coastal Engineering*, 53(2-3):191–208.

MacMahan, J. H., Thornton, E. B., Stanton, T. P., and Reniers, A. J. H. M. (2005). Ripex: Observations of a rip current system. *Marine Geology*, 218(1-4):113–134.

Madsen, A. J. and Plant, N. G. (2001). Intertidal beach slope predictions compared to field data. *Marine Geology*, 173(1-4):121–139.

Marcoe, K. (2007). Slides lidar: an introduction and overview. *Portland State University*.

Marcos, M., Chust, G., Jordà, G., and Caballero, A. (2012). Effect of sea level extremes on the western basque coast during the 21st century. *Climate Research*, 51(3):237–248.

Marroni, M. and Perilli, N. (1990). The age of the ophiolite sedimentary cover from the mt. gottero unit (internal ligurid units, northern apennines): new data from calcareous nannofossils. *Ofioliti*, 15(2):232–251.

Martens, D., Williams, T., and Cowell, P. J. (1999). Mega-rip dimensional analysis on the sydney coast australia, and implications for beach-state recognition and prediction. *Journal of Coastal Research*, 17:34–42.

Mastronuzzi, G., Aringoli, D., Pietro P. C., A., Maurizio A., B., Bellotti, P., Bini, M., Biolchi, S., Bontempi, S., Brandolini, P., Chelli, A., Davoli, L., Deiana, G., De Muro, S., Devoto, S., Di Paola, G., Donadio, C., Fago, P., Ferrari, M., Furlani, S., Ibba, A., Lupia Palmieri, E., Marsico, A., Rita T., M., Milella, M., Mucerino, L., Nesci, O., Orr, P. E., Panizza, V., Pennetta, M., Piacentini, D., Piscitelli, A., Pusceddu, N., Raffi, R., Carmen M., R., Sans, P., Stanislao, C., Tarragoni, C., and Valente, A. (2017). Geomorphological map of the italian coast: From a descriptive to a morphodynamic approach. *Geografia Fisica e Dinamica Quaternaria*, 40:161–196.

McCarroll, R. J., Brander, R. W., Turner, I. L., Power, H. E., and Mortlock, T. R. (2014). Lagrangian observations of circulation on an embayed beach with headland rip currents. *Marine Geology*, 355:173–188.

McCool, J. P., Moran, K., Ameratunga, S., Robinson, E., et al. (2008). New zealand beachgoers swimming behaviors, swimming abilities, and perception of drowning risk. *International Journal of Aquatic Research and Education*, 2(1):7–15.

McKenzie, P. (1958). Rip-current systems. *The Journal of Geology*, 66(2):103–113.

Meadows, G., Purcell, H., Guenther, D., Meadows, L., Kinnunen, R. E., and Clark, G. (2011). Rip currents in the great lakes: an unfortunate truth.

Mei, C. C. and Liu, P. L. F. (1977). Effects of topography on the circulation in and near the surf zonelinear theory. *Estuarine and Coastal Marine Science*, 5(1):25–37.

Meinshausen, M., Smith, S. J., Calvin, K., Daniel, J. S., Kainuma, M. L. T., Lamarque, J. F., Matsumoto, K. M., Montzka, S. A., Raper, S. C. B., Riahi, K., et al. (2011). The rcp greenhouse gas concentrations and their extensions from 1765 to 2300. *Climatic change*, 109(1-2):213.

Mentaschi, L., Besio, G., Cassola, F., and Mazzino, A. (2013). Developing and validating a forecast/hindcast system for the Mediterranean Sea. *Journal of Coastal Research*, 65(sp2):1551–1556.

Mentaschi, L., Besio, G., Cassola, F., and Mazzino, A. (2015). Performance evaluation of WAVEWATCH III in the Mediterranean Sea. *Ocean Modelling*, 90:82–94.

Mimura, N. (2013). Sea-level rise caused by climate change and its implications for society. *Proceedings of the Japan Academy, Series B*, 89(7):281–301.

Moksness, E., Dahl, E., and Støttrup, J. (2009). *Integrated coastal zone management*. John Wiley & Sons.

Morris, B. D., Davidson, M. A., and Huntley, D. A. (2001). Measurements of the response of a coastal inlet using video monitoring techniques. *Marine Geology*, 175(1-4):251–272.

Mucchi, A. M., Pellegrini, M., and Mantovani, M. P. (1968). Le serie stratigrafiche di spezia e dei monti d'oltre serchio. *Mem.Soc.Geol.It*, 7:195–225.

Murray, A. B. (2004). Rip channel development on nonbarred beaches: The importance of a lag in suspended-sediment transport. *Journal of Geophysical Research: Oceans*, 109(C4).

Murray, T., Cartwright, N., and Tomlinson, R. (2013). Video-imaging of transient rip currents on the gold coast open beaches. *Journal of Coastal Research*, 65(sp2):1809–1814.

Nelko, V. and Dalrymple, R. A. (2011). Rip current prediction at ocean city, maryland. *Rip currents: Beach safety, physical oceanography, and wave modeling, Florida: CRC Press International*, pages 45–57.

Nicholson, J., Broker, I., Roelvink, J. A., Price, D., Tanguy, J. M., and Moreno, L. (1997). Intercomparison of coastal area morphodynamic models. *Coastal Engineering*, 31(1-4):97–123.

Nieto, M. A., Garau, B., Balle, S., Simarro, G., Zarruk, G. A., Ortiz, A., Tintoré, J., Álvarez-Ellacuría, A., Gómez-Pujol, L., and Orfila, A. (2010). An open source, low cost video-based coastal monitoring system. *Earth Surface Processes and Landforms*, 35(14):1712–1719.

Noda, E. K. (1974). Wave-induced nearshore circulation. *Journal of Geophysical Research*, 79(27):4097–4106.

Ojeda, E., Ruessink, B. G., and Guillén, J. (2008). Morphodynamic response of a two-barred beach to a shoreface nourishment. *Coastal Engineering*, 55(12):1185–1196.

O'Rourke, J. C. and LeBlond, P. H. (1972). Longshore currents in a semicircular bay. *Journal of Geophysical Research*, 77(3):444–452.

Paduan, J. D. and Niiler, P. P. (1993). Structure of velocity and temperature in the northeast pacific as measured with lagrangian drifters in fall 1987. *Journal of Physical Oceanography*, 23(4):585–600.

Parlagreco, L. (2011). *Video-monitoraggio della variabilità morfologica delle barre sommerse: il caso del litorale di Terracina.* PhD thesis, Università degli Studi di Ferrara.

Pattiaratchi, C., James, A., and Collins, M. (1987). Island wakes and headland eddies: a comparison between remotely sensed data and laboratory experiments. *Journal of Geophysical Research: Oceans*, 92(C1):783–794.

Pattiaratchi, C., Olsson, D., Hetzel, Y., and Lowe, R. (2009). Wave-driven circulation patterns in the lee of groynes. *Continental Shelf Research*, 29(16):1961–1974.

Pearre, N. S. and Puleo, J. A. (2009). Quantifying seasonal shoreline variability at rehoboth beach, delaware, using automated imaging techniques. *Journal of Coastal Research*, 25(4):900–914.

Pender, D. and Karunarathna, H. (2013). A statistical-process based approach for modelling beach profile variability. *Coastal Engineering*, 81:19–29.

Peynaud, F. and Pijanowski, J. (1979). An acoustic doppler current meter. In *Offshore Technology Conference.* Offshore Technology Conference.

Piccardo, G. B., Rampone, E., Vannucci, R., and Cimmino, F. (1994). Upper mantle evolution of ophiolitic peridotites from the northern apennine:

petrological constraints to the geodynamic processes. *Mem. Soc. Geol. It*, 48:137–148.

Pickaver, A. H., Gilbert, C., and Breton, F. (2004). An indicator set to measure the progress in the implementation of integrated coastal zone management in europe. *Ocean & Coastal Management*, 47(9-10):449–462.

Plant, N. G. and Holman, R. A. (1997). Intertidal beach profile estimation using video images. *Marine Geology*, 140(1-2):1–24.

Poulain, P. M. and Zambianchi, E. (2007). Surface circulation in the central mediterranean sea as deduced from lagrangian drifters in the 1990s. *Continental Shelf Research*, 27(7):981–1001.

Quartel, S., Addink, E. A., and Ruessink, B. G. (2006). Object-oriented extraction of beach morphology from video images. *International journal of applied earth observation and geoinformation*, 8(4):256–269.

Ranasinghe, R., Turner, I. L., and Symonds, G. (2006). Shoreline response to multi-functional artificial surfing reefs: A numerical and physical modelling study. *Coastal Engineering*, 53(7):589–611.

Rea, C. C. and Komar, P. D. (1975). Computer simulation models of a hooked beach shoreline configuration. *Journal of Sedimentary Research*, 45(4):866–872.

Regione Liguria (2008). [https://geoportal.regione.liguria.it].

Roelvink, D. (2011). *A guide to modeling coastal morphology*, volume 12. world scientific.

Roelvink, D., Reniers, A., Van Dongeren, A. P., de Vries, J. v. T., McCall, R., and Lescinski, J. (2009). Modelling storm impacts on beaches, dunes and barrier islands. *Coastal engineering*, 56(11-12):1133–1152.

Roelvink, D., Van Dongeren, A., McCall, R., Hoonhout, B., Van Rooijen, A., Van Geer, P., De Vet, L., Nederhoff, K., and Quataert, E. (2015). Xbeach technical reference: Kingsday release. *Delft, The Netherlands: Deltares, Technical report.*

Roelvink, J. A. and Brøker, I. (1993). Cross-shore profile models. *Coastal Engineering*, 21(1-3):163–191.

Russell, R. J. and McIntire, W. G. (1965). Beach cusps. *Geological Society of America Bulletin*, 76(3):307–320.

Sabet, B. S. and Barani, G. A. (2011). Field investigation of rip currents along the southern coast of the caspian sea. *Scientia Iranica*, 18(4):878–884.

Salmon, S. A., Bryan, K. R., and Coco, G. (2007). The use of video systems to measure run-up on beaches. *Journal of Coastal Research*, 50:211–215.

Schiaffino, C. F., Brignone, M., Corradi, N., Cevasco, A., Iannotta, M. A., Cavallo, C., and Ferrari, M. (2013). The ligurian webcam network and database for coastal management. *Coastal erosion monitoring*, page 79.

Schiaffino, C. F., Dessy, C., Corradi, N., Fierro, G., and Ferrari, M. (2015). Morphodynamics of a gravel beach protected by a detached low-crested breakwater. the case of levanto (eastern ligurian sea, italy). *Italian Journal of Engineering Geology and Environment*, 15(1):31–39.

Schoonees, J. S. and Theron, A. K. (1995). Evaluation of 10 cross-shore sediment transport / morphological models. *Coastal Engineering*, 25:1–41.

Schwartz, M. L. (1982). The encyclopedia of beaches and coastal environments.

Scott, T., Austin, M., Masselink, G., and Russell, P. (2016). Dynamics of rip currents associated with groynesfield measurements, modelling and implications for beach safety. *Coastal Engineering*, 107:53–69.

Scott, T., Russell, P., Masselink, G., and Wooler, A. (2009). Rip current variability and hazard along a macro-tidal coast. *Journal of Coastal Research*, 56:895–898.

Shanks, A. L., Morgan, S. G., MacMahan, J., and Reniers, A. J. H. M. (2010). Surf zone physical and morphological regime as determinants of temporal and spatial variation in larval recruitment. *Journal of Experimental Marine Biology and Ecology*, 392(1-2):140–150.

Shepard, F. P. (1936). Undertow, rip tide or" rip current". *Science*, 84(2173):181–182.

Shepard, F. P., Emery, K. O., and La Fond, E. C. (1941). Rip currents: a process of geological importance. *The Journal of Geology*, 49(4):337–369.

Shepard, F. P. and Inman, D. L. (1950). Nearshore water circulation related to bottom topography and wave refraction. *Eos, Transactions American Geophysical Union*, 31(2):196–212.

Shepard, F. P. and Inman, D. L. (1951). Nearshore circulation. Technical report, Scripps Institution of Oceanography La Jolla Calif.

Sherker, S., Brander, R. W., Finch, C., and Hatfield, J. (2008). Why australia needs an effective national campaign to reduce coastal drowning. *Journal of science and medicine in sport*, 11(2):81.

Short, A. D. (1985). Rip-current type, spacing and persistence, narrabeen beach, australia. *Marine geology*, 65(1-2):47–71.

Short, A. D. (1991). Macro-meso tidal beach morphodynamics: an overview. *Journal of Coastal Research*, 7(2):417–436.

Short, A. D. (1996). *Beaches of the Victorian coast & Port Phillip Bay: a guide to their nature, characteristics, surf and safety.* Sydney University Press.

Short, A. D. (1999). *Handbook of beach and shoreface morphodynamics.* Number 551.468 HAN. John Willey and Sons.

Short, A. D. (2007). Australian rip systems–friend or foe? *Journal of Coastal Research*, 50:7–11.

Short, A. D. and Hogan, C. L. (1994). Rip currents and beach hazards: their impact on public safety and implications for coastal management. *Journal of Coastal Research*, 12:197–209.

Short, A. D. and Masselink, G. (1999). Structurally controlled beaches. *Handbook of Beach and Shoreface Morphodynamics; Short, AD, Ed.; John Wiley and Sons Ltd: Chichester, UK*, pages 230–250.

Signell, R. P., Beardsley, R. C., Graber, H. C., and Capotondi, A. (1990). Effect of wave-current interaction on wind-driven circulation in narrow, shallow embayments. *Journal of Geophysical Research: Oceans*, 95(C6):9671–9678.

Silva, A. N., Taborda, R., Catalão, J., and Freire, P. (2009). Dtm extraction using video-monitoring techniques: application to a fetch limited beach. *Journal of Coastal Research*, 1:203–207.

Silvester, R., Hsu, J. R., and Dean, R. (1994). Coastal stabilization: innovative concepts. *Sedimentary Geology*, 88(3):153–153.

Silvester, R., Tsuchtya, Y., and Shibano, Y. (1980). Zeta bays, pocket beaches and headland control. In *Coastal Engineering 1980*, pages 1306–1319.

Simeoni, U., Corbau, C., Pranzini, E., Ginesu, S., et al. (2012). *Le pocket beach. Dinamica e gestione delle piccole spiagge: Dinamica e gestione delle piccole spiagge*. FrancoAngeli.

Sinnett, G. and Feddersen, F. (2014). The surf zone heat budget: The effect of wave heating. *Geophysical Research Letters*, 41(20):7217–7226.

Skamarock, W. C. and Klemp, J. B. (2008). A time-split nonhydrostatic atmospheric model for weather research and forecasting applications. *Journal of Computational Physics*, 227(7):3465–3485.

Sonu, C. J. (1972). Field observation of nearshore circulation and meandering currents. *Journal of Geophysical Research*, 77(18):3232–3247.

Sonu, C. J., McCloy, J. M., and McArthur, D. S. (1967). Longshore currents and nearshore topographies. In *Coastal Engineering 1966*, pages 525–549.

Soulsby, R. L., Hamm, L., Klopman, G., Myrhaug, D., Simons, R. R., and Thomas, G. P. (1993). Wave-current interaction within and outside the bottom boundary layer. *Coastal engineering*, 21(1-3):41–69.

Surf Life Saving Australia, S. L. S. (2009). National coastal safety report 2009. *Sydney, Australia*.

Szmytkiewicz, M., Biegowski, J., Kaczmarek, L. M., Okroj, T., Ostrowski, R., Pruszak, Z., Różyńsky, G., and Skaja, M. (2000). Coastline changes

nearby harbour structures: comparative analysis of one-line models versus field data. *Coastal Engineering*, 40(2):119–139.

Taborda, R. and Silva, A. (2012). Cosmos: A lightweight coastal video monitoring system. *Computers & geosciences*, 49:248–255.

Takewaka, S. and Nakamura, T. (2001). Surf zone imaging with a moored video system. In *Coastal Engineering 2000*, pages 1211–1216.

Talbot, M. M. B. and Bate, G. C. (1987). Rip current charactersitics and their role in the exchange of water and surf diatoms between the surf zone and nearshore. *Estuarine, Coastal and Shelf Science*, 25(6):707–720.

Thia-Eng, C. (1993). Essential elements of integrated coastal zone management. *Ocean & Coastal Management*, 21(1-3):81–108.

Thornton, E. B., MacMahan, J., and Sallenger Jr, A. H. (2007). Rip currents, mega-cusps, and eroding dunes. *Marine geology*, 240(1-4):151–167.

Tolman, H. L. et al. (2009). User manual and system documentation of wavewatch iii tm version 3.14. *Technical note, MMAB Contribution*, 276:220.

Vousdoukas, M. I., Ferreira, P. M., Almeida, L. P., Dodet, G., Psaros, F., Andriolo, U., Taborda, R., Silva, A. N., Ruano, A., and Ferreira, Ó. (2011). Performance of intertidal topography video monitoring of a meso-tidal reflective beach in south portugal. *Ocean Dynamics*, 61(10):1521–1540.

Wang, L., Zimmermann, N., Trouw, K., De Maerschalck, B., Delgado, R., Verwaest, T., and Mostaert, F. (2015). Scientific support regarding hydrodynamics and sand transport in the coastal zone: Calibration of a long term morphological model of the belgian shelf. *WL Rapporten*.

Wentworth, C. K. (1922). A scale of grade and class terms for clastic sediments. *The journal of geology*, 30(5):377–392.

Wright, L. D. and Short, A. D. (1984). Morphodynamic variability of surf zones and beaches: a synthesis. *Marine geology*, 56(1-4):93–118.

Wright, L. D. and Thom, B. G. (1977). Coastal depositional landforms: a morphodynamic approach. *Progress in Physical Geography*, 1(3):412–459.

Yasso, W. E. (1965). Plan geometry of headland-bay beaches. *The Journal of geology*, 73(5):702–714.

Yoon, S. B., Park, W. K., and Choi, J. (2014). Observation of rip current velocity at an accidental event by using video image analysis. *Journal of Coastal Research*, 72(sp1):16–21.

Zaccagna, D. (1935). *La geologia del golfo della Spezia*.

Zhang, S. and Zhang, C. (2008). Application of ridgelet transform to wave direction estimation. In *2008 Congress on Image and Signal Processing*, pages 690–693. IEEE.

Zikra, M. (2008). Wave speed estimation using video coastal imagery. *Neptunus*, 14(1).